PEOPLE'S DEMOCRATIC REPUBLIC OF ALGERIA
MINISTERY OF HIGHER EDUCATION AND SCIENTIFIC RESEARCH

MOHAMED BOUDIAF UNIVERSITY -M'SILA
Faculty of Mathematics and Computer Science
Department of Mathematics

N° d'ordre: ....

Thesis

Submitted for the Doctorate (Third Cycle) degree

Domain : Mathematics and Computer Science
Specialty : Mathematics
Option : Numerical Analysis, PDEs and Applications

Title

Fractional PDEs for image restoration and denoising

Presented by :
Imane BOUDRISSA

Publicly defended on : April 23, 2026

Before the Jury Committee composed of :

Yacine Arioua,	Prof.,	University of M'sila,	Chair
Noureddine Benhamidouche,	Prof.,	University of M'sila,	Supervisor
Rafaa Chouder,	Dr.,	University of M'sila,	Co-Supervisor
Mohammed Hachama,	Prof.,	NHSM,	Examiner
Abdelkrim Merzougui,	Prof.,	University of Msila,	Examiner

University year: 2025/2026

Acknowledgements

First and foremost, I thank Almighty Allah for granting me the strength and determination to complete this work.

I would like to express my sincere thanks and profound gratitude to my supervisor, Prof. Noureddine Benhamidouche, for his guidance, valuable advice, and continuous support throughout the preparation of this thesis. I also wish to extend my sincere appreciation to Dr. Rafaa Chouder, for his constructive suggestions and constant encouragement throughout the course of this research.

I am also grateful to the members of the examination committee, Prof. Yacine Arioua, Prof. Mohammed Hachama, and Prof. Abdelkrim Merzougui, for their time and for agreeing to review and assess this thesis.

I would like to express my deep appreciation to my family, who have always been an inexhaustible source of encouragement and support.

Dedication

I dedicate this work to those who are dearest to me:

To my mother, whose constant support has been a source of strength throughout this journey.

To my father, for his invaluable support and guidance in helping me reach this stage.

To my brothers and sisters.

To my entire family.

To all my friends.

To my fellow students.

Contents

List of Tables

List of Figures

Notation

$\mathbb{N}$	The set of positive integers $\{1, 2, 3, ...\}$.
$\mathbb{R}$	The set of real numbers.
$\mathbb{R}^+$	The set of positive real numbers.
$\mathbb{R}^n$	The real vector space of dimension n.
$\Re(\alpha)$	The real part of the complex number α.
$\mathcal{W}^{m,p}(\Omega)$	The Sobolev space.
$\mathcal{W}^{\alpha,p}(\Omega)$	The fractional-order Sobolev space.
$\mathcal{H}^m(\Omega)$	$= \mathcal{W}^{m,2}(\Omega)$.
$\mathcal{H}^\alpha(\Omega)$	$= \mathcal{W}^{\alpha,2}(\Omega)$.
$\mathcal{K}_\rho$	The Gaussian kernel with standard deviation ρ.
$\Gamma(.)$	The Euler's Gamma function.
$e^{(.)}$	The Exponential function.
$\mathcal{I}^\alpha$	The Riemann-Liouville fractional integral of order α.
${}^{C}\mathcal{D}^\alpha$	The Caputo fractional derivative of order α.
${}^{CF}\mathcal{D}^\alpha$	The Caputo-Fabrizio fractional derivative of order α.
∇	The gradient operator.
∇^α	The fractional gradient operator.
div(.)	The divergence operator.
$\mathrm{div}^\alpha(.)$	The fractional divergence operator.
PDEs	Partial differential equations.
FPDEs	Fractional partial differential equations.
PM	The Perona-Malik model.
ROF	The Rudin-Osher-Fatemi model.
AOS	Additive Operator Splitting schemes.
PSNR	Peak Signal-to-Noise Ratio.
SSIM	Structural Similarity Index Measure.

Introduction

Partial differential equations (PDEs) play a central role in the mathematical modeling of a wide range of natural and physical processes. They describe how quantities evolve in space and time according to fundamental principles such as conservation laws, transport, and diffusion. In particular, diffusion-type equations are used to model processes involving the spreading or equalization of physical quantities, such as heat conduction, particle dispersion, and fluid dynamics. The strength of PDEs lies in their ability to capture both local interactions and global behaviors within well-established analytical and numerical frameworks.

In recent decades, PDEs have also emerged as powerful tools beyond classical physics-based applications, providing a rigorous mathematical foundation for diverse problems in engineering, biology, and image processing. The use of PDEs in image processing was popularized by the seminal work of Perona and Malik [39], who introduced an anisotropic diffusion model that adapts the amount of smoothing according to the local image gradient. This formulation represented a major departure from conventional linear filtering, as it enabled selective noise removal while preserving essential structures such as edges and contours. Since then, numerous PDE-based models have been developed to address various image processing tasks, including denoising, deblurring, and edge detection. Among these approaches, the total variation (TV) model proposed by Rudin, Osher, and Fatemi [44] has become one of the most influential, as it minimizes the total variation of the image to produce smoothing while preserving edges. Higher-order PDEs [36, 58] and curvature-driven flows [38, 42, 57] were later introduced to mitigate drawbacks such as staircasing artifacts and excessive smoothing. Despite their effectiveness, classical PDE-based models remain fundamentally local: the diffusion process at each point depends only on its immediate neighborhood. This locality limits their ability to capture long-range spatial dependencies and fine textures, which are intrinsic to natural images.

Numerous image denoising strategies have been proposed over the past decades, each based on distinct assumptions and mathematical frameworks. These include classical spatial filters [29, 47], transform-domain methods [29, 48], and more recently, data-driven [15, 25] and learning-based approaches [31, 63]. While such methods offer particular advantages, they often suffer from drawbacks such as insufficient edge preservation, inadequate texture recovery, or, in the case of deep learning models [63], a reliance on large annotated datasets and limited interpretability. Among these methodologies, variational and PDE-based models have gained special prominence due to their solid theoretical foundations and superior ability to preserve structural details compared with traditional filtering or transform-based methods [3, 7, 17, 19, 36, 37, 39, 44, 55, 64]. Nevertheless, even classical PDE-based models, including TV regularization, may oversmooth fine textures or fail to reconstruct subtle image structures accurately.

To overcome these limitations, researchers have increasingly turned to fractional-order models, which extend classical PDE formulations by incorporating fractional (non-integer) derivatives. This generalization introduces nonlocal and scale-dependent interactions, providing a more flexible and powerful framework for image restoration. The nonlocal nature of fractional derivatives enables these models to preserve both global structures and fine textures while effectively reducing various types of noise. Fractional-order diffusion models have shown remarkable success in removing additive Gaussian noise [5, 9, 23], while other formulations have been adapted to address multiplicative noise [1, 21, 45, 56, 61, 65].

In this context, fractional partial differential equations (FPDEs) provide a natural bridge between local and nonlocal models, combining the analytical depth of classical PDEs with the modeling versatility of fractional calculus. By adjusting the fractional order, one can interpolate between strong smoothing and fine-detail preservation, allowing for precise control of the restoration process. Motivated by these developments, the present work investigates fractional PDE-based models for image restoration and denoising, combining rigorous mathematical analysis with numerical implementation and experimental validation.

Objectives and contributions of the thesis

The primary objective of this thesis is to develop, analyze, and numerically solve advanced fractional-order models for image denoising, addressing the limitations of traditional methods while ensuring high-quality image restoration. The focus is on incorporating fractional-order derivatives into nonlinear diffusion equations to enhance both noise suppression and edge preservation. The key contributions of this thesis are as follows:

1. **Incorporation of fractional derivatives into nonlinear diffusion models**

   This thesis introduces novel models that integrate fractional-order derivatives within the diffusivity functions of nonlinear diffusion equations. These fractional derivatives improve the preservation of fine image structures and textures, which are essential for high-quality image restoration in noisy image. By extending traditional diffusion equations with fractional components, the proposed models enhance noise suppression while maintaining edge integrity and structural features.

2. **Theoretical analysis and well-posedness of the models**

   A comprehensive mathematical analysis is conducted to establish the existence, uniqueness, and boundedness of weak solutions to the nonlinear fractional diffusion equations. The analysis is based on Schauder's fixed-point theorem, ensuring the well-posedness of the models and providing a robust foundation for the subsequent numerical methods developed in this thesis.

3. **Development of efficient numerical methods**

   To solve the fractional diffusion equations efficiently, this thesis proposes a numerically stable semi-implicit method based on the additive operator splitting (AOS) technique. This method ensures unconditional stability, making the numerical solution stable even for large time steps, without sacrificing computational efficiency.

4. **Evaluation and comparison of denoising performance**

   Extensive numerical experiments are performed on a range of images corrupted by various types of noise, such as Gaussian, salt-and-pepper, and speckle noise. The performance of the proposed models is quantitatively assessed using standard metrics, including peak signal-to-noise ratio (PSNR) and structural similarity index (SSIM). The results show that the proposed models significantly outperform traditional denoising methods, achieving superior denoising performance while preserving fine image details and edges.

5. **Comparison with existing methods**

   The proposed models are compared with classical diffusion models and other existing fractional diffusion models. Experimental results demonstrate that the new models, which incorporate fractional derivatives, offer superior denoising quality and enhanced edge preservation, making them more effective and suitable for image processing applications.

Structure of the thesis

This thesis is organized into several chapters, each of which is based on one of our published or submitted research articles. At the beginning of each chapter, a statement is provided to indicated the corresponding publication on which the chapter is based. The overall structure of the thesis is summarized below.

Chapter 1: Image processing: fundamentals, diffusion-based models, and mathematical background. This chapter introduces the theoretical and numerical background required throughout the thesis. It begins with an overview of essential image processing concepts related to image restoration and denoising, such as the main sources and types of noise in digital images and commonly used image quality assessment metrics. The chapter then reviews diffusion-based models in image processing, covering both classical and fractional formulations. Next, it recalls essential mathematical preliminaries, including functional spaces, basic definitions of fractional calculus, and several fundamental inequalities and theorems, which provide the analytical framework for studying the well-posedness of solutions. Finally, the finite difference framework is presented, with emphasis on explicit, implicit, and semi-implicit schemes, in particular the additive operator splitting (AOS) technique. This chapter therefore establishes a self-contained foundation for the theoretical analysis and numerical implementation developed in the subsequent chapters.

Chapter 2: Fractional gradient-based nonlinear diffusion model for image denoising. This chapter is devoted to the development of a fractional gradient-based nonlinear diffusion model for image denoising. The model extends the classical Rudin-Osher-Fatemi (ROF) framework [44] by incorporating the Caputo-Fabrizio fractional derivative into the diffusion coefficient, introducing nonlocal effects that enhance the preservation of image structures and edges. The chapter also addresses the well-posedness of the model and employs a semi-implicit finite difference scheme based on additive operator splitting (AOS) to ensure computational efficiency. A comparative study with the Caputo derivative and the classical ROF model is presented, demonstrating that the proposed approach achieves superior denoising performance while maintaining lower computational costs. This chapter thus provides a foundation for further extensions and applications presented in subsequent chapters.

Chapter 3: A nonlinear diffusion equation with gray-level and fractional gradient dependent coefficients: well-posedness analysis. This chapter develops a nonlinear diffusion model in which the diffusion coefficient depends on the image gradient, gray-level information, and fractional derivatives in the Caputo sense. The gray-level indicator plays a central role in adapting the diffusion to local intensity variations, thereby addressing the limitations observed in the Caputo model. Theoretical results on the existence and uniqueness of the weak solution are established, and a semi-implicit AOS numerical scheme is implemented. Compared to the Caputo model presented in Chapter 2, the inclusion of a gray-level indicator enhances adaptability to image intensities, leading to improved denoising performance and better preservation of fine details.

Chapter 4: Weak solution of a spatial fractional nonlinear diffusion equation: existence and uniqueness. This chapter focuses on the theoretical analysis of a spatial fractional nonlinear diffusion equation designed for image denoising. The model is formulated as a parabolic PDE that interpolates between second- and fourth-order diffusion, achieved by replacing the integer-order derivatives in the classical Perona-Malik equation with Caputo fractional derivatives. This fractional extension provides greater flexibility in balancing noise removal with the preservation of fine structures. Moreover, a fidelity term, following the formulation in [7], is added to reinforce the denoising process by enforcing consistency with the observed image data. A rigorous mathematical framework is established to study the existence and uniqueness of the weak solution, providing solid theoretical foundations for this class of fractional diffusion models.

Chapter 5: Fractional gradient-based nonlinear telegraph diffusion model for image restoration. This chapter introduces an enhanced nonlinear telegraph diffusion model in which fractional-order derivatives are incorporated into the diffusivity function to improve image denoising performance. Theoretical analysis is carried out to establish the existence, uniqueness, and boundedness of the weak solution, ensuring a solid foundation for the model. On the numerical side, a semi-implicit AOS scheme is employed for stable and efficient implementation. Extensive experiments demonstrate that the proposed approach outperforms the classical telegraph diffusion method, achieving higher denoising quality and better preservation of image structures. In addition, the study highlights the influence of the fractional order parameter α, showing that its optimal value depends on the noise density, thereby enhancing adaptability and denoising performance.

Finally, the thesis concludes by summarizing the main theoretical and numerical findings and emphasizing their relevance to image denoising applications.

CHAPTER 1

IMAGE PROCESSING: FUNDAMENTALS, DIFFUSION-BASED MODELS, AND MATHEMATICAL BACKGROUND

The objective of this chapter is to lay the groundwork for the theoretical and numerical contributions developed in the subsequent chapters. To this end, the chapter is structured into five main parts. First, we introduce the fundamentals of image processing, including the basic concepts of image restoration and denoising, the main sources and types of noise encountered in digital images, and common image quality assessment metrics. Second, we provide an overview of classical diffusion models in image processing, emphasizing their key features and applications. Third, we present fractional diffusion models, highlighting their main motivations and advantages compared to classical approaches. Fourth, we recall several mathematical preliminaries, including Sobolev spaces, fundamental analytical results, and basic definitions of fractional calculus, which are essential tools for analyzing existence, and uniqueness of weak solutions. Finally, we introduce the finite difference framework that underpins the numerical schemes employed throughout this thesis and serves as the basis for their implementation and analysis.

1.1 Fundamentals of image processing

Digital images play a pivotal role in a wide range of scientific, industrial, and societal applications. From medical diagnostics and satellite imaging to autonomous navigation, the reliability of visual data is crucial for both human interpretation and automated analysis. However, image degradation is almost inevitable during acquisition, transmission, or storage, potentially hindering downstream analysis and decision-making. Consequently, improving image quality has become a central focus in image processing and computer vision.

1.1.1 Image restoration

Image restoration refers to the process of estimating a clean, original image from a corrupted observation, with the aim of enhancing visual quality and enabling reliable interpretation or analysis. The degradation may result from various sources, including motion blur, sensor noise, optical distortions, or partial occlusions. Restoration techniques are therefore essential across a wide range of domains, including:

- **Medical imaging,** where visual clarity is critical for accurate diagnosis.
- **Astronomical imaging,** where faint and distant objects must be reconstructed from noisy measurements.
- **Remote sensing,** where satellite images are affected by atmospheric interference and sensor imperfections.
- **Microscopy,** where fine structural details must be recovered despite physical and optical limitations.

From a mathematical perspective, image restoration is typically formulated as an inverse problem, where the observed image u_0 is modeled as a degraded version of the true image u, through a forward operator $\mathcal{A}$ and an additive noise term η:

$$u_0 = \mathcal{A}(u) + \eta.$$

Such problems are generally ill-posed in the sense of Hadamard [32], lacking existence, uniqueness, or stability of the solution. Consequently, suitable regularization techniques are required to ensure the well-posedness of the reconstruction process. Common restoration problems include denoising, deblurring, inpainting, super-resolution, and decomposition. Each of these tasks poses unique challenges, but they all share the fundamental goal of recovering meaningful structure from incomplete or corrupted data.

1.1.2 Image denoising

Among all image restoration tasks, denoising plays a foundational role, as it addresses one of the most prevalent and fundamental forms of degradation. The objective is to reconstruct a clean image from a corrupted input affected solely by noise. Image denoising is essential not only as a standalone task but also as a critical preprocessing step in various image analysis pipelines, including segmentation, object detection, feature extraction, and image compression.

Despite its apparent simplicity, image denoising remains a challenging and delicate problem. An effective denoising algorithm must suppress noise while preserving essential image structures. Over-smoothing can lead to the loss of textures, edges, and fine details, whereas under-smoothing may leave residual noise that degrades subsequent analysis. This challenge is further compounded by the diversity of noise types, each with distinct statistical properties and degradation patterns, thus necessitating specialized modeling and filtering strategies.

Noise in digital images: Sources and types

In the context of image denoising, understanding the nature and origin of noise is fundamental to designing effective restoration models. Noise refers to any undesired or random fluctuation in pixel intensity values that degrades the visual quality or obscures relevant image content. It typically arises from sensor imperfection, environmental disturbances, quantization errors, or transmission faults during the image acquisition process.

Regardless of its source, noise compromises image quality and reduces the reliability of image-based analysis in critical applications. In medical imaging, for instance, noise may obscure fine anatomical structures and lead to misdiagnoses. In computer vision and machine learning systems, it can degraded the accuracy and robustness of object detection, classification, and recognition tasks.

Accordingly, image noise is commonly categorized into three principle types:

- **Additive noise** is the most extensively studied type of noise and is characterized by its independence from the underlying image content. The most common instance is **additive white Gaussian noise (AWGN)**, where the noise values are sampled from a zero-mean Gaussian distribution with constant variance. AWGN effectively models the cumulative effect of numerous small, independent disturbances and is widely used as a standard approximation for sensor noise in imaging systems such as CCD or CMOS cameras.

- **Impulse noise**, on the other hand, arises from sudden disturbances such as bit errors during transmission or defective sensor elements. A typical example is **salt-and-pepper noise**, in which a certain percentage of pixels is randomly corrupted by replacing their original values with either the minimum (e.g., 0) or the maximum (e.g., 255) intensity levels. This results in sparsely distributed black and white pixels across the image, significantly degrading visual quality, especially in smooth or low-texture regions.

- **Multiplicative noise** differs fundamentally from additive noise in that it depends on the image signal itself, resulting in more complex, signal-dependent degradation. A prominent example is **speckle noise**, commonly observed in coherent imaging modalities such as ultrasound, synthetic aperture radar (SAR), and laser imaging. In these systems, speckle originates from the interference of multiple coherent wavefronts, producing granular noise patterns that degrade structural detail. Mathematically, speckle is often modeled using statistical distributions such as Rayleigh, Gamma, or log-normal, and its multiplicative nature poses significant challenges for image restoration, as conventional linear and additive-based filtering techniques are generally ineffective.

Each type of noise exhibits distinct statistical and structural characteristics, necessitating specialized modeling and denoising strategies tailored to its behavior. Figure 1.1 illustrates representative examples of these three noise types as they appear in corrupted images.

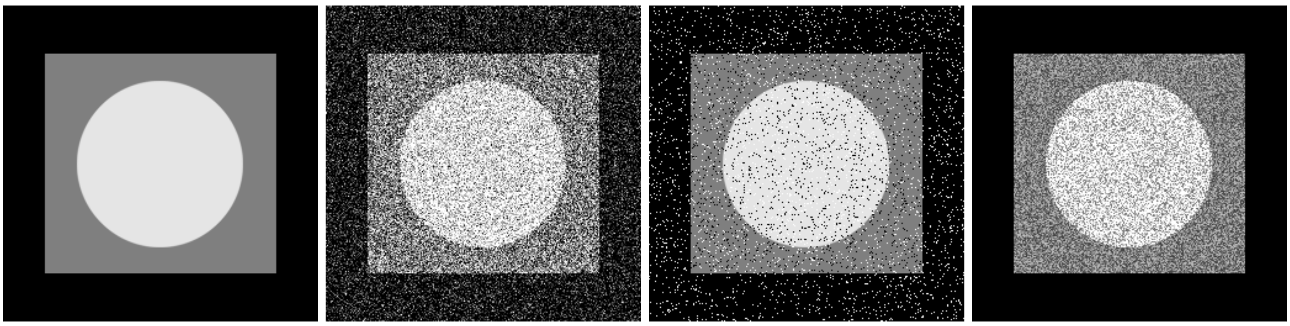

(a) (b) (c) (d)

Figure 1.1: Illustration of common types of noise in digital images. (a) Clean image without noise. (b) Image corrupted by additive white Gaussian noise (AWGN). (c) Image affected by salt-and-pepper impulse noise. (d) Image degraded by multiplicative speckle noise.

1.1.3 Image quality assessment metrics

Evaluating the performance of image denoising algorithms requires appropriate quantitative metrics. These metrics serve two main purposes: enabling comparison between different methods and assisting in the tuning of algorithmic parameters during model development. Among the various available measures, the peak signal-to-noise ratio (PSNR) [51] and the structural similarity index (SSIM) [52] are among the most widely used objective evaluation criteria.

PSNR: Peak signal-to-noise ratio is a signal fidelity metric that compares the pixel-wise difference between the original and restored images. It is defined as:

$$\mathrm{PSNR}(U_0, U) = 10\log_{10}\left(\frac{\max^2}{\frac{1}{MN}\sum_{i=1}^{M}\sum_{j=1}^{N}\left((U_0)_{i,j} - U_{i,j}\right)^2}\right),$$

where U_0 denotes the ground truth image of size $M \times N$, max is the maximum possible pixel value of U_0 (typically 255 for 8-bit images), U denotes the restored image.

Higher PSNR values indicate greater similarity to the ground truth image, and hence, better restoration performance. However, PSNR does not always correlate well with perceived visual quality.

SSIM: To address the perceptual limitations of PSNR, the structural similarity index SSIM metric was introduced to better reflect human visual perception. Instead of comparing absolute pixel differences, SSIM evaluates local patterns of luminance, contrast, and structural similarity between the original and restored images. It is defined as:

$$\mathrm{SSIM}(x, y) = \frac{\left(2\mu_x\mu_y + k_1\right)\left(2\sigma_{xy} + k_2\right)}{\left(\mu_x^2 + \mu_y^2 + k_1\right)\left(\sigma_x^2 + \sigma_y^2 + k_2\right)},$$

where μ_x, μ_y are local means, σ_x^2, σ_y^2 are local variances, and σ_{xy} is the covariance between the local patches x and y. The constants k_1 and k_2 stabilize the division.

The SSIM value ranges from -1 to 1, where value of 1 indicates perfect structural similarity.

1.2 Diffusion models based on PDEs

Partial differential equations (PDEs) are among the most fundamental mathematical tools in image processing and computer vision. They naturally arise in both diffusion-based techniques and as Euler-Lagrange equations derived from variational models. Owing to their versatility and solid theoretical foundation, PDEs have been widely employed in a board range of image processing tasks, particularly image denoising. In what follows, we first review the classical linear isotropic diffusion model and then discuss nonlinear diffusion models.

1.2.1 Linear isotropic diffusion

The linear isotropic diffusion equation, commonly referred to as the heat equation, is one of the oldest and most extensively studied partial differential equations in image processing. Its introduction into the field was motivated by the early work of Koenderink [34], who emphasized its intrinsic connection to Gaussian smoothing, a classical method in signal and image analysis. The equation can be written as:

$$\begin{cases} \dfrac{\partial u}{\partial t} = \Delta u(x,y,t), & \Omega \times (0,T], \\ u(x,y,0) = u_0(x,y), & \Omega. \end{cases} \tag{1.1}$$

The explicit solution of (1.1) is expressed as a convolution with the Gaussian kernel [8, 53]:

$$u(x,y,t) = \begin{cases} u_0(x,y) & t = 0, \\ \left(\mathcal{K}_{\sqrt{2t}} * \tilde{u_0}\right)(x,y) & t > 0, \end{cases} \tag{1.2}$$

where the kernel $\mathcal{K}_{\sqrt{2t}}$ is a two-dimensional Gaussian function, defined as follows:

$$\mathcal{K}_\rho(x,y) = \frac{1}{2\pi\rho^2} e^{\left(-\frac{x^2+y^2}{2\rho^2}\right)}, \quad (x,y) \in \mathbb{R}^2,\ \rho > 0, \tag{1.3}$$

and $\tilde{u_0}$ denotes an extension of u_0 from Ω to $\mathbb{R}^2$.

Convolution with this positive kernel acts as a low-pass filter, effectively suppressing noise while inevitably blurring important image structures such as edges. This drawback compromises the performance of subsequent tasks such as segmentation. To address this issue, nonlinear diffusion filters have been proposed, which adapt to the local image structure and better preserve significant features.

1.2.2 Nonlinear diffusion models

The Perona-Malik model

To overcome the limitations of linear isotropic diffusion, such as excessive blurring and poor edge localization, Perona and Malik introduced a nonlinear diffusion model [39] that adapts to the local image structure. Their method relies on an inhomogeneous diffusion process in which the diffusivity is a function of the image gradient: strong diffusion is applied in regions with small gradient magnitude, while diffusion is reduced near edges, where the gradient is large. The model, known as the Perona-Malik (PM) equation, is expressed as:

$$\begin{cases} \dfrac{\partial u}{\partial t} = \operatorname{div}\left(g\left(|\nabla u|\right)\nabla u\right), & \Omega \times (0,T), \\ u(x,y,0) = u_0(x,y), & \Omega, \end{cases} \tag{1.4}$$

where the diffusion coefficient function g is referred to as the edge-stopping function. It is a non-negative, decreasing function that satisfies:

- $g(s) \to 1$ as $s \to 0$, which ensures a high diffusion rate within homogeneous or interior regions.
- $g(s) \to 0$ as $s \to \infty$, which suppresses diffusion across object boundaries.

As an example, the authors proposed the following definitions:

$$g_1(s) = \frac{1}{1 + (s/k)^2}, \quad g_2(s) = e^{(s/k)^2}, \tag{1.5}$$

here, k denotes the edge threshold parameter that controls the sensitivity of the diffusion process to image gradients. Alternative formulations of the diffusion coefficient can be found in [33, 53, 59].

To illustrates the difference between nonlinear and linear diffusion-based approaches, Figure 1.2 shows the denoising results for a noisy image corrupted by Gaussian noise, where the Perona-Malik model (1.4) is compared with the heat equation (1.1).

(a) (b) (c)

Figure 1.2: Comparison of image denoising results for the local Barbara image. (a) Noisy image corrupted by Gaussian noise. (b) Denoising result using the heat equation (1.1). (c) Denoising result using the PM model (1.4).

The Perona-Malik equation has proven effective in achieving a reasonable balance between noise reduction and edge preservation. However, the model is subject to both theoretical and practical limitations. From a theoretical standpoint, the equation is ill-posed due to the occurrence of forward-backward diffusion induced by edge-stopping functions [53]. In particular, when the squared gradient exceeds a certain threshold, the diffusion becomes backward, leading to instability. On the practical side, the model is highly sensitive to noise: oscillations in the image gradient may generate spurious edges, thereby reducing the effectiveness of adaptive smoothing. Consequently, even very similar images can produce divergent solutions and inconsistent edge representations. To mitigate these drawbacks, modified formulations have been proposed, for instance in [3, 4, 19], to obtain regularized versions of the model.

Regularized Perona-Malik model

To transform the aforementioned model (1.4) into a more stable and well-posed one, adjustments are made by incorporating a Gaussian kernel function (1.3) into the diffusion coefficient. In particular, this approach, proposed by Catte et al. [19], lead to the following model:

$$\begin{cases} \dfrac{\partial u}{\partial t} = \operatorname{div}\left(g\left(\left|\nabla \mathcal{K}_\rho * u\right|\right)\nabla u\right), & \Omega \times (0,T), \\ u(x,y,0) = u_0(x,y), & \Omega. \end{cases} \tag{1.6}$$

Another approach to regularizing the PM equation (1.4) was proposed by Amann [4]. Rather than employing spatial regularization, he suggested introducing regularization in time.

These examples demonstrate that regularization extends beyond merely stabilizing an ill-posed process: it constitutes a form of modeling. When appropriately designed, regularizations can impart the desired characteristics to the resulting filter.

The Weickert model

Despite the advantages of nonlinear isotropic diffusion filters, a notable limitation remains. When the diffusion process is halted near object boundaries, edges are preserved, but noise may still persist in these regions. To overcome this issue, Weickert [53] proposed a modification of the diffusion operator, promoting diffusion along directions parallel to edges while restricting it in the perpendicular direction. In this approach, the image is first smoothed using a Gaussian kernel to reduce the influence of noise. The local gradient information is then analyzed to construct a symmetric, positive semidefinite structure tensor, which captures the predominant orientations and local image structures. The diffusion tensor is subsequently designed to share the same eigenvectors as the structure tensor, with eigenvalues chosen according to the desired filtering objectives. This nonlinear anisotropic diffusion framework effectively smooths homogeneous regions while preserving edges and suppressing noise along object boundaries, providing a robust and adaptive filtering approach.

Figure 1.3 illustrates the different diffusion approaches discussed above, highlighting their respective impacts on noise suppression and edge preservation.

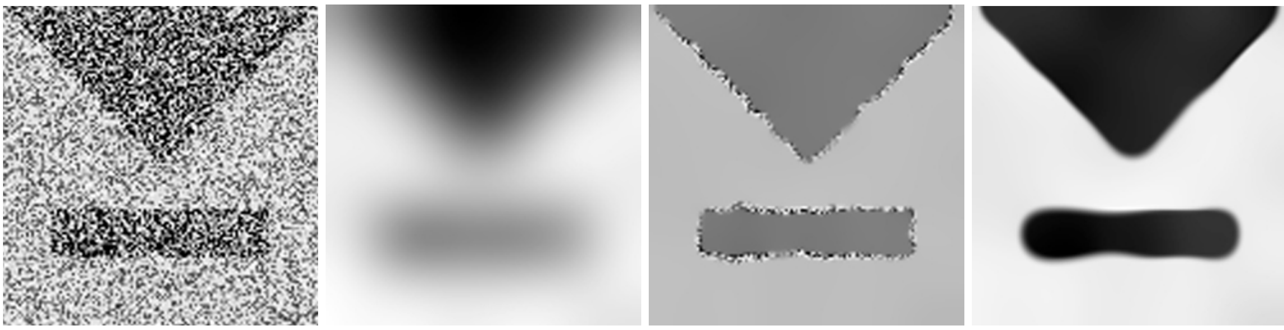

Figure 1.3: Comparison of image restoration capabilities of diffusion filters. (a) Noisy image. (b) Linear isotropic diffusion. (c) Nonlinear isotropic diffusion. (d) Nonlinear anisotropic diffusion.

1.3 Diffusion models based on fractional-order PDEs

Fractional-order partial differential equations (FPDEs) extend classical integer-order PDEs by incorporating derivatives of non-integer order. Unlike integer-order derivatives, fractional derivatives provide enhanced flexibility by capturing long-range interactions and memory effects that classical models cannot. As a result, fractional-order PDEs have attracted significant attention in image processing, particularly for achieving a balance between effective denoising and enhanced edge preservation and texture fidelity. In what follows, we present two representative fractional-order diffusion models for image restoration.

Time-fractional heat equation

Fractional extensions of the heat equation have been investigated to provide better control over the diffusion process in image denoising. Cuesta and Finat [23] observed that the intensity of the diffusion process governed by the linear heat equation can be modulated by introducing a fractional time derivative of order $1 < \alpha < 2$; as $\alpha \to 2$, the diffusion intensity becomes weaker than that of the classical linear heat equation (1.1). Accordingly, they proposed to regulate the diffusion process of the linear heat equation by selecting the order of the fractional time derivative in the corresponding equation as follows:

$$\begin{cases} \dfrac{\partial^\alpha u}{\partial t^\alpha} = \Delta u(x, y, t), & \Omega \times (0, T], \\ u(x, y, 0) = u_0(x, y), & \Omega, \end{cases} \tag{1.7}$$

where $\dfrac{\partial^\alpha u}{\partial t^\alpha}$ denotes the fractional time derivative of order $1 < \alpha < 2$ in the Riemann-Liouville sense [35]. Since the equation (1.7) provides an interpolation between a linear parabolic equation and a linear hyperbolic equation [27, 28], its solution exhibits intermediate characteristics.

Figure1.4 illustrates the denoising performance of the Perona-Malik model (1.4) and the Time-fractional heat equation (1.7) on a textured image corrupted by Gaussian noise.

(a) (b) (c) (d)

Figure 1.4: Comparison of denoising methods on a textured image. (a) Original image. (b) Noisy image. (c) Denoised image using the PM model (1.4). (d) Denoised image using the Time-fractional heat equation (1.7).

Fractional-order nonlinear diffusion model

Anisotropic diffusion models are formulated through energy minimization principles, where the choice of the underlying energy functional determines the nature of the diffusion process. To overcome the speckle effect and other undesirable artifacts arising in the Perona-Malik model and related approaches [20, 22], Bai and Feng [9] proposed a modification of the Perona-Malik energy functional by incorporating the fractional derivative of the image intensity, defined in the Fourier domain. The corresponding Euler-Lagrange equation yields the fractional-order anisotropic diffusion process, expressed as:

$$\frac{\partial u}{\partial t} = -\mathcal{D}_x^{\alpha *}\left(g\left(|\mathcal{D}^\alpha u|\right)\mathcal{D}_x^\alpha u\right) - \mathcal{D}_y^{\alpha *}\left(g\left(|\mathcal{D}^\alpha u|\right)\mathcal{D}_y^\alpha u\right), \tag{1.8}$$

where, $\mathcal{D}_x^{\alpha *}$ is the adjoint of $\mathcal{D}_x^\alpha$, $\mathcal{D}_y^{\alpha *}$ is the adjoint of $\mathcal{D}_y^\alpha$, and $|\mathcal{D}^\alpha|$ denotes the magnitude of the fractional gradient operator defined by: $|\mathcal{D}^\alpha u| = \sqrt{(\mathcal{D}_x^\alpha u)^2 + (\mathcal{D}_y^\alpha u)^2}$.

The proposed equation (1.8) provides an interpolation between the classical Perona-Malik equation (1.4) and the fourth-order anisotropic diffusion equations presented in [45].

To investigate the influence of the fractional order, Figure 1.5 presents the denoising results for the noisy Boat image obtained by applying the equation (1.8) with three different values of α, which allows a visual comparison of how the choice of α influences the restoration quality.


(a)


(b)


(c)


(d)


(e)

Figure 1.5: Denoising results of the noisy Boat image using fractional-order nonlinear diffusion equation (1.8). (a) original image. (b) Noisy image corrupted by additive white Gaussian noise. (c) For $\alpha = 1.2$. (d) For $\alpha = 1.6$. (e) For $\alpha = 2$.

1.4 Analytical tools and concepts

1.4.1 Functional Spaces

For any Banach space F, $L^p(0,T;F)$ represents the normed space consisting of all functions $v : [0,T] \to F$ that satisfy:

$$||v||_{L^p(0,T;F)} = \left(\int_0^T ||v||_F^p \, dt \right)^{\frac{1}{p}}, \quad 1 \leq p < \infty,$$

and

$$||v||_{L^\infty(0,T;F)} = \operatorname*{ess\,sup}_{0 \leq t \leq T} ||v||_F, \quad p = \infty.$$

Sobolev space

Let Ω be an open, bounded subset of $\mathbb{R}^n$. For $r \in \mathbb{N}$, the Hilbert space $\mathcal{H}^r(\Omega)$ is defined as the space of all functions in $L^2(\Omega)$ whose partial derivatives, in the distributional sense, of all orders up to r also belong to $L^2(\Omega)$. This space is equipped with the norm:

$$\|v\|_{\mathcal{H}^r(\Omega)} = \left(\sum_{|m|\leq r} \|D^m v\|^2_{L^2(\Omega)} \right)^{\frac{1}{2}}.$$

The dual space of $\mathcal{H}^1(\Omega)$, denoted by $\left(\mathcal{H}^1(\Omega)\right)'$, is endowed with the norm defined as follows:

$$\|v\|_{\left(\mathcal{H}^1(\Omega)\right)'} = \left\{ \sup \langle v, u\rangle : u \in \mathcal{H}^1(\Omega), \|u\|_{\mathcal{H}^1(\Omega)} \leq 1 \right\}.$$

Fractional-order Sobolev space

The fractional-order Sobolev space is defined as follows [1], [16]. Let Ω be an open bounded subset of $\mathbb{R}^n$. We define the fractional-order Sobolev space $\mathcal{W}^{\alpha,p}$ for each $\alpha > 0$, where $\alpha = m + s$, with m being the integer part of α and $0 < s < 1$, and $1 \leq p < \infty$, as follows:

$$\mathcal{W}^{\alpha,p}(\Omega) = \left\{ u \in \mathcal{W}^{m,p}(\Omega), \frac{\left|D^\mu u(x) - D^\mu u(y)\right|}{\left|x-y\right|^{n+ps}} \in L^p(\Omega \times \Omega), \left|\mu\right| = m \right\},$$

equipped with the norm:

$$\|u\|_{\mathcal{W}^{\alpha,p}(\Omega)} = \left(\|u\|^p_{\mathcal{W}^{m,p}(\Omega)} + \sum_{|\mu|=m} \int_\Omega \int_\Omega \frac{\left|D^\mu u(x) - D^\mu u(y)\right|^p}{\left|x-y\right|^{n+ps}} dx\, dy \right)^{\frac{1}{p}}.$$

In the case $p = 2$, we write $\mathcal{H}^\alpha(\Omega) = \mathcal{W}^{\alpha,2}(\Omega)$, with its norm:

$$\|u\|_{\mathcal{H}^\alpha(\Omega)} = \left(\|u\|^2_{\mathcal{H}^m(\Omega)} + \sum_{|\mu|=m} \int_\Omega \int_\Omega \frac{\left|D^\mu u(x) - D^\mu u(y)\right|^2}{\left|x-y\right|^{n+2s}} dx\, dy \right)^{\frac{1}{2}}.$$

Denote the dual of $\mathcal{H}^\alpha(\Omega)$ by $(\mathcal{H}^\alpha(\Omega))'$, and define its norm:

$$\|u\|_{(\mathcal{H}^\alpha(\Omega))'} = \left\{ \sup \langle u, v\rangle : v \in \mathcal{H}^\alpha(\Omega), \|v\|_{\mathcal{H}^\alpha(\Omega)} \leq 1 \right\}.$$

1.4.2 Fractional calculus

Euler Gamma function

The Euler Gamma function, denoted by $\Gamma(\alpha)$, is one of the fundamental functions in fractional calculus. It provides a continuous extension of the factorial function to real and complex arguments and plays an important role in defining fractional integrals and derivatives.

Definition 1.1. [35]. The Euler Gamma function is defined for all complex numbers α with a positive real part by the integral:

$$\Gamma(\alpha) = \int_0^{\infty} x^{\alpha-1} e^{-x} dx, \quad \Re(\alpha) > 0. \tag{1.9}$$

By applying integrating by parts, one obtains the following basic property of the Gamma function:

$$\Gamma(1+\alpha) = \alpha\,\Gamma(\alpha), \quad \Re(\alpha) > 0. \tag{1.10}$$

Riemann-Liouville fractional integral

Definition 1.2. (Left Riemann-Liouville fractional integral) [35].

The Left Riemann-Liouville fractional integral of order $\alpha > 0$ of an integrable function $u : [0, \nu] \to \mathbb{R}$ with $\nu > 0$, is defined by:

$${}_0\mathcal{I}_y^{\alpha} u(y) = \frac{1}{\Gamma(\alpha)} \int_0^y (y-\delta)^{\alpha-1}\, u(\delta)\, d\delta, \quad y > 0, \tag{1.11}$$

$\Gamma(\alpha)$ denotes Euler's continuous Gamma function (1.9).

Caputo-type fractional derivative

Definition 1.3. (Left Caputo fractional derivative) [35].

The left Caputo fractional derivative of order $\alpha > 0$ of a function $v : [0, \nu] \to \mathbb{R}$, with $\nu > 0$, is defined by:

$${}^{C}\mathcal{D}_y^{\alpha} u(y) = {}_0\mathcal{I}_y^{n-\alpha} \frac{d^n}{dy^n} u(y) = \frac{1}{\Gamma(n-\alpha)} \int_0^y (y-\delta)^{n-\alpha-1} \frac{d^n u(\delta)}{d\delta^n}\, d\delta, \;\; n-1 < \alpha < n \in \mathbb{N}. \tag{1.12}$$

Caputo-Fabrizio-type fractional derivative

Definition 1.4. (Caputo-Fabrizio fractional derivative) [18].

The Caputo-Fabrizio fractional derivative of order $\alpha > 0$ for a function $u \in \mathcal{H}^1(a, b)$, where $b > a$, is defined as follows:

$${}^{CF}\mathcal{D}_x^{\alpha} u(x) = \frac{M(\alpha)}{1-\alpha} \int_0^x e^{-\left(\frac{\alpha}{1-\alpha}\right)(x-\eta)} \frac{du(\eta)}{d\eta}\, d\eta, \;\; 0 < \alpha < 1, \tag{1.13}$$

where $M(\alpha)$ is a normalization function, which is typically set as $M(\alpha) = 1$.

1.4.3 Useful inequalities

In this subsection, we recall some inequalities that will be used in the subsequent chapters.

Young's inequality [10]. Let $1 \leq p, q \leq \infty$ and $\frac{1}{p} + \frac{1}{q} = 1$. Then:

$$ab \leq \frac{a^p}{p} + \frac{b^q}{q}, \quad a, b \in \mathbb{R}^+. \tag{1.14}$$

Lemma 1.1. *[2]. If $1 \leq p \leq \infty$ and $r, d \geq 0$, thus:*

$$(r+d)^p \leq 2^{p-1}\left(r^p + d^p\right). \tag{1.15}$$

Lemma 1.2. *(Gronwall [30]). Let $\mathcal{J}$ represent an interval on the real line. For $\zeta(s)$ and $\theta(s)$ be continuous and non negative functions on $\mathcal{J}$, there is the inequality:*

$$\theta(s) \leq \mu + \int_0^s \zeta(z)\theta(z)dz,\ s \in \mathcal{J}, \tag{1.16}$$

where μ is a positive constant, consequently

$$\theta(s) \leq \mu\, e^{\left(\int_0^s \zeta(z)dz\right)},\ s \in \mathcal{J}. \tag{1.17}$$

1.4.4 Fixed point theorem

Theorem 1.1. *(Schauder's fixed point [26]). Let Y be a real Banach space and $Q \subset Y$ is a compact and convex, and assume also*

$$F : Q \to Q,$$

is continuous. Then, F has a fixed point in Q.

1.5 Numerical schemes for partial differential equations

Partial differential equation (PDE) models constitute a fundamental framework in image processing, particularly for tasks such as image denoising and restoration. These models describe the continuous evolution of image intensity over an artificial time variable, governed by diffusion or variational principles designed to remove noise while preserving significant image structures such as edges and textures. As analytical solutions are seldom attainable and digital images are inherently defined on discrete grids, numerical schemes are essential for approximating the solutions of these PDEs.

This section delineates the fundamental concepts of spatial and temporal discretization, followed by the formulation of explicit, implicit, and semi-implicit finite difference schemes. Particular emphasis is placed on the Additive Operator Splitting (AOS) technique, renowned for its computational efficiency and stability in tackling multi-dimensional image restoration problems. The numerical schemes discussed herein form the computational foundation for a wide range of PDE-based image processing algorithms.

1.5.1 Spatial and temporal discretization

The image domain is discretized into a uniform grid with spatial step sizes Δx and Δy, and the temporal domain is discretized with a time step Δt. Each grid point (i, j) corresponds to a pixel, and the continuous intensity function $u(x, y, t)$ is approximated by $u^n_{i,j}$, representing the discretized intensity at pixel (i, j) and iteration n.

Spatial derivatives are approximated using finite difference formulas. For instance, the first-order partial derivatives can be discretized using forward, backward, or central difference approximations as follows:

$$\left(\frac{\partial u}{\partial x}\right)^n_{i,j} = \begin{cases} \dfrac{u^n_{i+1,j} - u^n_{i,j}}{\Delta x} + O\left(\Delta x\right), & \text{(forward difference)}, \\ \dfrac{u^n_{i,j} - u^n_{i-1,j}}{\Delta x} + O\left(\Delta x\right), & \text{(backward difference)}, \\ \dfrac{u^n_{i+1,j} - u^n_{i-1,j}}{2\Delta x} + O\left(\Delta x^2\right), & \text{(central difference)}. \end{cases}$$

Similarly, the second-order partial derivatives are usually approximated by the central difference formula:

$$\left(\frac{\partial^2 u}{\partial x^2}\right)^n_{i,j} = \frac{u^n_{i+1,j} - 2u^n_{i,j} + u^n_{i-1,j}}{(\Delta x)^2} + O\left(\Delta x^2\right).$$

Temporal derivatives can also be approximated using different finite difference schemes, depending on the desired accuracy and stability properties. For the first-order time derivative, the most common approaches are the forward, backward, and central differences, expressed as follows:

$$\left(\frac{\partial u}{\partial t}\right)^n_{i,j} = \begin{cases} \dfrac{u^{n+1}_{i,j} - u^n_{i,j}}{\Delta t} + O\left(\Delta t\right), & \text{(forward Euler)}, \\ \dfrac{u^n_{i,j} - u^{n-1}_{i,j}}{\Delta t} + O\left(\Delta t\right), & \text{(backward Euler)}, \\ \dfrac{u^{n+1}_{i,j} - u^{n-1}_{i,j}}{2\Delta t} + O\left(\Delta t^2\right), & \text{(central difference)}. \end{cases}$$

For the second-order time derivative, a standard central difference formula is given by:

$$\left(\frac{\partial^2 u}{\partial t^2}\right)_{i,j}^n = \frac{u_{i,j}^{n+1} - 2u_{i,j}^n + u_{i,j}^{n-1}}{(\Delta t)^2} + O\left(\Delta t^2\right).$$

1.5.2 Explicit finite difference schemes

In explicit finite difference schemes, the image state at the next time iteration u^{n+1} is computed directly from the known values at the current iteration u^n. These schemes are straightforward to implement and offer intuitive control over the diffusion process.

Explicit schemes are widely used in nonlinear diffusion and total variation models [39, 44]. However, a significant drawback is their conditional stability, often requiring a restrictive bound on the time step Δt (e.g., the Courant-Friedrichs-Lewy (CFL) condition) to prevent numerical instability. This limitation can lead to high computational costs when simulating long evolution times or processing high-resolution images.

1.5.3 Implicit finite difference schemes

Implicit schemes compute the new image state u^{n+1} by solving a system of algebraic equations that couples the unknown intensities at time $n+1$. This approach leads to a nonlinear system of equations, Since the diffusion coefficient in nonlinear diffusion models depends on the updated image u^{n+1}. Such nonlinear systems are typically solved through iterative procedures, such as Newton method, until convergence is achieved. The primary advantage of implicit methods lies in their unconditional stability for a wide class of diffusion processes. This property allows for significantly larger time steps compared to explicit schemes, thereby reducing the overall computational time required to reach a steady-state solution.

1.5.4 Semi-implicit schemes and the additive operator splitting (AOS) technique

Semi-implicit schemes combine the desirable properties of explicit and implicit methods. Typically, linear or stiff components of the PDE are treated implicitly to ensure stability, while nonlinear or data-driven terms are handled explicitly to reduce computational complexity. In practical implementations, the diffusion coefficients in nonlinear diffusion models are usually evaluated at the previous time level to avoid solving a nonlinear system at each iteration, thereby yielding a linear system that can be efficiently solved. Semi-implicit schemes are particularly suitable for one-dimensional problems, where the computational cost of solving the resulting linear system remains moderate. However, in higher-dimensional cases, the associated system matrices become considerably larger and more complex to handle, leading to significant computational challenges.

Applying direct algorithms such as Gaussian elimination would destroy the sparsity pattern and result in excessive storage requirements and computational effort. Therefore, iterative algorithms are typically employed. Classical iterative methods such as Gauss-Seidel do not require additional storage, and their convergence can be guaranteed due to the favorable properties of these matrices. Nonetheless, convergence tends to be slow, and the rate further deteriorates for larger image sizes, as the condition number of the system matrix increases. Consequently, although the semi-implicit scheme is unconditionally stable, it is often not significantly faster than the explicit scheme in practical applications.

To overcome these limitations, the additive operator splitting (AOS) technique [54] provides an efficient semi-implicit alternative for multidimensional diffusion processes. The key idea of AOS is to decompose a multidimensional diffusion operator into a sum of one-dimensional operators, each of which can be solved independently and implicitly. This decomposition substantially reduces computational complexity and enables efficient parallel implementation while maintaining unconditional stability even for nonlinear diffusion models.

In the context of image restoration and denoising, AOS schemes provides an efficient numerical framework for solving nonlinear diffusion equations that underlie various PDE-based models. From a computational perspective, AOS methods require solving only tri-diagonal linear systems along each spatial direction, which significantly reduces computational cost compared to solving fully coupled multidimensional systems. Owing to their stability and efficiency, AOS schemes have become a standard choice for implementing nonlinear diffusion processes in image processing.

1.5.5 Comparison of numerical schemes

A comparative summary of the main characteristics of the discussed numerical schemes is presented below:

- **Explicit schemes:** These methods are straightforward to implement and computationally inexpensive per time step. However, they are subject to strict stability constraints on the time step size, which can make them inefficient for problems requiring long evolution times or high spatial resolution.

- **Implicit schemes:** These approaches offer unconditional stability for a broad class of problems, allowing the use of larger time steps. Their main disadvantage lies in the increased computational cost due to the need to solve a coupled system of equations at each iteration, which may become demanding for large-scale image data.

- **Semi-implicit and AOS schemes:** These methods provide a compromise between explicit and implicit approaches. They combine the simplicity of explicit treatments for nonlinear terms with the stability of implicit treatments for linear diffusive terms. The Additive Operator Splitting (AOS) technique, in particular, offers a highly efficient and unconditionally stable framework for multidimensional problems by decomposing them into a series of one-dimensional subproblems.

The choice of the numerical scheme thus represents a trade-off between stability, computational efficiency, and algorithmic complexity, depending on the specific characteristics and objectives of the image restoration task.

Remark 1.1. ***(Stability analysis)***
Stability is a fundamental requirement in the numerical solution of time-dependent partial differential equations, as it ensures that small perturbations in the initial data or numerical errors do not grow uncontrollably during the iterative process. A stable numerical scheme produces bounded solutions as the number of time steps increases, whereas instability leads to divergence or nonphysical oscillations in the computed results.

Although a detailed stability analysis is not presented in this thesis, the numerical schemes employed in the following chapters are designed to ensure stable and reliable behavior throughout the evolution process.

CHAPTER 2

FRACTIONAL GRADIENT-BASED NONLINEAR DIFFUSION MODEL FOR IMAGE DENOISING

The results presented in this chapter are based on the findings reported in [13].

2.1 Introduction

In this chapter, we propose a model that integrates the nonlinear diffusion equation with a fractional gradient in the diffusion coefficient, where the fractional gradient is defined using the Caputo-Fabrizio fractional derivative. This approach extends the ROF model [44] by incorporating fractional derivatives to enhance denoising performance. The Caputo-Fabrizio operator exhibits a nonlocal behavior; unlike classical derivatives, it depends on the global behavior of the function rather than solely on local values, which enables improved preservation of image features. As a result, the proposed model plays a significant role in maintaining edges and structural details while effectively reducing noise. Additionally, the integration of a Gaussian kernel into the diffusion coefficient contributes to the well-posedness of the model.

Since explicit finite difference schemes are subject to stringent stability constraints that require very small time steps-thereby limiting their practical utility-we employ a semi-implicit numerical scheme based on additive operator splitting (AOS), as originally introduced by Weickert [54], to improve computational efficiency.

To justify the selection of the Caputo-Fabrizio operator, we carried out a comparative study with the Caputo derivative using the same model formulation. While both variants yield comparable denoising results, the Caputo-Fabrizio-based model exhibits significantly faster convergence, requiring fewer iterations and shorter computational time. This advantage makes it particularly suitable for practical image processing tasks that demand both accuracy and efficiency.

Furthermore, we compared our proposed model with the classical ROF model [44]. The numerical results demonstrate that our approach offers improved denoising performance, especially in preserving fine details and sharp edges, which are often blurred or lost in the ROF solution due to its reliance on local regularization. The use of a fractional gradient provides a more effective balance between noise suppression and detail retention.

The structure of this chapter is as follows. Section 2.2 introduces the preliminaries, including fundamental definitions and key theoretical results. In section 2.3, we propose our model and its motivation. In section 2.4 we investigate the existence and uniqueness of the weak solution to the proposed model. Section 2.5 describes the numerical scheme used to solve the model. Section 2.6 presents the experimental results, which evaluate the model's performance. Finally, section 2.7 provides the conclusions of this chapter.

2.2 Preliminaries

The fractional gradient of $\mathcal{K}_\rho$ of order α is given by the following definition:

$$\nabla^\alpha \mathcal{K}_\rho(x,y) = \left({}^{CF}\mathcal{D}_x^\alpha \mathcal{K}_\rho(x,y), {}^{CF}\mathcal{D}_y^\alpha \mathcal{K}_\rho(x,y)\right),$$

where ${}^{CF}\mathcal{D}_x^\alpha \mathcal{K}_\rho(x,y)$ represents the fractional derivative of order α of $\mathcal{K}_\rho(x,y)$ in terms of the variable x, and ${}^{CF}\mathcal{D}_y^\alpha \mathcal{K}_\rho(x,y)$ represents the fractional derivative of order α of $\mathcal{K}_\rho(x,y)$ in terms of the variable y.

From(1.13), we get:

$${}^{CF}\mathcal{D}_x^\alpha \mathcal{K}_\rho(x,y) = \frac{1}{(1-\alpha)} \int_0^x e^{-\left(\frac{\alpha}{1-\alpha}\right)(x-\eta)} \frac{\partial \mathcal{K}_\rho(\eta,y)}{\partial \eta}\, d\eta, \quad 0 < \alpha < 1,$$

which is equivalent to:

$${}^{CF}\mathcal{D}_x^\alpha \mathcal{K}_\rho(x,y) = \frac{1}{(1-\alpha)} \left(\mathcal{K}_\rho(x,y) - e^{-\left(\frac{\alpha}{1-\alpha}\right)x} \mathcal{K}_\rho(0,y)\right) - \frac{\alpha}{(1-\alpha)^2} \int_0^x e^{-\left(\frac{\alpha}{1-\alpha}\right)(x-\eta)} \mathcal{K}_\rho(\eta,y)\, d\eta,$$

and, we have:

$$\begin{aligned}
{}^{CF}\mathcal{D}_y^\alpha \mathcal{K}_\rho(x,y) &= \frac{1}{(1-\alpha)} \int_0^y e^{-\left(\frac{\alpha}{1-\alpha}\right)(y-\eta)} \frac{\partial \mathcal{K}_\rho(x,\eta)}{\partial \eta}\, d\eta, \quad 0 < \alpha < 1 \\
&= \frac{1}{(1-\alpha)} \left(\mathcal{K}_\rho(x,y) - e^{-\left(\frac{\alpha}{1-\alpha}\right)y} \mathcal{K}_\rho(x,0)\right) - \frac{\alpha}{(1-\alpha)^2} \int_0^y e^{-\left(\frac{\alpha}{1-\alpha}\right)(y-\eta)} \mathcal{K}_\rho(x,\eta)\, d\eta,
\end{aligned}$$

Claim 2.1. *Let $\Omega \subset \mathbb{R}^2$, $\upsilon \in L^2(\Omega)$, and $\mu \in L^2(\Omega)$ then there is a constant C_ρ such that*

$$\left\|\nabla^\alpha \upsilon_\rho\right\|_{L^\infty(\Omega)} \leq C_\rho \left\|\upsilon\right\|_{L^2(\Omega)}. \tag{2.1}$$

Additionally, there exists a constant ψ, where

$$\left\|\hbar(\left|\nabla^\alpha \mu_\rho\right|) - \hbar(\left|\nabla^\alpha \upsilon_\rho\right|)\right\|_{L^\infty(\Omega)} \leq \psi \left\|\mu - \upsilon\right\|_{L^2(\Omega)}, \tag{2.2}$$

where $\hbar$ is a non-negative, smooth, Lipschitz, and decreasing function.

Proof. By convolution property, we have

$$\begin{aligned}\left|\nabla^\alpha \upsilon_\rho\right| &\leq \left|(\nabla^\alpha \mathcal{K}_\rho) * \upsilon\right| \\ &\leq C_\rho \left\|\upsilon\right\|_{L^2(\Omega)}.\end{aligned}$$

Furthermore, since $\hbar$ and $\nabla^\alpha \mu_\rho$ are C^∞, it follows that $\hbar(\left|\nabla^\alpha \mu_\rho\right|)$ is C^∞. Indeed, we have:

$$\begin{aligned}\left\|\hbar(\left|\nabla^\alpha \mu_\rho\right|) - \hbar(\left|\nabla^\alpha \upsilon_\rho\right|)\right\|_{L^\infty(\Omega)} &\leq C \left\|\left|\nabla^\alpha \mu_\rho\right| - \left|\nabla^\alpha \upsilon_\rho\right|\right\|_{L^\infty(\Omega)} \\ &\leq C \left\|\left|(\nabla^\alpha \mathcal{K}_\rho) * \mu\right| - \left|(\nabla^\alpha \mathcal{K}_\rho) * \upsilon\right|\right\|_{L^\infty(\Omega)} \\ &\leq C \left\|\left|(\nabla^\alpha \mathcal{K}_\rho) * \mu - (\nabla^\alpha \mathcal{K}_\rho) * \upsilon\right|\right\|_{L^\infty(\Omega)} \\ &= C \left\|\left|(\nabla^\alpha \mathcal{K}_\rho) * (\mu - \upsilon)\right|\right\|_{L^\infty(\Omega)} \\ &\leq C\, C_\rho \left\|\mu - \upsilon\right\|_{L^2(\Omega)} \\ &= \psi \left\|\mu - \upsilon\right\|_{L^2(\Omega)},\end{aligned}$$

where $\psi = CC_\rho$.

This completes the proof of the claim. □

2.3 The proposed model and its motivation

Diffusion-based methods in image processing are fundamentally influenced by principles from the calculus of variations [8]. These methods generally rely on an energy functional that balances two competing objectives: a data fidelity component, which ensures that the restored image remains close to the observed data, and a regularization component, which imposes smoothness. One of the earliest variational models for denoising images corrupted by additive noise was introduced by Rudin, Osher, and Fatemi, and is commonly referred to as the ROF model [44]. In this model, image denoising is achieved by minimizing the following energy functional:

$$E(u) = \int_\Omega |\nabla u| \, dx \, dy + \frac{\gamma}{2} \int_\Omega (u - u_0)^2 dx \, dy,$$

where the first term corresponds to the regularization component, and the second represents the fidelity to the observed image u_0. The parameter $\gamma > 0$ controls the trade-off between regularity and data adherence. The Euler-Lagrange equation associated with this functional is given by:

$$-\operatorname{div}\left(\frac{\nabla u}{|\nabla u|}\right) + \gamma (u - u_0) = 0 \qquad \text{in } \Omega. \tag{2.3}$$

Using the gradient projection method [41], equation (2.3) leads to the time-dependent evolution equation:

$$\frac{\partial u}{\partial t} = \operatorname{div}\left(\frac{\nabla u}{|\nabla u|}\right) + \gamma (u_0 - u) \qquad \text{in } \Omega \times (0, T),$$

Due to the nonlocal nature of the fractional-order derivative operator, it becomes necessary to develop a new mathematical framework capable of addressing both additive and multiplicative noise in image restoration. In this work, we propose a novel model based on a nonlinear diffusion equation, in which the diffusion coefficient depends on a fractional gradient defined in terms of the Caputo-Fabrizio fractional derivative. This formulation generalizes the classical ROF model by incorporating fractional order derivatives to improve noise removal while preserving essential image features. By exploiting the intrinsic properties of the fractional operator, including memory effects and nonlocal interactions, the model effectively preserves edge sharpness and structural details. Furthermore, the inclusion of a Gaussian kernel within the diffusion coefficient enhances the well-posedness, and robustness of the denoising process.

Our model is given by:

$$\frac{\partial u}{\partial t} = \operatorname{div}\left(\hbar\left(\left|\nabla^\alpha u_\rho\right|\right) \nabla u\right) + \gamma (u_0 - u), \qquad \text{in } \Omega \times (0, T), \tag{2.4}$$

$$u(x, y, 0) = u_0(x, y), \qquad \text{in } \Omega, \tag{2.5}$$

$$\nabla u . \vec{n} = 0, \qquad \text{on } \partial\Omega \times (0, T), \tag{2.6}$$

where:

- Ω is a bounded domain of $\mathbb{R}^2$, and u_0 is the original image.

- $0<\alpha<1$, $\gamma>0$, and $u_\rho=\mathcal{K}_\rho * u$. $\vec{n}$ denote the unit outward normal to $\partial\Omega$.

- ∇ (respectively. div(.)) denotes the gradient (respectively divergence) operator, and $\left|\nabla^\alpha u_\rho\right| = \sqrt{\left|{}^{CF}\mathcal{D}_x^\alpha u_\rho\right|^2+\left|{}^{CF}\mathcal{D}_y^\alpha u_\rho\right|^2}$.

- $\hbar$ is a positive, smooth, Lipschitz, decreasing function and satisfies the following assumption:

$$\hbar(0)=1,\quad \lim_{s\to+\infty}\hbar(s)=0. \tag{2.7}$$

2.4 Theoretical analysis

In this section, we establish the existence and uniqueness of the weak solution to the proposed model (2.4)-(2.6). Since the problem (2.4)-(2.6) is nonlinear, we start by considering the linearized problem, and then we apply Schauder's fixed point theorem to prove the existence of a weak solution. We introduce the space:

$$W(0,T)=\left\{w\in L^2(0,T;\mathcal{H}^1(\Omega)), \frac{dw}{dt}\in L^2\left(0,T;(\mathcal{H}^1(\Omega))'\right)\right\}.$$

Evidently, $W(0,T)$ is a Hilbert space with the norm:

$$||w||_W=||w||_{L^2(0,T;\mathcal{H}^1(\Omega))}+\left\|\frac{\partial w}{\partial t}\right\|_{L^2\left(0,T;(\mathcal{H}^1(\Omega))'\right)}.$$

Definition 2.1. A function $u\in W(0,T)$ is said to be a weak solution of (2.4)-(2.6) if it satisfies the following relation:

$$\left\langle\frac{\partial u}{\partial t},\varphi\right\rangle+\int_\Omega \hbar\left(\left|\nabla^\alpha u_\rho\right|\right)\nabla u.\nabla\varphi\,dx\,dy=\gamma\int_\Omega(u_0-u)\,\varphi\,dx\,dy,$$

$$u(x,y,0)=u_0(x,y),\quad \text{in}\,\Omega,$$

for almost every $t\in(0,T)$ and for all $\varphi\in\mathcal{H}^1(\Omega)$.

In the follows, we assume that the initial value $u_0\in\mathcal{H}^1(\Omega)$ fulfills:

$$0<m:=\text{ess}\inf_{x,y\in\Omega}\ u_0(x,y)\ \text{and}\ S:=\text{ess}\sup_{x,y\in\Omega}\ u_0(x,y)<\infty. \tag{2.8}$$

2.4.1 The linearized problem

We define the following space:

$$\Psi = \left\{ \quad w \in W(0,T) \cap L^{\infty}(0,T;L^2(\Omega)) : m \leq w(x,y,t) \leq S, \text{ a.e in } \Omega \times (0,T) \right\}.$$

For any $w \in \Psi$ such that

$$\|w\|_{L^{\infty}(0,T;L^2(\Omega))} \leq \|u_0\|_{L^2(\Omega)}, \tag{2.9}$$

and

$$\left\|\frac{\partial w}{\partial t}\right\|_{L^2(0,T;L^2(\Omega))} \leq \|u_0\|_{\mathcal{H}^1(\Omega)}, \tag{2.10}$$

we formulate the linearized problem as follows:

$$\frac{\partial u_w}{\partial t} = \operatorname{div}\left(\hbar\left(\left|\nabla^{\alpha} w_\rho\right|\right)\nabla u_w\right) + \gamma\left(u_0 - u_w\right), \qquad \text{in } \Omega \times (0,T), \tag{2.11}$$

$$u_w(x,y,0) = u_0(x,y), \qquad \text{in } \Omega, \tag{2.12}$$

$$\nabla u_w.\vec{n} = 0, \qquad \text{on } \partial\Omega \times (0,T). \tag{2.13}$$

Lemma 2.1. *The following inequalities hold:*

$$\xi \leq \hbar\left(\left|\nabla^{\alpha} w_\rho\right|\right) \leq 1, \tag{2.14}$$

$$\left|\frac{\partial \hbar\left(\left|\nabla^{\alpha} w_\rho\right|\right)}{\partial t}\right| \leq \theta, \tag{2.15}$$

where the positive constant ξ, and θ depend only on $\mathcal{K}_\rho$ and u_0.

Proof. Let $w \in \Psi$. Then we have:

$$\begin{aligned}\left|\nabla^{\alpha} w_\rho\right| &\leq C_\rho \|w\|_{L^2(\Omega)} \\ &\leq C_\rho C \|u_0\|_{\mathcal{H}^1(\Omega)}.\end{aligned}$$

Since $\hbar$ is decreasing, positive, and satisfies (2.7), it follows that

$$\xi \leq \hbar\left(\left|\nabla^{\alpha} w_\rho\right|\right) \leq 1, \text{for } \xi = \hbar\left(C_\rho C \|u_0\|_{\mathcal{H}^1(\Omega)}\right).$$

To verify inequality (2.15), we note that:

$$\begin{aligned}
\left|\frac{\partial \hbar\left(\left|\nabla^{\alpha} w_{\rho}\right|\right)}{\partial t}\right| &= \left|\hbar'\left(\left|\nabla^{\alpha} w_{\rho}\right|\right) \frac{\partial}{\partial t}(\left|\nabla^{\alpha} w_{\rho}\right|)\right| \\
&\leq \left|\hbar'\left(\left|\nabla^{\alpha} w_{\rho}\right|\right)\right| \left|\nabla^{\alpha} \mathcal{K}_{\rho} * \frac{\partial w}{\partial t}\right| \\
&\leq C C_{\rho} \left\|\frac{\partial w}{\partial t}\right\|_{L^2(\Omega)} \\
&\leq C C_{\rho} \left\|u_0\right\|_{\mathcal{H}^1(\Omega)} \\
&= \theta.
\end{aligned}$$

This completes the proof of Lemma. □

By using Lemma 2.1, we can apply the classical Galerkin method [26] to prove that the linearized problem (2.11)-(2.13) has a unique weak solution $u_w \in W(0,T)$.

Lemma 2.2. *Let $u_w \in W(0,T)$ be the weak solution of the problem (2.11)-(2.13). Then*

$$0 < m \leq u_w(x,y,t) \leq S \text{ for a.e. } (x,y,t) \in \Omega \times (0,T). \tag{2.16}$$

Proof. We define $(u_w - S)_+$ as $(u_w - S)_+ = \max\{0, u_w - S\}$.

Multiplying equation (2.11) by $(u_w - S)_+$ and then integrating over Ω, to get

$$\frac{1}{2}\frac{d}{dt}\int_{\Omega} |(u_w - S)_+|^2 \, dx\, dy = \int_{\Omega} \operatorname{div}\left(\hbar\left(\left|\nabla^{\alpha} w_{\rho}\right|\right) \nabla u_w\right)(u_w - S)_+ dx\, dy + \gamma \int_{\Omega} (u_0 - u_w)(u_w - S)_+ \, dx\, dy,$$

by applying integration by parts and the Neumann boundary condition (2.13), we obtain

$$\begin{aligned}
&\frac{1}{2}\frac{d}{dt}\int_{\Omega} |(u_w - S)_+|^2 \, dx\, dy \\
&= -\int_{\{u_w \geq S\}} \hbar\left(\left|\nabla^{\alpha} w_{\rho}\right|\right) \nabla u_w \cdot \nabla u_w \, dx\, dy + \gamma \int_{\{u_w \geq S\}} (u_0 - u_w)(u_w - S)_+ \, dx\, dy,
\end{aligned}$$

this is equivalent to the following:

$$\begin{aligned}
&\frac{1}{2}\frac{d}{dt}\int_{\Omega} |(u_w - S)_+|^2 \, dx\, dy + \int_{\{u_w \geq S\}} \hbar\left(\left|\nabla^{\alpha} w_{\rho}\right|\right) |\nabla u_w|^2 \, dx\, dy \\
&+ \gamma \int_{\{u_w \geq S\}} (u_w - u_0)(u_w - S)_+ \, dx\, dy = 0.
\end{aligned}$$

Since $\hbar\left(\left|\nabla^{\alpha} w_{\rho}\right|\right) > 0$ and $(u_w - u_0)(u_w - S)_+ \geq 0$, it follows that:

$$\frac{d}{dt}\int_{\Omega} |(u_w - S)_+|^2 \, dx\, dy \leq 0,$$

integrating over $(0, t)$ yields:

$$\int_\Omega |(u_w - S)_+|^2 \, dx \, dy \le \int_\Omega |(u_0 - S)_+|^2 \, dx \, dy,$$

because of $u_0 \le S$, we obtain

$$\int_\Omega |(u_w - S)_+|^2 \, dx \, dy \le \int_\Omega |(u_0 - S)_+|^2 \, dx \, dy \le 0.$$

As a result,

$$u_w(x, y, t) \le S \quad \text{for a.e. } (x, y, t) \in \Omega \times (0, T).$$

In the same way, we define $(u_w - m)_-$ as $(u_w - m)_- = \min\{0, u_w - m\}$, multiplying the equation (2.11) by $(u_w - m)_-$ and then integrating over Ω, we find:

$$0 < m \le u_w(x, y, t) \ \text{ for a.e. } (x, y, t) \in \Omega \times (0, T).$$

□

Lemma 2.3. *The linearized problem (2.11)-(2.13) has a unique weak solution $u_w \in W(0, T)$ that satisfies the given estimates:*

a)

$$\|u_w\|_{L^\infty(0,T;L^2(\Omega))} \le \|u_0\|_{L^2(\Omega)} + K_1,$$

b)

$$\|u_w\|_{L^\infty(0,T;\mathcal{H}^1\Omega))} \le K_2,$$

c)

$$\int_0^T \left\| \frac{\partial u_w}{\partial t} \right\|^2_{(\mathcal{H}^1(\Omega))'} dt \le K_3,$$

where the constants K_1, K_2, and K_3 are positive and depend on $\|u_0\|_{\mathcal{H}^1(\Omega)}$, $\mathcal{K}_\rho$, ξ, m, and S.

Proof. a): Multiplying equation (2.11) by u_w, integrating by parts over Ω, and using (2.13) yield:

$$\frac{1}{2}\frac{d}{dt}\int_\Omega |u_w|^2 \, dx \, dy + \int_\Omega \hbar\left(\left|\nabla^\alpha w_\rho\right|\right)|\nabla u_w|^2 \, dx \, dy = \gamma \int_\Omega (u_0 - u_w) \, u_w \, dx \, dy.$$

Applying Young's inequality and (2.14), we get:

$$\frac{1}{2}\frac{d}{dt}\int_\Omega |u_w|^2 \, dx \, dy + \xi \int_\Omega |\nabla u_w|^2 \, dx \, dy \le \frac{\gamma^2}{2}\|u_0 - u_w\|^2_{L^2(\Omega)} + \frac{1}{2}\|u_w\|^2_{L^2(\Omega)}.$$

By using Lemma 2.2, we obtain

$$\begin{aligned} \|u_0 - u_w\|^2_{L^2(\Omega)} &\leq 2\left(\|u_0\|^2_{\mathcal{H}^1(\Omega)} + \|u_w\|^2_{L^2(\Omega)}\right) \\ &\leq 2\,\|u_0\|^2_{\mathcal{H}^1(\Omega)} + 2S^2|\Omega|. \end{aligned} \tag{2.17}$$

From (2.17), we have

$$\begin{aligned} \frac{1}{2}\frac{d}{dt}\int_\Omega |u_w|^2\,dx\,dy + \xi\int_\Omega |\nabla u_w|^2\,dx\,dy &\leq \gamma^2\,\|u_0\|^2_{\mathcal{H}^1(\Omega)} + \gamma^2 S^2|\Omega| + \frac{S^2}{2}|\Omega|, \\ &= C. \end{aligned} \tag{2.18}$$

By integrating inequality (2.18) over $(0,t)$, we find:

$$\frac{1}{2}\int_0^t \frac{d}{d\tau}\,\|u_w\|^2_{L^2(\Omega)}\,d\tau + \xi\int_0^t\int_\Omega |\nabla u_w|^2\,dx\,dy\,d\tau \leq Ct,$$

hence, for a.e. $t \in (0,T]$,

$$\frac{1}{2}\,\|u_w(t)\|^2_{L^2(\Omega)} + \xi\int_0^t\int_\Omega |\nabla u_w|^2\,dx\,dy\,d\tau \leq CT + \frac{1}{2}\,\|u_0\|^2_{L^2(\Omega)},$$

we deduce that

$$\|u_w\|_{L^\infty(0,T;L^2(\Omega))} \leq \|u_0\|_{L^2(\Omega)} + K_1.$$

b): Multiplying equation (2.11) by $\frac{\partial u_w}{\partial t}$, integrating by parts over Ω, and using (2.13) imply that:

$$\int_\Omega \left|\frac{\partial u_w}{\partial t}\right|^2 dx\,dy + \int_\Omega \hbar\left(\left|\nabla^\alpha w_\rho\right|\right)\nabla u_w\cdot\nabla\left(\frac{\partial u_w}{\partial t}\right)dx\,dy = \gamma\int_\Omega (u_0 - u_w)\,\frac{\partial u_w}{\partial t}\,dx\,dy.$$

According to Young's inequality, we get that:

$$\int_\Omega \left|\frac{\partial u_w}{\partial t}\right|^2 dx\,dy + \int_\Omega \hbar\left(\left|\nabla^\alpha w_\rho\right|\right)\nabla u_w\cdot\nabla\left(\frac{\partial u_w}{\partial t}\right)dx\,dy \leq \frac{\gamma^2}{2}\,\|u_0 - u_w\|^2_{L^2(\Omega)} + \frac{1}{2}\left\|\frac{\partial u_w}{\partial t}\right\|^2_{L^2(\Omega)}.$$

Noting that:

$$\begin{aligned} \int_\Omega \hbar\left(\left|\nabla^\alpha w_\rho\right|\right)\nabla u_w\cdot\nabla\left(\frac{\partial u_w}{\partial t}\right)dx\,dy &= \int_\Omega \hbar\left(\left|\nabla^\alpha w_\rho\right|\right)\nabla u_w\cdot\frac{\partial}{\partial t}(\nabla u_w)\,dx\,dy \\ &= \frac{1}{2}\int_\Omega \hbar\left(\left|\nabla^\alpha w_\rho\right|\right)\frac{d}{dt}\,|\nabla u_w|^2\,dx\,dy. \end{aligned}$$

On the other hand, we have also

$$\begin{aligned} &\frac{1}{2}\int_\Omega \hbar\left(\left|\nabla^\alpha w_\rho\right|\right)\frac{d}{dt}\,|\nabla u_w|^2\,dx\,dy \\ &= \frac{1}{2}\frac{d}{dt}\int_\Omega \hbar\left(\left|\nabla^\alpha w_\rho\right|\right)|\nabla u_w|^2\,dx\,dy - \frac{1}{2}\int_\Omega \frac{d\hbar\left(\left|\nabla^\alpha w_\rho\right|\right)}{dt}\,|\nabla u_w|^2\,dx\,dy. \end{aligned}$$

Therefore, by using the inequality (2.15), we conclude that

$$\int_\Omega \hbar\left(\left|\nabla^\alpha w_\rho\right|\right)\nabla u_w \cdot \nabla\left(\frac{\partial u_w}{\partial t}\right) dx\,dy \\ \geq \frac{1}{2}\frac{d}{dt}\int_\Omega \hbar\left(\left|\nabla^\alpha w_\rho\right|\right)|\nabla u_w|^2\,dx\,dy - \frac{\theta}{2}\|\nabla u_w\|^2_{L^2(\Omega)}. \tag{2.19}$$

Combining (2.17) and (2.19), we obtain

$$\frac{1}{2}\left\|\frac{\partial u_w}{\partial t}\right\|^2_{L^2(\Omega)} + \frac{1}{2}\frac{d}{dt}\int_\Omega \hbar\left(\left|\nabla^\alpha w_\rho\right|\right)|\nabla u_w|^2\,dx\,dy \\ \leq \gamma^2\|u_0\|^2_{\mathcal{H}^1(\Omega)} + \gamma^2 S^2|\Omega| + \frac{\theta}{2}\|\nabla u_w\|^2_{L^2(\Omega)}.$$

Observing in (2.14) that $0 < \xi \leq h\left(\left|\nabla^\alpha w_\rho\right|\right)$ gives the following:

$$\xi\,\|\nabla u_w\|^2_{L^2(\Omega)} \leq \int_\Omega \hbar\left(\left|\nabla^\alpha w_\rho\right|\right)|\nabla u_w|^2\,dx\,dy,$$

which implies

$$\|\nabla u_w\|^2_{L^2(\Omega)} \leq \frac{1}{\xi}\int_\Omega \hbar\left(\left|\nabla^\alpha w_\rho\right|\right)|\nabla u_w|^2\,dx\,dy. \tag{2.20}$$

Using (2.20) and substituting $C_0 = \gamma^2\|u_0\|^2_{\mathcal{H}^1(\Omega)} + \gamma^2 S^2|\Omega|$, we have:

$$\frac{1}{2}\left\|\frac{\partial u_w}{\partial t}\right\|^2_{L^2(\Omega)} + \frac{1}{2}\frac{d}{dt}\int_\Omega \hbar\left(\left|\nabla^\alpha w_\rho\right|\right)|\nabla u_w|^2\,dx\,dy \\ \leq C_0 + \frac{C_1}{2}\int_\Omega \hbar\left(\left|\nabla^\alpha w_\rho\right|\right)|\nabla u_w|^2\,dx\,dy, \tag{2.21}$$

where $C_1 = \dfrac{\theta}{\xi}$.

It is evident that

$$\frac{d}{dt}\int_\Omega h\left(\left|\nabla^\alpha w_\rho\right|\right)|\nabla u_w|^2\,dx\,dy \leq 2C_0 + C_1\int_\Omega \hbar\left(\left|\nabla^\alpha w_\rho\right|\right)|\nabla u_w|^2\,dx\,dy.$$

Through the use of Gronwall's lemma, we obtain

$$\int_\Omega \hbar\left(\left|\nabla^\alpha w_\rho(x,y,t)\right|\right)\left|\nabla u_w(x,y,t)\right|^2\,dx\,dy \leq e^{C_1 t}(C_2 + 2C_0 t),$$

for a.e. $t \in (0,T]$, where $C_2 = \int_\Omega \hbar\left(\left|\nabla^\alpha w_\rho(x,y,0)\right|\right)\left|\nabla u_w(x,y,0)\right|^2\,dx\,dy$.

From (2.20), we have

$$\|\nabla u_w\|^2_{L^2(\Omega)} \leq \frac{1}{\xi}e^{C_1 T}(C_2 + 2C_0 T). \tag{2.22}$$

Moreover, from (2.21), we can deduce that

$$\frac{1}{2}\left\|\frac{\partial u_w}{\partial t}\right\|^2_{L^2(\Omega)} + \frac{1}{2}\frac{d}{dt}\int_\Omega \hbar\left(\left|\nabla^\alpha w_\rho\right|\right)|\nabla u_w|^2\,dx\,dy \;\le\; C_0 + \frac{C_1}{2}\,e^{C_1 T}(C_2 + 2C_0 T). \tag{2.23}$$

By integrating (2.23) over $(0,t)$, we get to that

$$\begin{aligned}&\int_0^t \left\|\frac{\partial u_w}{\partial \tau}\right\|^2_{L^2(\Omega)} d\tau + \int_\Omega \hbar\left(\left|\nabla^\alpha w_\rho(x,y,t)\right|\right)\left|\nabla u_w(x,y,t)\right|^2 dx\,dy\\ &\le \left(2C_0 + C_1\,e^{C_1 T}(C_2 + 2C_0 T)\right)t + C_2,\end{aligned}$$

for a.e $t \in (0,T]$.

We see that:

$$\int_0^t \left\|\frac{\partial u_w}{\partial \tau}\right\|^2_{L^2(\Omega)} d\tau \;\le\; \left(2C_0 + C_1\,e^{C_1 T}(C_2 + 2C_0 T)\right)T + C_2. \tag{2.24}$$

According to $u_w(x,y,t) = u_w(x,y,0) + \int_0^t \frac{\partial u_w}{\partial \tau} d\tau$, inequalities (1.15), and (2.24), we have

$$\begin{aligned}\|u_w\|^2_{L^2(\Omega)} &\le\; 2\,\|u_0\|^2_{\mathcal{H}^1(\Omega)} + 2T\int_0^t \left\|\frac{\partial u_w(\tau)}{\partial \tau}\right\|^2_{L^2(\Omega)} d\tau\\ &\le\; 2\,\|u_0\|^2_{\mathcal{H}^1(\Omega)} + 2T^2\left(2C_0 + C_1\,e^{C_1 t}(C_2 + 2C_0 t)\right) + C_2 T.\end{aligned} \tag{2.25}$$

From (2.25) and (2.22), it follows that

$$\|u_w\|_{L^\infty(0,T;\mathcal{H}^1(\Omega))} \;\le\; K_2. \tag{2.26}$$

c): Multiplying (2.11) by $\varphi \in \mathcal{H}^1(\Omega)$ where $\left\|\varphi\right\|_{\mathcal{H}^1(\Omega)} \le 1$, applying Cauchy-Schwarz's inequality, and combining (2.17) and (2.26), we acquire that:

$$\begin{aligned}\left|\left\langle\frac{\partial u_w}{\partial t},\varphi\right\rangle\right| &= \left|\int_\Omega \hbar\left(\left|\nabla^\alpha w_\rho\right|\right)\nabla u_w\cdot\nabla\varphi\,dx\,dy \;+\gamma\int_\Omega (u_0 - u_w)\,\varphi\,dx\,dy\right|\\ &\le \left(\left|\hbar\left(\left|\nabla^\alpha w_\rho\right|\right)\right|\,\|\nabla u_w\|_{L^2(\Omega)} + \gamma\,\|u_0 - u_w\|_{L^2(\Omega)}\right)\left\|\varphi\right\|_{\mathcal{H}^1(\Omega)}\\ &\le \left(K_2 + \sqrt{2}\gamma\,\|u_0\|_{\mathcal{H}^1(\Omega)} + \sqrt{2|\Omega|}\gamma S\right)\left\|\varphi\right\|_{\mathcal{H}^1(\Omega)}.\end{aligned}$$

Consequently, we find

$$\left\|\frac{\partial u_w}{\partial t}\right\|_{(\mathcal{H}^1(\Omega))'} \le\; K_0 + \sqrt{2}\gamma\,\|u_0\|_{\mathcal{H}^1(\Omega)}, \tag{2.27}$$

where $K_0 = K_2 + \sqrt{2|\Omega|}\gamma S$.

Additionally, by squaring (2.27) and integrating over $(0,T)$, we obtain:

$$\int_0^T \left\| \frac{\partial u_w}{\partial t} \right\|^2_{(\mathcal{H}^1(\Omega))'} dt \ \leq K_3.$$

The proof is complete. □

2.4.2 Existence of a weak solution

Theorem 2.1. *Assuming that $u_0 \in \mathcal{H}^1(\Omega)$ and that (2.8) holds, the problem defined by (2.4)-(2.6) admits a weak solution $u \in W(0,T)$.*

Proof. Through lemma 2.3, we give the subset $\bar{W}$ of $W(0,T)$ as described by:

$$\bar{W} = \left\{ \begin{array}{l} w \in W(0,T); \|w\|_{L^\infty(0,T;\mathcal{H}^1(\Omega))} \leq K_2, \|w\|_{L^\infty(0,T;L^2(\Omega))} \leq \|u_0\|_{L^2(\Omega)}, \left\| \frac{\partial w}{\partial t} \right\|_{L^2(0,T;(\mathcal{H}^1(\Omega))')} \leq K_3, \\ 0 < m \leq w(x,y,t) \leq S \text{ for a.e. } (x,y,t) \in \Omega \times (0,T), w(0) = u_0 \end{array} \right\}.$$

Furthermore, it can be shown that $\bar{W}$ is a nonempty and convex subset of $W(0,T)$. Since the functions in $\bar{W}$ satisfy uniform bounds, the set is bounded in $W(0,T)$ and is also weakly closed. As $W(0,T)$ is a reflexive Banach space, the Banach-Alaoglu theorem [43] ensures that $\bar{W}$ is weakly compact in $W(0,T)$. Moreover, by the Eberlein-Smulaian theorem [24], weak compactness and weak sequential compactness are equivalent in Banach spaces. Therefore, $\bar{W}$ is weakly sequential compact in $W(0,T)$. Subsequently, we define the next mapping:

$$Q : \bar{W} \to \bar{W}$$
$$w \mapsto u_w.$$

To apply Schauder's fixed-point theorem, we must prove that the mapping $Q : w \mapsto u_w$ is weakly continuous from $\bar{W}$ into $\bar{W}$. Consider a sequence w_j in $\bar{W}$ that weakly converges to some w in $\bar{W}$, and let $u_j = Q(w_j)$. Our objective is to demonstrate that $Q(w_j) := u_j$ weakly converges to $Q(w) := u_w$. By applying lemma 2.3 and using classical results of compact inclusion in Sobolev spaces [2], we can extract sub-sequences of w_j and u_j (still denoted by w_j and u_j), hence we obtain:

$$w_j \to w \text{ in } L^2((0,T);L^2(\Omega)) \text{ and a.e. on } \Omega\times(0,T), \tag{2.28}$$

$$^{CF}\mathcal{D}_x^{\alpha}(w_j)_\rho \to^{CF} \mathcal{D}_x^{\alpha}w_\rho, ^{CF}\mathcal{D}_y^{\alpha}(w_j)_\rho \to^{CF} \mathcal{D}_y^{\alpha}w_\rho \text{ in } L^2((0,T);L^2(\Omega)) \tag{2.29}$$

and a.e. on $\Omega\times(0,T)$,

$$\left|\nabla^{\alpha}(w_j)_\rho\right| \to \left|\nabla^{\alpha}w_\rho\right| \text{ in } L^2((0,T);L^2(\Omega)) \text{ and a.e. on } \Omega\times(0,T), \tag{2.30}$$

$$\hbar\left(\left|\nabla^{\alpha}(w_j)_\rho\right|\right) \to \hbar\left(\left|\nabla^{\alpha}w_\rho\right|\right) \text{ in } L^2((0,T);L^2(\Omega)) \text{ and a.e. on } \Omega\times(0,T), \tag{2.31}$$

$$u_j \to u \text{ weakly in } L^{\infty}((0,T);\mathcal{H}^1(\Omega)), \tag{2.32}$$

$$\frac{\partial u_j}{\partial t} \to \frac{\partial u}{\partial t} \text{ weakly in } L^2((0,T);(\mathcal{H}^1(\Omega))'), \tag{2.33}$$

$$u_j \to u \text{ in } L^2((0,T);L^2(\Omega)) \text{ and a.e. on } \Omega\times(0,T), \tag{2.34}$$

$$\nabla u_j \to \nabla u \text{ weakly in } L^{\infty}((0,T);L^2(\Omega)), \tag{2.35}$$

$$u_j(0) \to u(0) \text{ in } L^2(\Omega). \tag{2.36}$$

The (2.31) is acquired by applying the dominated convergence theorem [10].

Since u_j is the weak solution of (2.11) corresponding to w_j, we have, for almost every $t \in (0,T]$, and $\varphi \in \mathcal{H}^1(\Omega)$:

$$\int_{\Omega} \frac{\partial u_j}{\partial t}\varphi\, dx\, dy + \int_{\Omega} \hbar\left(\left|\nabla^{\alpha}(w_j)_\rho\right|\right)\nabla u_j.\nabla\varphi\, dx\, dy = \gamma\int_{\Omega}\left(u_j(0)-u_j\right)\varphi\, dx\, dy. \tag{2.37}$$

Integrating (2.37) over $(0,T)$ yields

$$\begin{aligned}&\int_0^T\int_{\Omega} \frac{\partial u_j}{\partial t}\varphi\, dx\, dy\, dt + \int_0^T\int_{\Omega} \hbar\left(\left|\nabla^{\alpha}(w_j)_\rho\right|\right)\nabla u_j.\nabla\varphi\, dx\, dy\, dt\\ &= \gamma\int_0^T\int_{\Omega}\left(u_j(0)-u_j\right)\varphi\, dx\, dy\, dt.\end{aligned} \tag{2.38}$$

From (2.33), we have

$$\int_0^T\int_{\Omega} \frac{\partial u_j}{\partial t}\varphi\, dx\, dy\, dt \to \int_0^T\int_{\Omega} \frac{\partial u}{\partial t}\varphi\, dx\, dy\, dt, \quad \text{as } j\to\infty.$$

Examining the second term in (2.38)

$$\begin{aligned}
&\left|\int_0^T\int_\Omega \hbar\left(\left|\nabla^\alpha (w_j)_\rho\right|\right)\nabla u_j\cdot\nabla\varphi\,dx\,dy\,dt - \int_0^T\int_\Omega \hbar\left(\left|\nabla^\alpha w_\rho\right|\right)\nabla u\cdot\nabla\varphi\,dx\,dy\,dt\right|\\
&\leq \int_0^T\int_\Omega \left|\hbar\left(\left|\nabla^\alpha (w_j)_\rho\right|\right) - \hbar\left(\left|\nabla^\alpha w_\rho\right|\right)\right| |\nabla u| \left|\nabla\varphi\right|\,dx\,dy\,dt\\
&+\left|\int_0^T\int_\Omega \hbar\left(\left|\nabla^\alpha (w_j)_\rho\right|\right)\nabla (u_j-u)\cdot\nabla\varphi\,dx\,dy\,dt\right|.
\end{aligned}$$

According to claim 2.1, we deduce, as $j\to\infty$

$$\begin{aligned}
&\int_0^T\int_\Omega \left|\hbar\left(\left|\nabla^\alpha (w_j)_\rho\right|\right) - \hbar\left(\left|\nabla^\alpha w_\rho\right|\right)\right| |\nabla u| \left|\nabla\varphi\right|\,dx\,dy\,dt\\
&\leq C\int_0^T\int_\Omega \left\|w_j - w\right\|_{L^2(\Omega)} |\nabla u| \left|\nabla\varphi\right|\,dx\,dy\,dt\\
&\leq C(\varphi)\left\|w_j - w\right\|_{L^2(\Omega)} \|\nabla u\|_{L^2((0,T);L^2(\Omega))}\to 0,
\end{aligned}$$

and also, as $j\to\infty$,

$$\left|\int_0^T\int_\Omega \hbar\left(\left|\nabla^\alpha (w_j)_\rho\right|\right)\nabla (u_j-u)\cdot\nabla\varphi\,dx\,dy\,dt\right|\to 0.$$

Through (2.34) and (2.36), we obtain

$$\int_0^T\int_\Omega \left(u_j(0)-u_j\right)\varphi\,dx\,dy\,dt \to \int_0^T\int_\Omega (u_0-u)\,\varphi\,dx\,dy\,dt.$$

Letting $j\to\infty$ in (2.38) implies that

$$\int_0^T\int_\Omega \frac{\partial u}{\partial t}\,\varphi\,dx\,dy\,dt + \int_0^T\int_\Omega \hbar\left(\left|\nabla^\alpha w_\rho\right|\right)\nabla u.\nabla\varphi\,dx\,dy\,dt = \gamma\int_0^T\int_\Omega (u_0-u)\,\varphi\,dx\,dy\,dt.$$

Therefore, by the arbitrariness of $\varphi\in\mathcal{H}^1(\Omega)$, we get for a.e $t\in(0,T]$

$$\int_\Omega \frac{\partial u}{\partial t}\,\varphi\,dx\,dy + \int_\Omega \hbar\left(\left|\nabla^\alpha w_\rho\right|\right)\nabla u.\nabla\varphi\,dx\,dy = \gamma\int_\Omega (u_0-u)\,\varphi\,dx\,dy.$$

Hence, it follows that

$$u = u_w = Q(w).$$

Furthermore, given the uniqueness of the solution to problem (2.11), the whole sequence $u_j = Q(w_j)$ converge weakly in $\bar{W}$ to $u = Q(w)$. This confirms that Q is weakly continuous.

Therefore, by Schauder's fixed-point theorem, there exists $w\in\bar{W}$ such that

$$w = Q(w) = u_w.$$

Consequently, the existence of the weak solution u_w to the problem (2.4)-(2.6), is proved. □

2.4.3 Uniqueness of the weak solution

Theorem 2.2. *Assuming that u is a weak solution to (2.4)-(2.6), then this solution is unique.*

Proof. Let u_1, u_2 be tow weak solutions of (2.4)-(2.6). Then for a.e $t \in (0,T)$, we have

$$\begin{cases} \dfrac{\partial u_i}{\partial t} = \operatorname{div}\left(\hbar\left(\left|\nabla^{\alpha}(u_i)_{\rho}\right|\right)\nabla u\right) + \gamma\,(u_0 - u_i) & \Omega \times (0,T)\,, \\ u_i(x,y,0) = u_0(x,y), & \Omega, \\ \nabla u_i.\vec{n} = 0, & \text{on } \partial\Omega \times (0,T)\,. \end{cases} \tag{2.39}$$

Such that $i = 1, 2$.

Denote $\bar{u} = u_1 - u_2$. Then we can get:

$$\frac{\partial \bar{u}}{\partial t} - \operatorname{div}(\hbar\left(\left|\nabla^{\alpha}(u_1)_{\rho}\right|\right)\nabla\bar{u}) = \operatorname{div}((\hbar\left(\left|\nabla^{\alpha}(u_1)_{\rho}\right|\right) - \hbar\left(\left|\nabla^{\alpha}(u_2)_{\rho}\right|\right))\nabla u_2) - \gamma\,\bar{u} \qquad \text{in } \Omega \times (0,T)\,, \tag{2.40}$$

$$\bar{u}(x,y,0) = 0 \qquad \Omega, \tag{2.41}$$

$$\nabla\bar{u}.\vec{n} = 0, \qquad \text{on } \partial\Omega \times (0,T)\,. \tag{2.42}$$

Multiplying (2.40) by $\bar{u}$, and integrating over Ω, we obtain:

$$\begin{aligned} &\int_{\Omega} \frac{\partial \bar{u}}{\partial t}\,\bar{u}\,dx\,dy - \int_{\Omega} \operatorname{div}(\hbar\left(\left|\nabla^{\alpha}(u_1)_{\rho}\right|\right)(\nabla\bar{u})\bar{u}\,dx\,dy \\ &= \int_{\Omega} \operatorname{div}((\hbar\left(\left|\nabla^{\alpha}(u_1)_{\rho}\right|\right) - \hbar\left(\left|\nabla^{\alpha}(u_2)_{\rho}\right|\right))\nabla u_2)\bar{u}\,dx\,dy - \gamma\int_{\Omega} |\bar{u}|^2\,dx\,dy. \end{aligned}$$

By applying the integration by parts formula and using (2.42), we have:

$$\begin{aligned} &\frac{1}{2}\frac{d}{dt}\int_{\Omega} |\bar{u}|^2\,dx\,dy + \int_{\Omega} \hbar\left(\left|\nabla^{\alpha}(u_1)_{\rho}\right|\right)|\nabla\bar{u}|^2\,dx\,dy \\ &= -\int_{\Omega} (\hbar\left(\left|\nabla^{\alpha}(u_1)_{\rho}\right|\right) - \hbar\left(\left|\nabla^{\alpha}(u_2)_{\rho}\right|\right))\nabla u_2.\nabla\bar{u}\,dx\,dy - \gamma\int_{\Omega} |\bar{u}|^2\,dx\,dy. \end{aligned} \tag{2.43}$$

In view of (2.14), there exists a constant $\xi_1 > 0$, such that:

$$\xi_1 \le \hbar\left(\left|\nabla^{\alpha}(u_1)_{\rho}(x,y,t)\right|\right) \le 1, \quad \text{for a.e. } (x,y,t) \in \Omega \times (0,T).$$

Furthermore, according to (2.2) we find

$$\left\| \hbar\left(\left|\nabla^{\alpha}(u_1)_{\rho}\right|\right) - \hbar\left(\left|\nabla^{\alpha}(u_2)_{\rho}\right|\right) \right\|_{L^{\infty}(\Omega)} \leq C \left\| \bar{u} \right\|_{L^2(\Omega)}, \tag{2.44}$$

where C is a positive constant.

Therefore, by substituting the estimate (2.44) into (2.43), we get

$$\frac{1}{2}\frac{d}{dt}\left\|\bar{u}\right\|^2_{L^2(\Omega)} + \xi_1 \left\|\nabla\bar{u}\right\|^2_{L^2(\Omega)} \leq C \left\|\bar{u}\right\|_{L^2(\Omega)} \left\|\nabla u_2\right\|_{L^2(\Omega)} \left\|\nabla\bar{u}\right\|_{L^2(\Omega)} - \gamma \left\|\bar{u}\right\|^2_{L^2(\Omega)}.$$

By applying the Young's inequality

$$p.q \leq \frac{\xi_1 p^2}{2} + \frac{q^2}{2\xi_1}, \quad p, q, \xi_1 \in \mathbb{R}^+.$$

We conclude that:

$$\frac{1}{2}\frac{d}{dt}\left\|\bar{u}\right\|^2_{L^2(\Omega)} + \xi_1 \left\|\nabla\bar{u}\right\|^2_{L^2(\Omega)} \leq \frac{C^2}{2\xi_1} \left\|\bar{u}\right\|^2_{L^2(\Omega)} \left\|\nabla u_2\right\|^2_{L^2(\Omega)} + \frac{\xi_1}{2} \left\|\nabla\bar{u}\right\|^2_{L^2(\Omega)} - \gamma \left\|\bar{u}\right\|^2_{L^2(\Omega)},$$

which implies

$$\frac{d}{dt}\left\|\bar{u}\right\|^2_{L^2(\Omega)} \leq \left(\frac{C^2}{\xi_1} \left\|\nabla u_2\right\|^2_{L^2(\Omega)} - 2\gamma\right) \left\|\bar{u}\right\|^2_{L^2(\Omega)}.$$

Since, $\bar{u}(0) = 0$, applying Gronwall's inequality yields

$$\left\|\bar{u}(t)\right\|^2_{L^2(\Omega)} \leq 0.$$

In other words, $u_1 = u_2$. □

Remark 2.1. *According to theorem 2.1, the weak solution of problem (2.4)-(2.6) belongs to $\bar{W}$ and $w = Q(w) = u_w$ is the fixed point of (2.4)-(2.6). Thus, u_w is also in $\bar{W}$. Given the uniqueness of the solution, we conclude that the unique weak solution $u = u_w$ satisfies the extremum principle:*

$$0 < m \leq u(x, y, t) \leq S \text{ for a.e. } (x, y, t) \in \Omega \times (0, T),$$

such that:

$$0 < m := \operatorname{ess}\inf_{x,y\in\Omega} u_0(x, y) \text{ and } S := \operatorname{ess}\sup_{x,y\in\Omega} u_0(x, y) < \infty.$$

2.5 Numerical schemes

Nonlinear diffusion equations are typically solved numerically using explicit schemes. However, these schemes are only stable for very small time steps, which results in poor efficiency and limits their practical applicability. In this section, we develop a semi-implicit discrete scheme to numerically solve the problem defined by (2.4)-(2.6). To achieve this, we first introduce the additive operator splitting and then discretize the Caputo-Fabrizio fractional derivative.

Additionally, to enable a fair numerical comparison with the Caputo-based version of our model, we also construct a corresponding numerical scheme involving the discretization of the Caputo fractional derivative. This allows both formulations to be evaluated within the same computational framework and ensures a consistent assessment of their efficiency and denoising performance.

2.5.1 Additive operator splitting (AOS) method

Additive operator splitting (AOS) schemes were introduced by Weickert et al. [54] as unconditionally stable methods for the nonlinear diffusion in image processing. In this subsection, we apply the AOS technique to our proposed model.

The equation (2.4) can be expressed as follows:

$$\frac{\partial u}{\partial t} = \left(O_x + O_y\right) u + \gamma \left(u_0 - u\right), \tag{2.45}$$

where, O_x and O_y are differential sub-operators, as mentioned below:

$$\begin{cases} O_x = \dfrac{\partial}{\partial x}\left(\hbar\left(\left|\nabla^\alpha u_\rho\right|\right)\dfrac{\partial}{\partial x}\right), \\ O_y = \dfrac{\partial}{\partial y}\left(\hbar(\left|\nabla^\alpha u_\rho\right|)\dfrac{\partial}{\partial y}\right). \end{cases} \tag{2.46}$$

Applying the forward difference formula to (2.45), we get:

$$\frac{u_{i,j}^{n+1} - u_{i,j}^{n}}{\Delta t} = \left(O_x + O_y\right) u_{i,j}^{n+1} + \gamma\left(u_{i,j}^{0} - u_{i,j}^{n}\right). \tag{2.47}$$

The superscript n refers to the current time step, while $n+1$ refers to the next time step, $\Delta t > 0$ is the time step size. The subscripts i and j index the discrete pixel locations, assuming a spatial step size

$\Delta x = \Delta y = \Delta s$. By $u^n_{i,j}$, we denote approximation to $u(x_i, y_j, t_n)$, which represents the known values, and $u^{n+1}_{i,j}$ are the values to be determined.

To compute the values of the diffusivity function $\hbar$ using the known values of u^n, the scheme is semi-implicit and unconditionally stable. Although $\hbar$ depends on the fractional gradient of u, it is treated as a given function of (x, y).

We can write (2.47) in matrix-vector notation as:

$$\frac{U^{n+1} - U^n}{\Delta t} = \left(O_x + O_y\right) U^{n+1} + \gamma \left(U^0 - U^n\right). \tag{2.48}$$

Where U^n as the vector with entries $u^n_{i,j}$.

Incorporating U^{n+1} on the right-hand side of equation (2.48) yields the following:

$$\left[I - \Delta t \left(O_x + O_y\right)\right] U^{n+1} = \widetilde{U}^n, \tag{2.49}$$

where $\widetilde{U}^n = U^n + \gamma\, \Delta t\, (U^0 - U^n)$, and I is the identity matrix.

Note that equation (2.49) involves a large bandwidth matrix because all the equations related to new pixel values U^{n+1} are coupled. Our objective is to decouple this system so that each row and column of pixels can be handled independently. To achieve this, we rearrange the equation into the following form:

$$\begin{aligned} U^{n+1} &= \left[I - \Delta t \left(O_x + O_y\right)\right]^{-1} \widetilde{U}^n \\ &= \left[\frac{1}{2}\left(I - 2\Delta t\, O_x\right) + \frac{1}{2}\left(I - 2\Delta t\, O_y\right)\right]^{-1} \widetilde{U}^n. \end{aligned} \tag{2.50}$$

Certainly, we do not intend to invert the matrix to solve the linear system. This formulation is purely symbolic and is intended for use in subsequent derivations.

Equation (2.50) has interesting form in that it decomposes the system matrix. However, the challenge is that the decomposed system matrix is within the $[\ ]^{-1}$ operator. Instead, we aim to construct the solution in parts as follows:

$$U^{n+1} = \left(\left[\frac{1}{2}\left(I - 2\Delta t\, O_x\right)\right]^{-1} + \left[\frac{1}{2}\left(I - 2\Delta t\, O_y\right)\right]^{-1}\right) \widetilde{U}^n. \tag{2.51}$$

The issue is that the right-hand sides of equations (2.50) and (2.51) are not equal, as can be easily verified. Hence, To ensure equality, we multiply the right-hand side of (2.51) by a scalar r.

$$r\left(\left[\frac{1}{2}\left(I - 2\Delta t\, O_x\right)\right]^{-1} + \left[\frac{1}{2}\left(I - 2\Delta t\, O_y\right)\right]^{-1}\right)\widetilde{U}^n = \left[\frac{1}{2}\left(I - 2\Delta t\, O_x\right) + \frac{1}{2}\left(I - 2\Delta t\, O_y\right)\right]^{-1}\widetilde{U}^n,$$

this can be simplified to:

$$r\sum_{l=1}^{2}\left[\frac{1}{2}\left(I - 2\Delta t\, O_l\right)\right]^{-1}\widetilde{U}^n = \left[\sum_{l=1}^{2}\frac{1}{2}\left(I - 2\Delta t\, O_l\right)\right]^{-1}\widetilde{U}^n.$$

By setting $I - 2\Delta t\, O_l = \bar{M}_l$, we obtain:

$$4r\bar{M}^{-1} = \bar{M}^{-1},$$

thus we have:

$$r = \frac{1}{4}.$$

Based on this, to apply the additive operator splitting scheme given by equation (2.50), we multiply the right-hand side by $\frac{1}{4}$, resulting in the following:

$$U^{n+1} = \frac{1}{4}\sum_{l=1}^{2}\left[\frac{1}{2}\left(I - 2\Delta t\, O_l\right)\right]^{-1}\widetilde{U}^n,$$

which is equivalent to:

$$U^{n+1} = \left(2I - 4\Delta t\, O_x\right)^{-1}\widetilde{U}^n + \left(2I - 4\Delta t\, O_y\right)^{-1}\widetilde{U}^n.$$

Thus, the purpose of this scheme is to transform the equation into a simpler form, enabling the use of efficient block-wise solvers, such as the Tri-diagonal Matrix Algorithm.

Introduce the notations $R = \left(2I - 4\Delta t\, O_x\right)^{-1}\widetilde{U}^n$ and $P = \left(2I - 4\Delta t\, O_y\right)^{-1}\widetilde{U}^n$. The solution now consists of two components:

$$U^{n+1} = R + P. \tag{2.52}$$

We finally obtain the equations for R and P as follows:

$$\begin{cases} \left(2I - 4\Delta t\, O_x\right)R = \widetilde{U}^n \\ \left(2I - 4\Delta t\, O_y\right)P = \widetilde{U}^n. \end{cases} \tag{2.53}$$

The differential sub-operators O_x and O_y are analogous. Therefore, we derive the difference equation for a single row of pixels here; the equation for a column of pixels is identical. Consider a row with $N+1$ pixels indexed from 0 to N.

The first derivative can be approximated using a central finite difference scheme as follows:

$$\left(\frac{\partial R}{\partial x}\right)_{i+\frac{1}{2}} = \frac{R_{i+1}-R_i}{\Delta s} + O(\Delta s^2)$$
$$\left(\frac{\partial R}{\partial x}\right)_{i-\frac{1}{2}} = \frac{R_{i}-R_{i-1}}{\Delta s} + O(\Delta s^2).$$

Note that the neglected error terms are of order Δs^2. We conclude that:

$$(O_x R)_i = \left[\frac{\hbar_{i+\frac{1}{2}}(R_{i+1}-R_i) - \hbar_{i-\frac{1}{2}}(R_i - R_{i-1})}{\Delta s^2}\right]. \tag{2.54}$$

We introduce the following notation:

$$\beta_i = \frac{4\Delta t}{\Delta s^2}\left(\hbar_{i-\frac{1}{2}}\right), \text{ and } \ell_i = \frac{4\Delta t}{\Delta s^2}\left(\hbar_{i+\frac{1}{2}}\right).$$

Where

$$\hbar_{i-\frac{1}{2}} \text{ is an approximation of } \hbar\left(\left|\nabla^\alpha u_\rho(x_{i-\frac{1}{2}}, y_j, t_n)\right|\right),$$

and also,

$$\hbar_{i+\frac{1}{2}} \text{ is an approximation of } \hbar\left(\left|\nabla^\alpha u_\rho(x_{i+\frac{1}{2}}, y_j, t_n)\right|\right).$$

From equations (2.53) and (2.54), the finite difference equation simplifies to:

$$-\beta_i R_{i-1}^{n+1} + (2+\beta_i+\ell_i)R_i^{n+1} - \ell_i R_{i+1}^{n+1} = \widetilde{U}_i^n. \tag{2.55}$$

At each time step, we need to solve an algebraic system where the matrix $(2I - 4\Delta t\, O_x)$ is an irreducible, strictly diagonal dominant matrix, and thus invertible. such systems can be efficiently solved using block-wise solvers, such as the Tri-diagonal Matrix Algorithm. Additionally, by applying the Von Neumann method, we can demonstrate that this semi-implicit scheme is unconditionally stable.

A similar equation applies to P in the y dimension, for $j = 0, 1, \ldots M$.

$$-\beta_j P_{j-1}^{n+1} + (2+\beta_j+\ell_j)P_j^{n+1} - \ell_j P_{j+1}^{n+1} = \widetilde{U}_j^n, \tag{2.56}$$

where

$$\beta_j = \frac{4\Delta t}{\Delta s^2}\left(\hbar_{j-\frac{1}{2}}\right), \text{ and } \ell_j = \frac{4\Delta t}{\Delta s^2}\left(\hbar_{j+\frac{1}{2}}\right),$$

such that

$$\hbar_{j-\frac{1}{2}} \text{ is an approximation of } \hbar\left(\left|\nabla^\alpha u_\rho(x_i, y_{j-\frac{1}{2}}, t_n)\right|\right),$$

and

$$\hbar_{j+\frac{1}{2}} \text{ is an approximation of } \hbar\left(\left|\nabla^\alpha u_\rho(x_i, y_{j+\frac{1}{2}}, t_n)\right|\right).$$

For the first and last nodes, the Neumann boundary conditions are applied:

$$R_0 = R_1 \,,\, R_N = R_{N-1} \qquad \text{and} \qquad P_0 = P_1 \,,\, P_M = P_{M-1}.$$

To establish the values of the diffusivity function $\hbar$ at the points $i+\frac{1}{2}, i-\frac{1}{2}, j+\frac{1}{2}$ and $j-\frac{1}{2}$, we propose discretizing the Caputo-Fabrizio fractional derivative, as detailed below. Moreover, a similar discretization is constructed for the Caputo derivative to allow a consistent numerical comparison between the two formulations.

2.5.2 Discretization of the Caputo-Fabrizio derivative

As mentioned above, to obtain the values of the diffusivity function $\hbar$, we discretize the Caputo-Fabrizio fractional derivative. The function

$$\hbar(\left|\nabla^\alpha u_\rho\right|) = \frac{1}{1 + \left|\nabla^\alpha u_\rho\right|^2}, \tag{2.57}$$

is used in this chapter.

Based on the definition of the Caputo-Fabrizio fractional derivative (1.13), the discretization of this derivative over the interval $[0, x]$ is performed using a forward finite difference scheme as follows:

$${}^{CF}\mathcal{D}_x^\alpha\, u_\rho(x_i, y_j, t_n) = \frac{1}{1-\alpha}\int_0^{x_i} e^{-\left(\frac{\alpha}{1-\alpha}\right)(x_i - s)} \frac{\partial}{\partial s} u_\rho(s, y_j, t_n) ds. \tag{2.58}$$

Equation (2.58) can be modified to:

$${}^{CF}\mathcal{D}_x^\alpha\, u_\rho(x_i, y_j, t_n) \approx \frac{1}{1-\alpha}\sum_{k=1}^{i-1}\left(\frac{u_{k+1,j}^n - u_{k,j}^n}{\Delta s}\right)\int_{x_k}^{x_{k+1}} e^{-\left(\frac{\alpha}{1-\alpha}\right)(x_i - s)}\, ds.$$

Using the space grid point $x_i = i\,\Delta s$ for $i = 0, 1, ...N$, and by integrating, we obtain:

$$ {}^{CF}\mathcal{D}_x^{\alpha}\, u_\rho(x_i, y_j, t_n) \approx \frac{1}{\alpha\,\Delta s}\sum_{k=1}^{i-1}\left(u_{k+1,j}^n - u_{k,j}^n\right)\left[e^{-\left(\frac{\alpha}{1-\alpha}\right)(i-(k+1))\Delta s} - e^{-\left(\frac{\alpha}{1-\alpha}\right)(i-k)\Delta s}\right]. $$

Thus, the discretization of the Caputo-Fabrizio fractional derivative based on the forward finite difference scheme at the points $i+\frac{1}{2}$, $j+\frac{1}{2}$, $i-\frac{1}{2}$ and $j-\frac{1}{2}$ with respect to the variable x is given by:

- At a point $i+\frac{1}{2}$:

$$ {}^{CF}\mathcal{D}_x^{\alpha}\, u_\rho(x_{i+\frac{1}{2}}, y_j, t_n) = \frac{1}{1-\alpha}\int_0^{x_{i+\frac{1}{2}}} e^{-\left(\frac{\alpha}{1-\alpha}\right)\left(x_{i+\frac{1}{2}}-s\right)}\frac{\partial}{\partial s}u_\rho(s, y_j, t_n)ds. $$

The above equation is converted to:

$$ \begin{aligned} {}^{CF}\mathcal{D}_x^{\alpha}\, u_\rho(x_{i+\frac{1}{2}}, y_j, t_n) \approx{}& \frac{1}{1-\alpha}\sum_{k=1}^{i-1}\left(\frac{u_{k+1,j}^n - u_{k,j}^n}{\Delta s}\right)\int_{x_k}^{x_{k+1}} e^{-\left(\frac{\alpha}{1-\alpha}\right)\left(x_{i+\frac{1}{2}}-s\right)}ds \\ &+ \frac{1}{1-\alpha}\left(\frac{u_{i+1,j}^n - u_{i,j}^n}{\Delta s}\right)\int_{x_i}^{x_{i+\frac{1}{2}}} e^{-\left(\frac{\alpha}{1-\alpha}\right)\left(x_{i+\frac{1}{2}}-s\right)}ds. \end{aligned} $$

Using the space grid point $x_{i+\frac{1}{2}} = \left(i+\frac{1}{2}\right)\Delta s$ for $i = 0, 1, ...N$, and by integrating, we obtain:

$$ \begin{aligned} {}^{CF}\mathcal{D}_x^{\alpha}\, u_\rho(x_{i+\frac{1}{2}}, y_j, t_n) \approx{}& \frac{1}{\alpha\,\Delta s}\sum_{k=1}^{i-1}\left(u_{k+1,j}^n - u_{k,j}^n\right)\left[e^{-\left(\frac{\alpha}{1-\alpha}\right)\left(i-(k+\frac{1}{2})\right)\Delta s} - e^{-\left(\frac{\alpha}{1-\alpha}\right)\left(i-(k-\frac{1}{2})\right)\Delta s}\right] \\ &+ \frac{1}{\alpha\,\Delta s}\left(u_{i+1,j}^n - u_{i,j}^n\right)\left[1 - e^{-\left(\frac{\alpha}{1-\alpha}\right)\left(\frac{1}{2}\right)\Delta s}\right]. \end{aligned} $$

In the same manner, we can obtain the derivative at the remaining points.

- At a point $j+\frac{1}{2}$:

$$ \begin{aligned} {}^{CF}\mathcal{D}_x^{\alpha}\, u_\rho(x_i, y_{j+\frac{1}{2}}, t_n) ={}& \frac{1}{1-\alpha}\int_0^{x_i} e^{-\left(\frac{\alpha}{1-\alpha}\right)(x_i-s)}\frac{\partial}{\partial s}u_\rho(s, y_{j+\frac{1}{2}}, t_n)ds \\ \approx{}& \frac{1}{1-\alpha}\sum_{k=1}^{i-1}\left(\frac{u_{k+1,j+1}^n - u_{k,j+1}^n + u_{k+1,j}^n - u_{k,j}^n}{2\Delta s}\right)\int_{x_k}^{x_{k+1}} e^{-\left(\frac{\alpha}{1-\alpha}\right)(x_i-s)}ds \\ ={}& \frac{1}{2\alpha\Delta s}\sum_{k=1}^{i-1}\left(u_{k+1,j+1}^n - u_{k,j+1}^n + u_{k+1,j}^n - u_{k,j}^n\right)\left[e^{-\left(\frac{\alpha}{1-\alpha}\right)(i-(k+1))\Delta s} - e^{-\left(\frac{\alpha}{1-\alpha}\right)(i-k)\Delta s}\right]. \end{aligned} $$

- At a point $i-\frac{1}{2}$:

$$
\begin{aligned}
{}^{CF}\mathcal{D}_x^{\alpha}\, u_\rho(x_{i-\frac{1}{2}}, y_j, t_n) &= \frac{1}{1-\alpha}\int_0^{x_{i-\frac{1}{2}}} e^{-\left(\frac{\alpha}{1-\alpha}\right)\left(x_{i-\frac{1}{2}}-s\right)}\frac{\partial}{\partial s}u_\rho(s, y_j, t_n)ds\\
&\approx \frac{1}{1-\alpha}\sum_{k=2}^{i-1}\left(\frac{u_{k,j}^n-u_{k-1,j}^n}{\Delta s}\right)\int_{x_{k-1}}^{x_k} e^{-\left(\frac{\alpha}{1-\alpha}\right)\left(x_{i-\frac{1}{2}}-s\right)}ds\\
&+\frac{1}{1-\alpha}\left(\frac{u_{i,j}^n-u_{i-1,j}^n}{\Delta s}\right)\int_{x_{i-1}}^{x_{i-\frac{1}{2}}} e^{-\left(\frac{\alpha}{1-\alpha}\right)\left(x_{i-\frac{1}{2}}-s\right)}ds\\
&= \frac{1}{\alpha\,\Delta s}\sum_{k=2}^{i-1}\left(u_{k,j}^n-u_{k-1,j}^n\right)\left[e^{-\left(\frac{\alpha}{1-\alpha}\right)\left(i-(k+\frac{1}{2})\right)\Delta s}-e^{-\left(\frac{\alpha}{1-\alpha}\right)\left(i-(k-\frac{1}{2})\right)\Delta s}\right]\\
&+\frac{1}{\alpha\,\Delta s}\left(u_{i,j}^n-u_{i-1,j}^n\right)\left[1-e^{-\left(\frac{\alpha}{1-\alpha}\right)\left(\frac{1}{2}\right)\Delta s}\right].
\end{aligned}
$$

- At a point $j-\frac{1}{2}$:

$$
\begin{aligned}
{}^{CF}\mathcal{D}_x^{\alpha}\, u_\rho(x_i, y_{j-\frac{1}{2}}, t_n) &= \frac{1}{1-\alpha}\int_0^{x_i} e^{-\left(\frac{\alpha}{1-\alpha}\right)(x_i-s)}\frac{\partial}{\partial s}u_\rho(s, y_{j-\frac{1}{2}}, t_n)ds\\
&\approx \frac{1}{1-\alpha}\sum_{k=1}^{i-1}\left(\frac{u_{k+1,j}^n-u_{k,j}^n+u_{k+1,j-1}^n-u_{k,j-1}^n}{2\Delta s}\right)\int_{x_k}^{x_{k+1}} e^{-\left(\frac{\alpha}{1-\alpha}\right)(x_i-s)}ds\\
&= \frac{1}{2\alpha\Delta s}\sum_{k=1}^{i-1}\left(u_{k+1,j}^n-u_{k,j}^n+u_{k+1,j-1}^n-u_{k,j-1}^n\right)\left[e^{-\left(\frac{\alpha}{1-\alpha}\right)(i-(k+1))\Delta s}-e^{-\left(\frac{\alpha}{1-\alpha}\right)(i-k)\Delta s}\right].
\end{aligned}
$$

An analogue expression is derived for ${}^{CF}\mathcal{D}_y^{\alpha}$.

2.5.3 Discretization of the Caputo derivative

Based on the definition of the Caputo fractional derivative [35], its discretization over the interval $[0, x]$ is carried out using a forward finite difference scheme as follows:

$$
{}^{C}\mathcal{D}_x^{\alpha}\, u_\rho(x_i, y_j, t_n) = \frac{1}{\Gamma(1-\alpha)}\int_0^{x}(x_i-s)^{-\alpha}\frac{\partial}{\partial s}u_\rho(s, y_j, t_n)\,ds,\quad 0<\alpha<1. \tag{2.59}
$$

Γ denotes Euler's continuous gamma function.

Equation (2.59) can be reformulated as follows:

$$
{}^{C}\mathcal{D}_x^{\alpha}\, u_\rho(x_i, y_j, t_n) \approx \frac{1}{\Gamma(1-\alpha)}\sum_{k=1}^{i-1}\left(\frac{u_{k+1,j}^n-u_{k,j}^n}{\Delta s}\right)\int_{x_k}^{x_{k+1}}(x_i-s)^{-\alpha}\,ds.
$$

Using the space grid point $x_i = i\,\Delta s$ for $i = 0, 1, ...N$, and by integrating, we obtain:

$$
{}^{C}\mathcal{D}_x^{\alpha}\, u_\rho(x_i, y_j, t_n) \approx \frac{(\Delta s)^{-\alpha}}{\Gamma(2-\alpha)}\sum_{k=1}^{i-1}\left(u_{k+1,j}^n-u_{k,j}^n\right)\left[(i-k)^{1-\alpha}-(i-k-1)^{1-\alpha}\right].
$$

Thus, the discretization of the Caputo fractional derivative with respect to the variable x, based on the forward finite difference scheme at the points $i+\frac{1}{2}$, $j+\frac{1}{2}$, $i-\frac{1}{2}$ and $j-\frac{1}{2}$, is given by:

• At a point $i+\frac{1}{2}$:

$$\begin{aligned}
{}^{C}\mathcal{D}_x^{\alpha}\, u_\rho(x_{i+\frac{1}{2}}, y_j, t_n) &= \frac{1}{\Gamma(1-\alpha)} \int_0^{x_{i+\frac{1}{2}}} \left(x_{i+\frac{1}{2}} - s\right)^{-\alpha} \frac{\partial}{\partial s} u_\rho(s, y_j, t_n) ds. \\
&\approx \frac{1}{\Gamma(1-\alpha)} \sum_{k=1}^{i-1} \left(\frac{u_{k+1,j}^n - u_{k,j}^n}{\Delta s}\right) \int_{x_k}^{x_{k+1}} \left(x_{i+\frac{1}{2}} - s\right)^{-\alpha} ds \\
&+ \frac{1}{\Gamma(1-\alpha)} \left(\frac{u_{i+1,j}^n - u_{i,j}^n}{\Delta s}\right) \int_{x_i}^{x_{i+\frac{1}{2}}} \left(x_{i+\frac{1}{2}} - s\right)^{-\alpha} ds \\
&= \frac{(\Delta s)^{-\alpha}}{\Gamma(2-\alpha)} \sum_{k=1}^{i-1} \left(u_{k+1,j}^n - u_{k,j}^n\right) \left[\left(i-k+\frac{1}{2}\right)^{1-\alpha} - \left(i-k-\frac{1}{2}\right)^{1-\alpha}\right] \\
&+ \frac{(\Delta s)^{-\alpha}}{\Gamma(2-\alpha)} \left(u_{i+1,j}^n - u_{i,j}^n\right) \left(\frac{1}{2}\right)^{1-\alpha}.
\end{aligned}$$

• At a point $j+\frac{1}{2}$:

$$\begin{aligned}
{}^{C}\mathcal{D}_x^{\alpha}\, u_\rho(x_i, y_{j+\frac{1}{2}}, t_n) &= \frac{1}{\Gamma(1-\alpha)} \int_0^{x_i} (x_i - s)^{-\alpha} \frac{\partial}{\partial s} u_\rho(s, y_{j+\frac{1}{2}}, t_n) ds \\
&\approx \frac{1}{\Gamma(1-\alpha)} \sum_{k=1}^{i-1} \left(\frac{u_{k+1,j+1}^n - u_{k,j+1}^n + u_{k+1,j}^n - u_{k,j}^n}{2\Delta s}\right) \int_{x_k}^{x_{k+1}} (x_i - s)^{-\alpha} ds \\
&= \frac{(\Delta s)^{-\alpha}}{2\Gamma(2-\alpha)} \sum_{k=1}^{i-1} \left(u_{k+1,j+1}^n - u_{k,j+1}^n + u_{k+1,j}^n - u_{k,j}^n\right) \left[(i-k)^{1-\alpha} - (i-k-1)^{1-\alpha}\right].
\end{aligned}$$

• At a point $i-\frac{1}{2}$:

$$\begin{aligned}
{}^{C}\mathcal{D}_x^{\alpha}\, u_\rho(x_{i-\frac{1}{2}}, y_j, t_n) &= \frac{1}{\Gamma(1-\alpha)} \int_0^{x_{i-\frac{1}{2}}} \left(x_{i-\frac{1}{2}} - s\right)^{-\alpha} \frac{\partial}{\partial s} u_\rho(s, y_j, t_n) ds \\
&\approx \frac{1}{\Gamma(1-\alpha)} \sum_{k=2}^{i-1} \left(\frac{u_{k,j}^n - u_{k-1,j}^n}{\Delta s}\right) \int_{x_{k-1}}^{x_k} \left(x_{i+\frac{1}{2}} - s\right)^{-\alpha} ds \\
&+ \frac{1}{\Gamma(1-\alpha)} \left(\frac{u_{i,j}^n - u_{i-1,j}^n}{\Delta s}\right) \int_{x_{i-1}}^{x_{i-\frac{1}{2}}} \left(x_{i+\frac{1}{2}} - s\right)^{-\alpha} ds \\
&= \frac{(\Delta s)^{-\alpha}}{\Gamma(2-\alpha)} \sum_{k=2}^{i-1} \left(u_{k,j}^n - u_{k-1,j}^n\right) \left[\left(i-k+\frac{1}{2}\right)^{1-\alpha} - \left(i-k-\frac{1}{2}\right)^{1-\alpha}\right] \\
&+ \frac{(\Delta s)^{-\alpha}}{\Gamma(2-\alpha)} \left(u_{i,j}^n - u_{i-1,j}^n\right) \left(\frac{1}{2}\right)^{1-\alpha}.
\end{aligned}$$

- At a point $j - \frac{1}{2}$:

$$
\begin{aligned}
{}^{C}\mathcal{D}_x^{\alpha}\, u_\rho(x_i, y_{j-\frac{1}{2}}, t_n) &= \frac{1}{\Gamma(1-\alpha)} \int_0^{x_i} (x_i - s)^{-\alpha} \frac{\partial}{\partial s} u_\rho(s, y_{j-\frac{1}{2}}, t_n) ds \\
&\approx \frac{1}{\Gamma(1-\alpha)} \sum_{k=1}^{i-1} \left(\frac{u_{k+1,j}^n - u_{k,j}^n + u_{k+1,j-1}^n - u_{k,j-1}^n}{2\Delta s} \right) \int_{x_k}^{x_{k+1}} (x_i - s)^{-\alpha}\, ds \\
&= \frac{(\Delta s)^{-\alpha}}{2\Gamma(2-\alpha)} \sum_{k=1}^{i-1} \left(u_{k+1,j}^n - u_{k,j}^n + u_{k+1,j-1}^n - u_{k,j-1}^n \right) \left[(i-k)^{1-\alpha} - (i-k-1)^{1-\alpha} \right].
\end{aligned}
$$

Similarly, an expression for ${}^{C}\mathcal{D}_y^{\alpha}$ is derived.

We summarize the numerical algorithm for the proposed model in Algorithm 1.

The same algorithm is applied to the Caputo-based model, with the only modification being the replacement of the Caputo-Fabrizio fractional derivative 2.5.2 by the Caputo fractional derivative 2.5.3 in the computation of the fractional gradient. This ensures a fair and consistent numerical comparison between the two formulations.

Algorithm 1 AOS algorithm with diffusivity based on the Caputo-Fabrizio derivative

Input: Original image U^0, time step Δt, number of iterations N_t, parameters α, ρ, γ

Initialize: $U^n := U^0$

1: **for** $n = 1$ to N_t **do**

2: **Compute** $\tilde{U} := U^n + \gamma\, \Delta t\, (U^0 - U^n)$

3: **Regularization:** Compute the smoothed version using convolution $v := \mathcal{K}_\rho * U^n$

4: **Compute the diffusivity:**

- Approximate the fractional gradient $\nabla^\alpha v$ using the Caputo-Fabrizio fractional derivative (Section 2.5.2)
- Compute the diffusivity function $\hbar := \hbar(|\nabla^\alpha v|)$ at each pixel

5: **Solve 1D system in x-direction:**

$$R := (2I - 4\Delta t\, O_x)^{-1} \tilde{U}$$

Solve tridiagonal system using Thomas algorithm

6: **Solve 1D system in y-direction:**

$$P := (2I - 4\Delta t\, O_y)^{-1} \tilde{U}$$

Solve tridiagonal system using Thomas algorithm

7: **Combine results:**

$$U^{n+1} := R + P$$

8: **end for**

Output: U^{n+1}

2.6 Experimental results and discussion

In this section, a series of numerical experiments were conducted to validate the effectiveness of the proposed model (2.4)-(2.6). These experiments, applied to a diverse set of gray scale images, were performed using the AOS method with $\Delta s = 1$ and $\rho = 2.5$. Furthermore, we selected images of varying dimensions. Figure 2.1 shows an image with dimensions 384×256 pixels. Figure 2.2 includes the Shepp-Logan head image with dimensions 600×600 pixels. Figures 2.3 and 2.4 represent medical images with dimensions 256×256 and 200×200 pixels, respectively. Figure 2.5 displays the Barbara image with dimensions 512×512 pixels. In addition, Figure 2.6, 2.7, and 2.8 present the Die image (384×256 pixels), the BMRI (256×256 pixels), and the Butterfly image (376×300 pixels), respectively, which are used specifically for the comparative, analysis with the ROF [44] and Caputo-based models.

The images in Figures 2.1, 2.2, 2.3, and 2.4 illustrate the effects of different α values on denoising performance, with smaller α values preserving image details more effectively than larger ones.

Figure 2.1 shows the results obtained by applying our proposed model to an image degraded by additive Gaussian noise. The denoising performance was evaluated using three different values of the parameter α to investigate the trade-off between noise removal and detail preservation. As α increased, the images became progressively smoother.

Figures 2.2 presents the results of applying our model to the Shepp-Logan head image corrupted by two types of noise: additive Gaussian noise and salt-and-pepper noise. The purpose of this experiment is to assess the robustness of the model under different noise characteristics. To this end, we tested four different values of the parameter α, allowing us to examine how the choice of α affects the balance between noise suppression and structural preservation in the reconstructed images.

Figure 2.3 displays a noisy medical image along with the results obtained after processing it using our proposed model. The processing was performed with a time step of 3 and 12 iterations. To evaluate the impact of fractional-order parameter, six different values of α were tested. The model effectively reduced the noise while preserving important structures and edges. This preservation is essential for maintaining diagnostic quality, ensuring that clinically relevant features remain clear and intact.

Figure 2.4 presents a medical image corrupted by speckle noise at two different density levels. The corrupted images were then processed using our model with three different values of the parameter α. This experiment aims to evaluate the model's ability to handle multiplicative noise while preserving essential anatomical structures.

Additionally, Figure 2.5 illustrates the influence of the parameter γ by demonstrating how varying its value affects the balance between data fidelity and smoothness in image processing. In this nonlinear diffusion model, γ governs the trade-off between adherence to the original image and the degree of nonlinear diffusion applied for noise reduction. To investigate this effect, six different values of γ were tested. Increasing γ enhances the contribution of the data fidelity term, leading to results that are more faithful to the original image, with better detail preservation and reduced distortion.

Summarizing the observations across all experiments, although a relatively large time step is used -particularly in Figure 2.2, where $\Delta t = 10$- the proposed model still achieves both stability and accuracy. Overall, the experimental results demonstrate that the model is highly effective in preserving edges and fine details during the denoising process, while also producing visually superior outcomes compared to conventional approaches.

To further asses the performance of the proposed model, we conducted a comparative study involving the ROF model and a Caputo-based formulation. The comparison was carried out on a set of representative test images (Die, BMRI, and Butterfly), using both qualitative visual evaluation and quantitative metrics, including PSNR and SSIM. The results of this comparison are presented in Figures 2.6-2.8 and Tables 2.1-2.3.

Figure 2.6 presents a die image corrupted by salt-and-pepper noise. The results clearly highlight the superiority of the proposed model in effectively removing noise while preserving fine image details. This is evident both in the visual quality and in the quantitative evaluation metrics (PSNR and SSIM) reported in Table 2.1. In contrast, the denoised image obtained using the Caputo-based model still contains noticeable residual noise, especially in homogeneous regions. This is primarily attributed to the slow convergence behavior of the Caputo derivative, which requires a higher number of iterations and significantly longer computational time to produce results comparable to those of the Caputo-Fabrizio-based formulation. Furthermore, although the ROF model [44] performs well in terms of noise smoothing, it tends to oversmooth critical image features, resulting in the loss of fine details and edge blurring. This limitation arises from the local nature of the ROF regularization, which lacks the capacity to capture long-range dependencies or preserve textures effectively. By comparison, the proposed model based on the Caputo-Fabrizio operator demonstrates superior denoising performance, combining efficient noise removal with enhanced edge and structure preservation. These advantages are corroborated by the higher PSNR and SSIM values reported in Table 2.1, confirming both the visual and numerical improvements achieved by our approach.

Figure 2.7 illustrates the denoising performance on a BMRI image degraded by speckle noise. The proposed Caputo-Fabrizio-based model demonstrates a remarkable ability to reduce the multiplicative noise while preserving anatomical structures and delicate textures within the image. This is particularly important in medical imaging, where retaining structural integrity is critical for interpretation and diagnosis. The Caputo-based model, although capable of attenuating the noise, exhibits a slower convergence and leaves behind residual artifacts, especially in regions with subtle intensity variations. This further emphasizes the computational and practical limitations associated with the Caputo operator. On the other hand, the ROF model [44] successfully suppresses noise but at the cost of smoothing out meaningful anatomical details, such as fine tissue boundaries and small structural features. This loss of detail can hinder the diagnostic quality of the output. In contrast, the proposed model achieves a better trade-off between noise suppression and structure preservation. This superiority is confirmed by the PSNR and SSIM values reported in Table 2.2, which clearly favor the Caputo-Fabrizio-based formulation over the alternatives.

Figure 2.8 presents the denoising results for the Butterfly image contaminated with Gaussian noise. The proposed model based on the Caputo-Fabrizio operator successfully suppresses the noise while preserving sharp edges and intricate patterns such as the wing textures and fine contours. This highlights the model's ability to maintain high-frequency details, which are often lost during the denoising process. The Caputo-based model manages to reduce the noise to a certain extent; however, residual Gaussian noise remains noticeable, particularly in smooth background regions. Moreover, due to the slower convergence of the Caputo operator, this model requires more iterations and longer computational time to approach the visual quality achieved by our proposed approach. In contrast, the ROF model [44] effectively eliminates a portion of the noise but overly smooths key features, resulting in blurred edges and a loss of delicate structures within the image. This limitation arises from the local nature of the total variation regularization, which cannot fully preserve global texture information. Quantitatively, as shown in Table 2.3, the Caputo-Fabrizio-based model outperforms both the Caputo and ROF models in terms of PSNR and SSIM metrics, confirming its superiority in balancing noise removal with detail preservation.

Collectively, the results of the numerical experiments across various test images and noise types demonstrate the effectiveness and versatility of the proposed Caputo-Fabrizio-based model. Compared to the ROF [44] and Caputo-based models, the proposed approach achieves better noise suppression while preserving fine structures and edges. These advantages are consistently reflected in both visual quality and objective evaluation metrics, confirming the model's practical relevance for advanced image denoising applications.

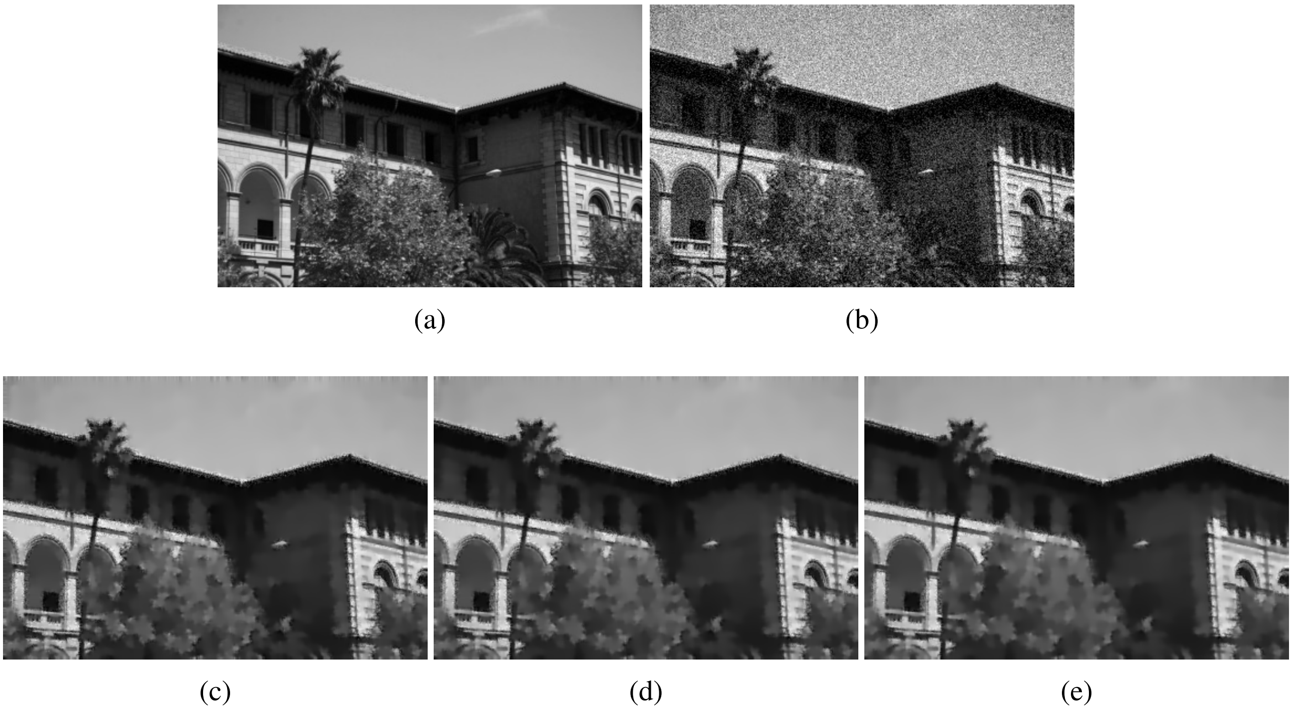

Figure 2.1: Results obtained by applying our model to the noisy image (b) after 10 iterations, with $\Delta t = 5$ and $\gamma = 0.001$. First row: (a) original image, (b) noisy image corrupted by Gaussian noise. Second row: Filtered versions of image (b) by the proposed Caputo-fabrizio-based model (2.4). First column: for $\alpha = 0.6$, second column: for $\alpha = 0.7$, third column: for $\alpha = 0.8$.

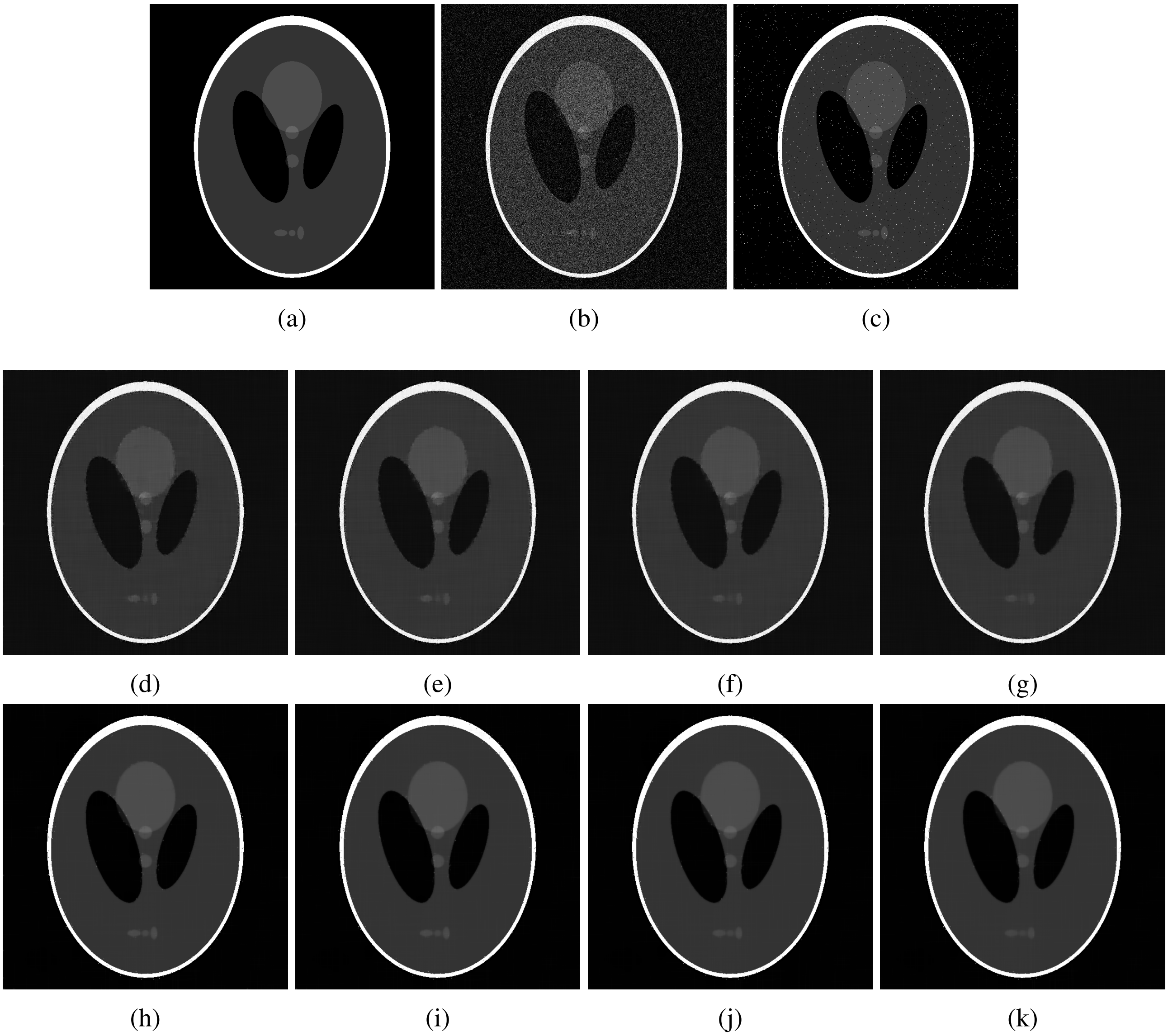

Figure 2.2: Results obtained by applying our model to the noisy Shepp-Logan head image after 17 iterations, with $\Delta t = 10$ and $\gamma = 0.03$. First row: (a) Shepp-Logan head original image, (b) noisy image corrupted by Gaussian noise, (c) noisy image corrupted by salt-and-pepper noise. Second and Third rows: Filtered versions of images (b) and (c) by the proposed Caputo-fabrizio-based model (2.4). First column: for $\alpha = 0.65$, second column: for $\alpha = 0.75$, third column: for $\alpha = 0.85$, fourth column: for $\alpha = 0.95$.

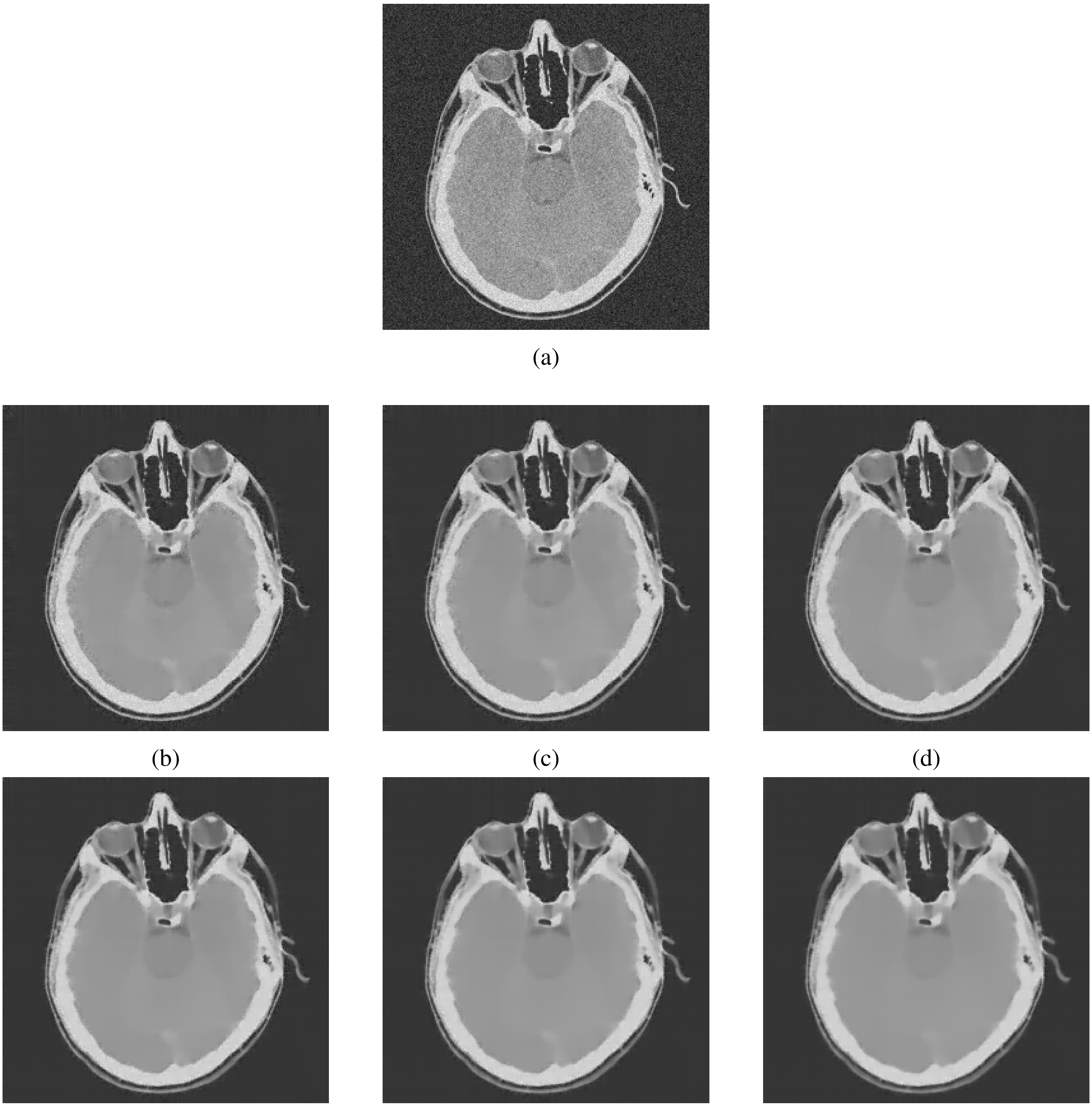

(a) (b) (c) (d) (e) (f) (g)

Figure 2.3: Comparison of the effects of different α values using our model on a noisy medical image after 12 iterations, with $\Delta t = 3$ and $\gamma = 0.04$. (a) Noisy image, (b-g) denoised images by the proposed Caputo-fabrizio-based model (2.4) for $\alpha = 0.3$, $\alpha = 0.4$, $\alpha = 0.5$, $\alpha = 0.6$, $\alpha = 0.7$, and $\alpha = 0.9$, respectively.

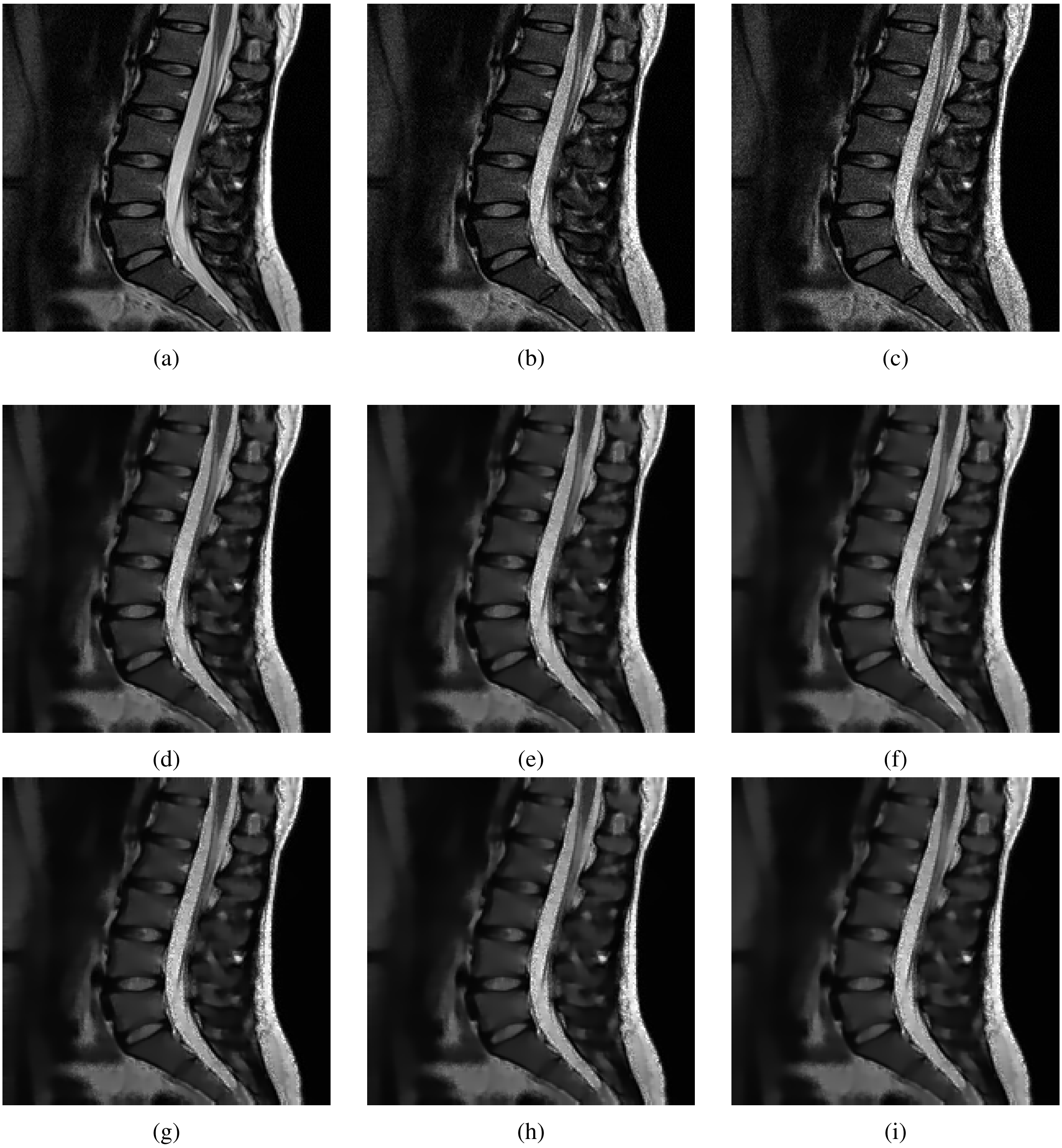

Figure 2.4: Results obtained by applying our model to the noisy medical image after 6 iterations, with $\Delta t = 4$ and $\gamma = 0.001$. First row: (a) original image, (b) noisy image corrupted by speckle noise at level of 0.01, (c) noisy image corrupted by speckle noise at level of 0.02. Second and third rows: Filtered versions of images (b) and (c) by the proposed Caputo-fabrizio-based model (2.4). First column: for $\alpha = 0.6$, second column: for $\alpha = 0.7$, third column: for $\alpha = 0.8$.

Figure 2.5: Comparison of the effects of different γ values using our model on the Barbara image after 40 iterations, with $\Delta t = 1$ and $\alpha = 0.65$. (a) Barbara original image, (b-g) processed images by the proposed Caputo-fabrizio-based model (2.4) for $\gamma = 2$, $\gamma = 1$, $\gamma = 0.5$, $\gamma = 0.2$, $\gamma = 0.07$, and $\gamma = 0.01$, respectively.

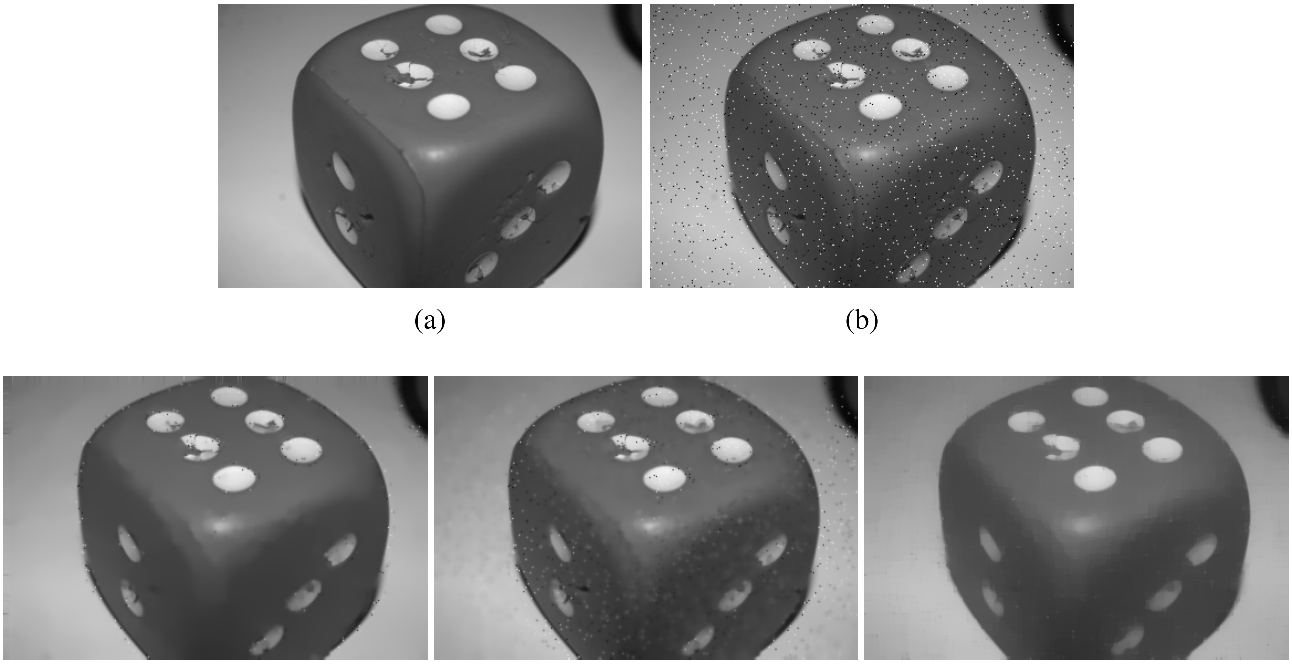

(a) (b)

(c) (d) (e)

Figure 2.6: Denoising results for Die image: (a) original image, (b) noisy image corrupted by salt-and-pepper noise, (c) result from the proposed Caputo-fabrizio-based model, (d) result from the Caputo-based model, (e) result from the ROF model. All results are shown after 10 iterations, with time step $\Delta t = 10$, $\gamma = 0.001$, and fractional order $\alpha = 0.5$.

Image	Caputo-Fabrizio-based model		Caputo-based model		ROF model [44]	
	PSNR	SSIM	PSNR	SSIM	PSNR	SSIM
Die image	**34.24**	**0.95**	32.21	0.89	29.19	0.93

Table 2.1: Quantitative comparison of denoising performance on the denoised Die image using PSNR and SSIM metrics for the proposed Caputo-Fabrizio-based model, the Caputo-based model, and the ROF model.

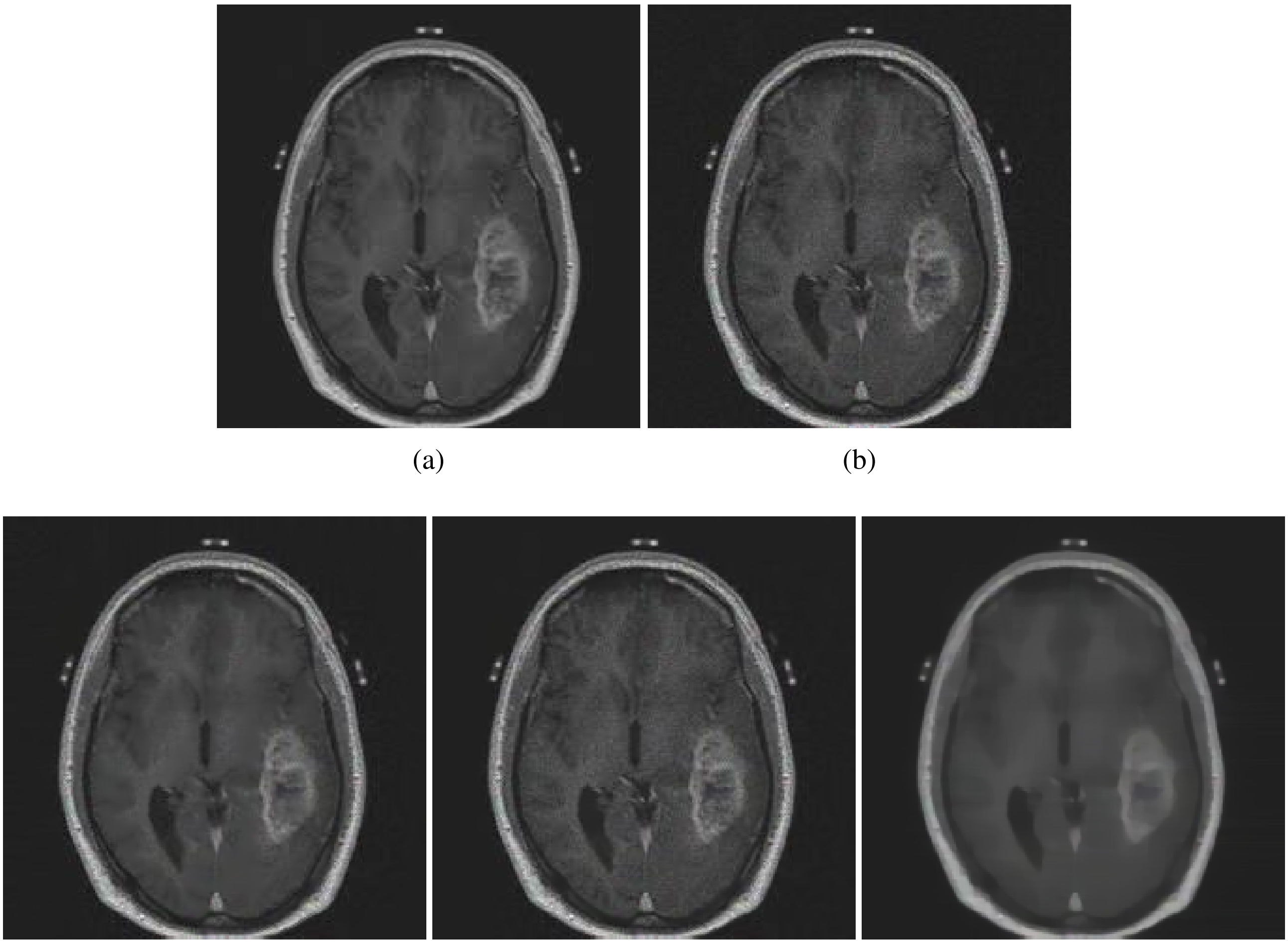

(a) (b)

(c) (d) (e)

Figure 2.7: Denoising results for BMRI: (a) original image, (b) noisy image corrupted by speckle noise, (c) result from the proposed Caputo-fabrizio-based model, (d) result from the Caputo-based model, (e) result from the ROF model. All results are shown after 4 iterations, with time step $\Delta t = 5$, $\gamma = 0.01$, and fractional order $\alpha = 0.1$.

Image	Caputo-Fabrizio-based model		Caputo-based model		ROF model [44]	
	PSNR	SSIM	PSNR	SSIM	PSNR	SSIM
BMRI	**37.27**	**0.97**	37.16	0.96	32.94	0.92

Table 2.2: Quantitative comparison of denoising performance on the denoised BMRI image using PSNR and SSIM metrics for the proposed Caputo-Fabrizio-based model, the Caputo-based model, and the ROF model.

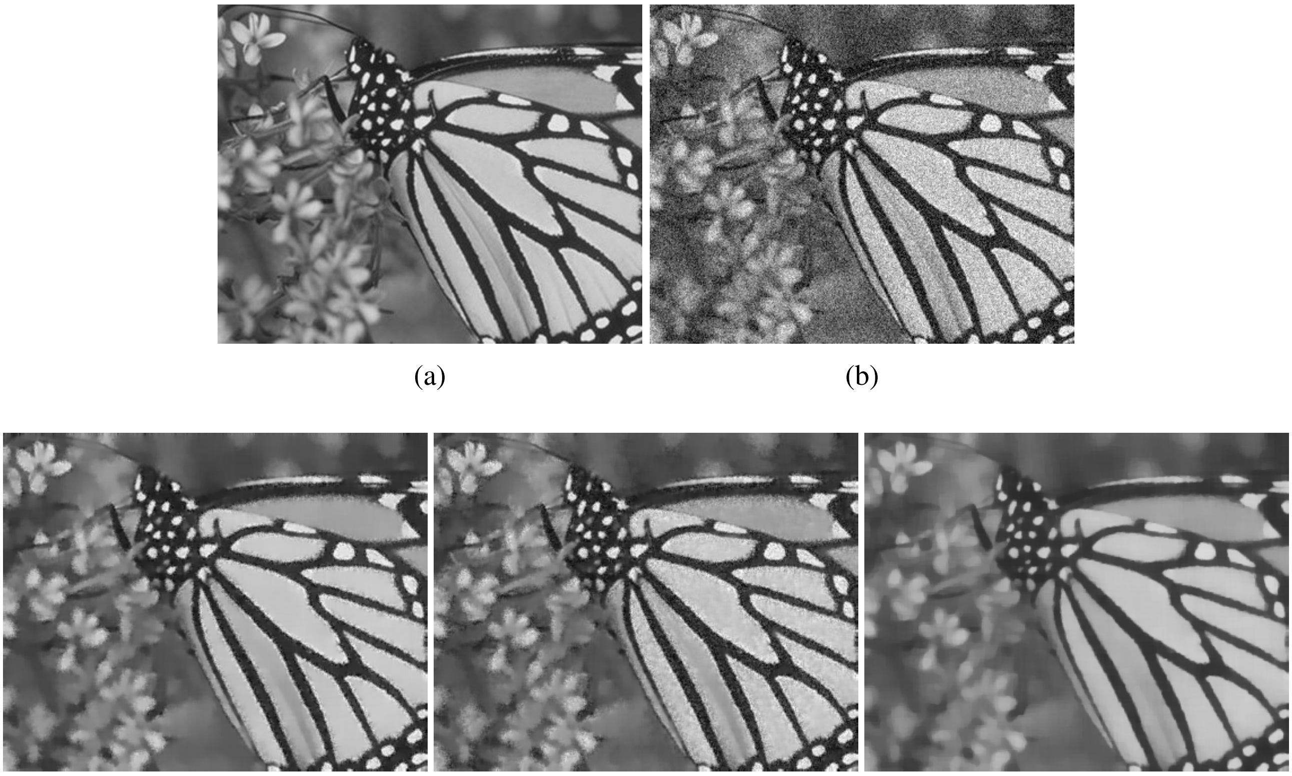

(a) (b)

(c) (d) (e)

Figure 2.8: Denoising results for Butterfly image: (a) original image, (b) noisy image corrupted by Gaussian noise, (c) result from the proposed Caputo-fabrizio-based model, (d) result from the Caputo-based model, (e) result from the ROF model. All results are shown after 10 iterations, with time step $\Delta t = 7$, $\gamma = 0.01$, and fractional order $\alpha = 0.7$.

Image	Caputo-Fabrizio-based model		Caputo-based model		ROF model [44]	
	PSNR	SSIM	PSNR	SSIM	PSNR	SSIM
Butterfly image	**26.55**	**0.82**	25.89	0.78	25.30	0.81

Table 2.3: Quantitative comparison of denoising performance on the denoised Butterfly image using PSNR and SSIM metrics for the proposed Caputo-Fabrizio-based model, the Caputo-based model, and the ROF model.

2.7 Conclusion

This chapter addressed the existence and uniqueness of the weak solution to a nonlinear diffusion model incorporating a fractional gradient, established through Schauder's fixed-point theorem. To complement the theoretical analysis, we have developed an unconditionally stable semi-implicit numerical scheme based on the additive operator splitting (AOS) method. The proposed scheme has been successfully applied to image denoising, with experimental results demonstrating its effectiveness in suppressing noise while preserving essential image structures such as edges and textures.

Moreover, we conducted a comparative study involving the proposed model, a Caputo-based formulation, and the classical ROF model [44]. The results show that our Caputo-Fabrizio-based approach consistently achieves higher denoising quality, as reflected in both visual outcomes and quantitative metrics such as PSNR and SSIM. Unlike the Caputo-based version, which requires more iterations and computational time due to slower convergence, or the ROF model, which often over-smooth and blurs image details, the proposed model offers a better trade-off between efficiency and preservation of fine structures.

An important aspect of the model is the inclusion of the fractional gradient, which introduces a degree of nonlocality. This contributes to more flexible control over the diffusion process, offering improved balance between noise reduction and feature preservation compared to classical models. Moreover, the use of the Caputo-Fabrizio operator-with its exponential kernel- further distinguishes the proposed approach from models based on traditional fractional derivatives. This kernel structure not only enhances computational efficiency but also improves convergence behavior, as confirmed by our comparative experiments.

Overall, this work provides a mathematically sound and computationally feasible framework for image processing tasks.

CHAPTER 3

A NONLINEAR DIFFUSION EQUATION WITH GRAY-LEVEL AND FRACTIONAL GRADIENT DEPENDENT COEFFICIENTS: WELL-POSEDNESS ANALYSIS

The results presented in this chapter are based on the findings reported in [12].

3.1 Introduction

In the previous chapter, a comparative study between the Caputo and Caputo-Fabrizio-based models was presented. While the Caputo-Fabrizio operator exhibited faster convergence and higher computational efficiency, the Caputo formulation revealed certain limitations, particularly regarding numerical performance. Motivated by these findings, this chapter introduces an improved Caputo-based diffusion model by incorporating a gray-level indicator into the diffusion coefficient. The gray-level indicator enhances the adaptability of the diffusion process to local intensity variations, thereby addressing the shortcomings of the Caputo model and improving practical denoising performance.

This chapter focuses on the theoretical and numerical analysis of a nonlinear diffusion equation in which we propose a model where the diffusion coefficient depends simultaneously depends on the image gradient, gray-level information, and fractional derivatives. The Caputo fractional derivative provides a nonlocal mechanism that enhances texture representation while preserving essential image features. To further suppress noise and retain structural information, a gray-level indicator is integrated into the diffusion coefficient. In addition, a Gaussian kernel function is employed to increase the model's robustness to noise and to play a crucial role in establishing its well-posedness. Finally, a fidelity term, originally proposed in [44], is incorporated as a source term to ensure that the restored image remains faithful to the observed data. The model is formulated as follows:

$$\frac{\partial u}{\partial t} = \operatorname{div}\left(\frac{\left|u_\rho\right|^\beta}{\left(M_\rho^u\right)^\beta}\frac{1}{1+\left|\nabla^\alpha u_\rho\right|^\lambda}\nabla u\right) + \gamma\left(u_0 - u\right), \qquad \text{in}\,\Omega\times(0,T), \tag{3.1}$$

$$u(x,y,0) = u_0(x,y), \qquad \text{in}\,\Omega, \tag{3.2}$$

$$\nabla u.\vec{n} = 0, \qquad \text{on}\,\partial\Omega\times(0,T), \tag{3.3}$$

where:

- Ω is a bounded domain of $\mathbb{R}^2$, and u_0 is the original image.
- $0 < \alpha < 1, \beta > 0, \lambda > 0, \gamma > 0$, and $\vec{n}$ denote the unit outward normal to $\partial\Omega$.
- $u_\rho = \mathcal{K}_\rho * u$, here "$*$" denotes convolution operator.
- We define:

$$M_\rho^u = \max_{x,y\in\Omega}\left|u_\rho(x,y,t)\right|.$$

- ∇ (respectively. div(.)) denotes the gradient (respectively divergence) operator, and $\left|\nabla^\alpha u_\rho\right| = \sqrt{\left|{}^C\mathcal{D}_x^\alpha u_\rho\right|^2 + \left|{}^C\mathcal{D}_y^\alpha u_\rho\right|^2}$, where ${}^C\mathcal{D}_x^\alpha u_\rho$ represents the Caputo fractional derivative of order α of u_ρ in terms of the variable x, and ${}^C\mathcal{D}_y^\alpha u_\rho$ represents the Caputo fractional derivative of order α of u_ρ in terms of the variable y.

The remainder of this work is organized as follows. Section 3.2 presents the preliminaries, including essential definitions and propositions. In section 3.3, we examine the existence and uniqueness of the weak solution for the proposed model. Section 3.4 outlines the numerical implementation developed for the model. Finally, section 3.5 concludes the study by summarizing the key findings.

3.2 Preliminaries

This section presents the essential definitions from fractional calculus.

The fractional gradient of $\mathcal{K}_\rho$ of order α is defined by:

$$\nabla^\alpha\mathcal{K}_\rho(x,y) = \left({}^C\mathcal{D}_x^\alpha\mathcal{K}_\rho(x,y), {}^C\mathcal{D}_y^\alpha\mathcal{K}_\rho(x,y)\right).$$

It follows from definition 1.12 that:

$$\begin{aligned} {}^{C}\mathcal{D}_x^{\alpha}\mathcal{K}_\rho(x,y) &= \frac{1}{\Gamma(1-\alpha)}\int_0^x (x-\delta)^{-\alpha}\,\frac{\partial \mathcal{K}_\rho(\delta,y)}{\partial\delta}\,d\delta, \quad 0<\alpha<1,\\ &= \frac{1}{\Gamma(2-\alpha)}\left(x^{1-\alpha}\,\frac{\partial \mathcal{K}_\rho(0,y)}{\partial\delta} + \int_0^x (x-\delta)^{1-\alpha}\frac{\partial^2 \mathcal{K}_\rho(\delta,y)}{\partial\delta^2}\,d\delta\right), \end{aligned}$$

similarly, we have:

$$\begin{aligned} {}^{C}\mathcal{D}_y^{\alpha}\mathcal{K}_\rho(x,y) &= \frac{1}{\Gamma(1-\alpha)}\int_0^y (y-\delta)^{-\alpha}\,\frac{\partial \mathcal{K}_\rho(x,\delta)}{\partial\delta}\,d\delta, \quad 0<\alpha<1\\ &= \frac{1}{\Gamma(2-\alpha)}\left(y^{1-\alpha}\,\frac{\partial \mathcal{K}_\rho(x,0)}{\partial\delta} + \int_0^y (y-\delta)^{1-\alpha}\frac{\partial^2 \mathcal{K}_\rho(x,\delta)}{\partial\delta^2}\,d\delta\right). \end{aligned}$$

3.3 Theoretical framework

In this section, we establish the existence and uniqueness of the weak solution to the proposed model (3.1)-(3.3). Owing to the nonlinearity of the problem, we begin by analyzing a linearized version, and subsequently apply Schauder's fixed point theorem to prove the existence of a weak solution.

We introduce the following functional space:

$$W(0,T) = \left\{ w \in L^2(0,T;\mathcal{H}^1(\Omega)),\, \frac{\partial w}{\partial t} \in L^2\left(0,T;(\mathcal{H}^1(\Omega))'\right)\right\}.$$

It is evident that $W(0,T)$ is a Hilbert space equipped with the norm:

$$\|w\|_W = \|w\|_{L^2(0,T;\mathcal{H}^1(\Omega))} + \left\|\frac{\partial w}{\partial t}\right\|_{L^2\left(0,T;(\mathcal{H}^1(\Omega))'\right)}.$$

Definition 3.1. A function $u \in W(0,T)$ is called a weak solution of (3.1)-(3.3) if it satisfies the following relation:

$$\left\langle \frac{\partial u}{\partial t},\varphi\right\rangle + \int_\Omega \left(\frac{|u_\rho|^\beta}{\left(M_\rho^u\right)^\beta}\,\frac{1}{1+|\nabla^\alpha u_\rho|^\lambda}\nabla u.\nabla\varphi\right) dx\,dy = \gamma\int_\Omega (u_0-u)\,\varphi\,dx\,dy,$$

$$u(x,y,0) = u_0(x,y), \quad \text{in}\,\Omega,$$

for almost every $t\in(0,T)$ and for all $\varphi\in\mathcal{H}^1(\Omega)$.

In what follows, we assume that the initial value $u_0 \in \mathcal{H}^1(\Omega)$ satisfies:

$$0 < m := \operatorname*{ess\,inf}_{x,y\in\Omega}\; u_0(x,y) \text{ and } \ell := \operatorname*{ess\,sup}_{x,y\in\Omega}\; u_0(x,y) < \infty. \tag{3.4}$$

The linearized problem

Let us define the following space:

$$\Psi = \left\{ \quad w \in W(0,T) \cap L^{\infty}(0,T;L^2(\Omega)) : m \leq w(x,y,t) \leq \ell, \text{ a.e in } \Omega \times (0,T) \right\}.$$

For any $w \in \Psi$ satisfying

$$\|w\|_{L^{\infty}(0,T;L^2(\Omega))} \leq \|u_0\|_{L^2(\Omega)}, \tag{3.5}$$

$$\left\| \frac{\partial w}{\partial t} \right\|_{L^2(0,T;L^2(\Omega))} \leq C \|u_0\|_{\mathcal{H}^1(\Omega)}, \tag{3.6}$$

where $C > 0$ is a constant .

The linearized problem is formulated as follows:

$$\frac{\partial u_w}{\partial t} = \operatorname{div}\left(\frac{|w_\rho|^\beta}{\left(M_\rho^w\right)^\beta} \frac{1}{1 + |\nabla^\alpha w_\rho|^\lambda} \nabla u_w \right) + \gamma\,(u_0 - u_w), \qquad \text{in } \Omega \times (0,T), \tag{3.7}$$

$$u_w(x,y,0) = u_0(x,y), \qquad \text{in } \Omega, \tag{3.8}$$

$$\nabla u_w.\vec{n} = 0, \qquad \text{on } \partial\Omega \times (0,T). \tag{3.9}$$

Proposition 3.1. *The following inequalities are valid:*

$$0 < \psi \leq \frac{|w_\rho|^\beta}{\left(M_\rho^w\right)^\beta} \frac{1}{1 + |\nabla^\alpha w_\rho|^\lambda} \leq 1, \tag{3.10}$$

$$\left| \frac{\partial}{\partial t} \left(\frac{|w_\rho|^\beta}{\left(M_\rho^w\right)^\beta} \frac{1}{1 + |\nabla^\alpha w_\rho|^\lambda} \right) \right| \leq \zeta, \tag{3.11}$$

$$\left\| \frac{|(w_1)_\rho|^\beta}{\left(M_\rho^{w_1}\right)^\beta} \frac{1}{1 + |\nabla^\alpha (w_1)_\rho|^\lambda} - \frac{|(w_2)_\rho|^\beta}{\left(M_\rho^{w_2}\right)^\beta} \frac{1}{1 + |\nabla^\alpha (w_2)_\rho|^\lambda} \right\|_{L^{\infty}(\Omega)} \leq \xi \|w_1 - w_2\|_{L^2(\Omega)}, \tag{3.12}$$

where positive constants ψ, ζ, and ξ depend only on $\mathcal{K}_\rho$, β, λ, m, and u_0, while w_1, $w_2 \in \Psi$.

Proof. Proof of (3.10). Let $w \in \Psi$. Since $0 < m \leq w_\rho$ and $\mathcal{K}_\rho$ is positive, it follows from the convolution property that:

$$m \left\|\mathcal{K}_\rho\right\|_{L^1(\Omega)} = \left|\mathcal{K}_\rho * m\right| \leq |w_\rho| \leq C_\rho C \|u_0\|_{\mathcal{H}^1(\Omega)}. \tag{3.13}$$

By definition, M_ρ^w is given by:

$$M_\rho^w = \max_{x,y \in \Omega} |w_\rho(x,y,t)|.$$

Using (3.13), we have:

$$\left|M_\rho^w\right| \leq C_\rho C \left\|u_0\right\|_{\mathcal{H}^1(\Omega)}.$$

Hence, for any $\beta > 0$, it holds that:

$$m^\beta \left\|\mathcal{K}_\rho\right\|_{L^1(\Omega)}^\beta \leq \left|w_\rho\right|^\beta \leq \left|M_\rho^w\right|^\beta \leq C_\rho^\beta C^\beta \left\|u_0\right\|_{\mathcal{H}^1(\Omega)}^\beta.$$

Therefore:

$$\frac{m^\beta \left\|\mathcal{K}_\rho\right\|_{L^1(\Omega)}^\beta}{C_\rho^\beta C^\beta \left\|u_0\right\|_{\mathcal{H}^1(\Omega)}^\beta} \leq \frac{\left|w_\rho\right|^\beta}{\left|M_\rho^w\right|^\beta} \leq 1. \tag{3.14}$$

Moreover, by applying Young's convolution inequality, we obtain:

$$\begin{aligned}
\left|\nabla^\alpha w_\rho\right| &\leq \left|(\nabla^\alpha \mathcal{K}_\rho) * w\right| \\
&\leq C_\rho \left\|w\right\|_{L^2(\Omega)} \\
&\leq C_\rho C \left\|u_0\right\|_{\mathcal{H}^1(\Omega)}.
\end{aligned}$$

Accordingly, for any $\lambda > 0$,

$$\begin{aligned}
1 \leq 1 + \left|\nabla^\alpha w_\rho\right|^\lambda &\leq 1 + C_\rho^\lambda C^\lambda \left\|u_0\right\|_{\mathcal{H}^1(\Omega)}^\lambda \\
\frac{1}{1 + C_\rho^\lambda C^\lambda \left\|u_0\right\|_{\mathcal{H}^1(\Omega)}^\lambda} \leq \frac{1}{1 + \left|\nabla^\alpha w_\rho\right|^\lambda} &\leq 1.
\end{aligned} \tag{3.15}$$

This implies that (3.10) follows from (3.14)-(3.15) for

$$\psi = \frac{m^\beta \left\|\mathcal{K}_\rho\right\|_{L^1(\Omega)}^\beta}{C_\rho^\beta C^\beta \left\|u_0\right\|_{\mathcal{H}^1(\Omega)}^\beta} \cdot \frac{1}{1 + C_\rho^\lambda C^\lambda \left\|u_0\right\|_{\mathcal{H}^1(\Omega)}^\lambda}.$$

Proof of (3.11). We note that:

$$\left|\frac{\partial}{\partial t}\left(\frac{\left|w_\rho\right|^\beta}{\left(M_\rho^w\right)^\beta} \frac{1}{1 + \left|\nabla^\alpha w_\rho\right|^\lambda}\right)\right| \leq \underbrace{\beta \frac{\left|w_\rho\right|^{\beta-1} \left|\mathcal{K}_\rho * \dfrac{\partial w}{\partial t}\right| (M_\rho^w)^\beta}{(M_\rho^w)^{2\beta}}}_{A_1} + \underbrace{\left|\frac{\dfrac{\partial}{\partial t}(\nabla^\alpha w_\rho)^\lambda}{(1 + |\nabla^\alpha w|^\lambda)^2}\right|}_{B_1}.$$

By the property of convolution and the condition $w \in \Psi$, it follows that

$$A_1 \leq \begin{cases} \dfrac{\beta C_\rho^\beta C^\beta \left\|u_0\right\|_{\mathcal{H}^1(\Omega)}^\beta}{m^\beta \left\|\mathcal{K}_\rho\right\|_{L^1(\Omega)}^\beta}, & \text{if } \beta > 1, \\[2ex] \dfrac{\beta C_\rho C \left\|u_0\right\|_{\mathcal{H}^1(\Omega)}}{m \left\|\mathcal{K}_\rho\right\|_{L^1(\Omega)}}, & \text{if } 0 < \beta \leq 1. \end{cases}$$

We also have:

$$\begin{aligned} B_1 &\leq \lambda C_\rho^{\lambda-1} N^{\lambda-1} \|u_0\|_{\mathcal{H}^1(\Omega)}^{\lambda-1} \left| \nabla^\alpha \mathcal{K}_\rho * \frac{\partial w}{\partial t} \right| \\ &\leq \lambda C_\rho^\lambda C^\lambda \|u_0\|_{\mathcal{H}^1(\Omega)}^\lambda . \end{aligned}$$

Hence,

$$\begin{aligned} \left| \frac{\partial}{\partial t} \left(\frac{\left|w_\rho\right|^\beta}{\left(M_\rho^w\right)^\beta} \frac{1}{1+\left|\nabla^\alpha w_\rho\right|^\lambda} \right) \right| &\leq C(\beta,\rho,m,\|u_0\|_{\mathcal{H}^1(\Omega)}) + C(\lambda,\rho,m,\|u_0\|_{\mathcal{H}^1(\Omega)}) \\ &= \zeta. \end{aligned}$$

Proof of (3.12). We have:

$$\begin{aligned} &\left\| \frac{\left|(w_1)_\rho\right|^\beta}{\left(M_\rho^{w_1}\right)^\beta} \frac{1}{1+\left|\nabla^\alpha (w_1)_\rho\right|^\lambda} - \frac{\left|(w_2)_\rho\right|^\beta}{\left(M_\rho^{w_2}\right)^\beta} \frac{1}{1+\left|\nabla^\alpha (w_2)_\rho\right|^\lambda} \right\|_{L^\infty(\Omega)} \\ &= \left\| \frac{\left|(w_1)_\rho\right|^\beta}{\left(M_\rho^{w_1}\right)^\beta} \left(\frac{1}{1+\left|\nabla^\alpha (w_1)_\rho\right|^\lambda} - \frac{1}{1+\left|\nabla^\alpha (w_2)_\rho\right|^\lambda} \right) + \frac{1}{1+\left|\nabla^\alpha (w_2)_\rho\right|^\lambda} \left(\frac{\left|(w_1)_\rho\right|^\beta}{\left(M_\rho^{w_1}\right)^\beta} - \frac{\left|(w_2)_\rho\right|^\beta}{\left(M_\rho^{w_2}\right)^\beta} \right) \right\|_{L^\infty(\Omega)} \\ &\leq \underbrace{\left\| \frac{1}{1+\left|\nabla^\alpha (w_1)_\rho\right|^\lambda} - \frac{1}{1+\left|\nabla^\alpha (w_2)_\rho\right|^\lambda} \right\|_{L^\infty(\Omega)}}_{A_2} + \underbrace{\left\| \frac{\left|(w_1)_\rho\right|^\beta \left(M_\rho^{w_2}\right)^\beta - \left|(w_2)_\rho\right|^\beta \left(M_\rho^{w_1}\right)^\beta}{\left(M_\rho^{w_1}\right)^\beta \left(M_\rho^{w_2}\right)^\beta} \right\|_{L^\infty(\Omega)}}_{B_2} . \end{aligned} \tag{3.16}$$

Using the convolution property, we obtain

$$\begin{aligned} A_2 &\leq C(\lambda) \left\| \left|\nabla^\alpha \mathcal{K}_\rho * w_1\right| - \left|\nabla^\alpha \mathcal{K}_\rho * w_2\right| \right\|_{L^\infty(\Omega)} \\ &\leq C(\lambda) \left\| \nabla^\alpha \mathcal{K}_\rho * w_1 - \nabla^\alpha \mathcal{K}_\rho * w_2 \right\|_{L^\infty(\Omega)} \\ &\leq C(\lambda) \left\| \nabla^\alpha \mathcal{K}_\rho * (w_1 - w_2) \right\|_{L^\infty(\Omega)} \\ &\leq C(\lambda,\rho) \|w_1 - w_2\|_{L^2(\Omega)} . \end{aligned} \tag{3.17}$$

Since $m^{\beta}\left\|\mathcal{K}_{\rho}\right\|_{L^1(\Omega)}^{\beta} \leq \left(M_{\rho}^{w_i}\right)^{\beta}$ for $i = 1, 2$, we observe that

$$\begin{aligned}
B_2 &\leq \frac{1}{m^{2\beta}\left\|\mathcal{K}_{\rho}\right\|_{L^1(\Omega)}^{2\beta}} \left\|\left|\mathcal{K}_{\rho} * w_1\right|^{\beta}\left(M_{\rho}^{w_2}\right)^{\beta} - \left|\mathcal{K}_{\rho} * w_2\right|^{\beta}\left(M_{\rho}^{w_1}\right)^{\beta}\right\|_{L^{\infty}(\Omega)} \\
&\leq C(m,\beta,\rho)\left(\left\|\left|\mathcal{K}_{\rho} * w_1\right|^{\beta}\left(\left(M_{\rho}^{w_2}\right)^{\beta} - \left(M_{\rho}^{w_1}\right)^{\beta}\right)\right\|_{L^{\infty}(\Omega)}\right. \\
&\left. + \left\|\left(M_{\rho}^{w_1}\right)^{\beta}\left(\left|\mathcal{K}_{\rho} * w_1\right|^{\beta} - \left|\mathcal{K}_{\rho} * w_2\right|^{\beta}\right)\right\|_{L^{\infty}(\Omega)}\right) \\
&\leq C(m,\beta,\rho,u_0)\left(\left\|\left|\mathcal{K}_{\rho} * w_1(x,y,t)\right|^{\beta} - \left|\mathcal{K}_{\rho} * w_2(x,y,t)\right|^{\beta}\right\|_{L^{\infty}(\Omega)}\right. \\
&\left. + \left\|\left|\mathcal{K}_{\rho} * w_1\right|^{\beta} - \left|\mathcal{K}_{\rho} * w_2\right|^{\beta}\right\|_{L^{\infty}(\Omega)}\right) \\
&\leq C(m,\beta,\rho,u_0)\left\|w_1 - w_2\right\|_{L^2(\Omega)}.
\end{aligned} \tag{3.18}$$

By substituting (3.17) and (3.18) into (3.16), we have:

$$\begin{aligned}
&\left\|\frac{\left|(w_1)_{\rho}\right|^{\beta}}{\left(M_{\rho}^{w_1}\right)^{\beta}}\frac{1}{1+\left|\nabla^{\alpha}(w_1)_{\rho}\right|^{\lambda}} - \frac{\left|(w_2)_{\rho}\right|^{\beta}}{\left(M_{\rho}^{w_2}\right)^{\beta}}\frac{1}{1+\left|\nabla^{\alpha}(w_2)_{\rho}\right|^{\lambda}}\right\|_{L^{\infty}(\Omega)} \\
&\leq C(\lambda,\rho)\left\|w_1 - w_2\right\|_{L^2(\Omega)} + C(m,\beta,\rho,u_0)\left\|w_1 - w_2\right\|_{L^2(\Omega)} \\
&= \xi\left\|w_1 - w_2\right\|_{L^2(\Omega)}.
\end{aligned}$$

This completes the proof of Proposition. □

By using (3.10) and (3.11), we can apply the classical Galerkin method [26] to prove that the linearized problem (3.7)-(3.9) has a unique weak solution $v_w \in W(0,T)$.

Lemma 3.1. *Let $v_w \in W(0,T)$ be the weak solution of the problem (3.7)-(3.9). Then*

$$0 < m \leq u_w(x,y,t) \leq \ell \text{ for a.e. } (x,y,t) \in \Omega \times (0,T). \tag{3.19}$$

Proof. We define $(u_w - \ell)_+$ as $(u_w - \ell)_+ = \max\{0, u_w - \ell\}$.

By multiplying equation (3.7) by $(u_w - \ell)_+$ and then integrating over Ω, we get:

$$\begin{aligned}
&\frac{1}{2}\frac{d}{dt}\int_{\Omega}\left|(u_w - \ell)_+\right|^2 dx\,dy \\
&= \int_{\Omega}\operatorname{div}\left(\frac{\left|w_{\rho}\right|^{\beta}}{\left(M_{\rho}^{w}\right)^{\beta}}\frac{1}{1+\left|\nabla^{\alpha}w_{\rho}\right|^{\lambda}}\nabla u_w\right)(u_w - \ell)_+ dx\,dy + \gamma\int_{\Omega}(u_0 - u_w)(u_w - \ell)_+\,dx\,dy,
\end{aligned}$$

using integration by parts and the Neumann boundary condition (3.9), we have

$$\begin{aligned}
&\frac{1}{2}\frac{d}{dt}\int_{\Omega}|(u_w-\ell)_+|^2\,dx\,dy\\
&=-\int_{\{u_w\geq\ell\}}\frac{|w_\rho|^\beta}{\left(M_\rho^w\right)^\beta}\frac{1}{1+\left|\nabla^\alpha w_\rho\right|^\lambda}\nabla u_w\cdot\nabla u_w\,dx\,dy+\gamma\int_{\{u_w\geq\ell\}}(u_0-u_w)\,(u_w-\ell)_+\,dx\,dy,
\end{aligned}$$

this implies that:

$$\begin{aligned}
&\frac{1}{2}\frac{d}{dt}\int_{\Omega}|(u_w-\ell)_+|^2\,dx\,dy+\int_{\{u_w\geq\ell\}}\frac{|w_\rho|^\beta}{\left(M_\rho^w\right)^\beta}\frac{1}{1+\left|\nabla^\alpha w_\rho\right|^\lambda}\,|\nabla u_w|^2\,dx\,dy\\
&+\gamma\int_{\{u_w\geq\ell\}}(u_w-u_0)\,(u_w-\ell)_+\;dx\,dy=0.
\end{aligned}$$

Since $\dfrac{|w_\rho|^\beta}{\left(M_\rho^w\right)^\beta}\dfrac{1}{1+\left|\nabla^\alpha w_\rho\right|^\lambda}>0$ and $(u_w-u_0)(u_w-\ell)_+\;\geq\;0$, we obtain:

$$\frac{d}{dt}\int_{\Omega}|(u_w-\ell)_+|^2\,dx\,dy\;\leq 0,$$

integrating over $(0,t)$ yields:

$$\int_{\Omega}|(u_w-\ell)_+|^2\,dx\,dy\;\leq\;\int_{\Omega}|(u_0-\ell)_+|^2\,dx\,dy,$$

given that $u_0\;\leq\;\ell$, it follows that:

$$\int_{\Omega}|(u_w-\ell)_+|^2\,dx\,dy\;\leq\;\int_{\Omega}|(u_0-\ell)_+|^2\,dx\,dy\;\leq 0.$$

As a result, the following inequality holds:

$$u_w(x,y,t)\;\leq\;\ell\quad\text{for a.e. }\;(x,y,t)\in\Omega\times(0,T).$$

Similarly, we define $(u_w-m)_-$ as $(u_w-m)_-=\min\{0,u_w-m\}$, multiplying the equation (3.7) by $(u_w-m)_-$ and then integrating over Ω, we conclude that:

$$0<\;m\leq\;u_w(x,y,t)\;\text{ for a.e. }\;(x,y,t)\in\Omega\times(0,T).$$

□

Lemma 3.2. *The linearized problem (3.7)-(3.9) admits a unique weak solution $u_w\in W(0,T)$ that satisfies the given estimates:*

i)

$$\|u_w\|_{L^\infty(0,T;L^2(\Omega))} \;\le\; \|u_0\|_{L^2(\Omega)} + \kappa_1,$$

ii)

$$\|u_w\|_{L^\infty(0,T;\mathcal{H}^1\Omega))} \;\le\; \kappa_2,$$

iii)

$$\int_0^T \left\|\frac{\partial u_w}{\partial t}\right\|^2_{(\mathcal{H}^1(\Omega))'} dt \;\le\; \kappa_3,$$

where the constants κ_1, κ_2, and κ_3 are positive and depend on $\|u_0\|_{\mathcal{H}^1(\Omega)}$, $\mathcal{K}_\rho$, ψ, m, and ℓ.

Proof. i): Multiplication of equation (3.7) by u_w, followed by integration by parts over Ω and the use of (3.9), leads to:

$$\frac{1}{2}\frac{d}{dt}\int_\Omega |u_w|^2\, dx\, dy + \int_\Omega \frac{\left|w_\rho\right|^\beta}{\left(M_\rho^w\right)^\beta}\frac{1}{1+\left|\nabla^\alpha w_\rho\right|^\lambda}\,|\nabla u_w|^2\, dx\, dy = \gamma \int_\Omega (u_0 - u_w)\, u_w\, dx\, dy.$$

Applying Young's inequality and (3.10), we obtain:

$$\frac{1}{2}\frac{d}{dt}\int_\Omega |u_w|^2\, dx\, dy + \psi\int_\Omega |\nabla u_w|^2\, dx\, dy \;\le\; \frac{\gamma^2}{2}\|u_0 - u_w\|^2_{L^2(\Omega)} + \frac{1}{2}\|u_w\|^2_{L^2(\Omega)}.$$

By using Lemma 3.1, we find

$$\begin{aligned} \|u_0 - u_w\|^2_{L^2(\Omega)} &\le 2\left(\|u_0\|^2_{\mathcal{H}^1(\Omega)} + \|u_w\|^2_{L^2(\Omega)}\right) \\ &\le 2\,\|u_0\|^2_{\mathcal{H}^1(\Omega)} + 2\ell^2|\Omega|. \end{aligned} \tag{3.20}$$

According to (3.20), we have

$$\begin{aligned} \frac{1}{2}\frac{d}{dt}\int_\Omega |u_w|^2\, dx\, dy + \psi\int_\Omega |\nabla u_w|^2\, dx\, dy &\le \gamma^2\,\|u_0\|^2_{\mathcal{H}^1(\Omega)} + \gamma^2\ell^2|\Omega| + \frac{\ell^2}{2}|\Omega| \\ &= C. \end{aligned} \tag{3.21}$$

By integrating inequality (3.21) over $(0,t)$, we get:

$$\frac{1}{2}\int_0^t \frac{d}{d\tau}\|u_w\|^2_{L^2(\Omega)}\, d\tau + \psi\int_0^t\int_\Omega |\nabla u_w|^2\, dx\, dy\, d\tau \;\le\; Ct,$$

hence, for a.e. $t \in (0,T]$,

$$\frac{1}{2}\|u_w(t)\|^2_{L^2(\Omega)} + \psi\int_0^t\int_\Omega |\nabla u_w|^2\, dx\, dy\, d\tau \;\le\; CT + \frac{1}{2}\|u_0\|^2_{L^2(\Omega)},$$

we conclude that

$$\|u_w\|_{L^\infty(0,T;L^2(\Omega))} \;\le\; \|u_0\|_{L^2(\Omega)} + \kappa_1.$$

ii): Multiplying equation (3.7) by $\dfrac{\partial u_w}{\partial t}$, integrating by parts over Ω, and using (3.9) imply that:

$$\int_\Omega \left|\frac{\partial u_w}{\partial t}\right|^2 dx\,dy + \int_\Omega \frac{\left|w_\rho\right|^\beta}{\left(M_\rho^w\right)^\beta} \frac{1}{1+\left|\nabla^\alpha w_\rho\right|^\lambda} \nabla u_w \cdot \nabla\left(\frac{\partial u_w}{\partial t}\right) dx\,dy$$
$$= \gamma \int_\Omega (u_0 - u_w) \frac{\partial u_w}{\partial t}\, dx\,dy.$$

According to Young's inequality, we obtain the result:

$$\int_\Omega \left|\frac{\partial u_w}{\partial t}\right|^2 dx\,dy + \int_\Omega \frac{\left|w_\rho\right|^\beta}{\left(M_\rho^w\right)^\beta} \frac{1}{1+\left|\nabla^\alpha w_\rho\right|^\lambda} \nabla u_w \cdot \nabla\left(\frac{\partial u_w}{\partial t}\right) dx\,dy$$
$$\leq \frac{\gamma^2}{2} \|u_0 - u_w\|^2_{L^2(\Omega)} + \frac{1}{2}\left\|\frac{\partial u_w}{\partial t}\right\|^2_{L^2(\Omega)}.$$

Observing that:

$$\int_\Omega \frac{\left|w_\rho\right|^\beta}{\left(M_\rho^w\right)^\beta} \frac{1}{1+\left|\nabla^\alpha w_\rho\right|^\lambda} \nabla u_w \cdot \nabla\left(\frac{\partial u_w}{\partial t}\right) dx\,dy$$
$$= \int_\Omega \frac{\left|w_\rho\right|^\beta}{\left(M_\rho^w\right)^\beta} \frac{1}{1+\left|\nabla^\alpha w_\rho\right|^\lambda} \nabla u_w \cdot \frac{\partial}{\partial t}(\nabla u_w)\, dx\,dy$$
$$= \frac{1}{2}\int_\Omega \frac{\left|w_\rho\right|^\beta}{\left(M_\rho^w\right)^\beta} \frac{1}{1+\left|\nabla^\alpha w_\rho\right|^\lambda} \frac{d}{dt}\left|\nabla u_w\right|^2 dx\,dy.$$

We also have:

$$\frac{1}{2}\int_\Omega \frac{\left|w_\rho\right|^\beta}{\left(M_\rho^w\right)^\beta} \frac{1}{1+\left|\nabla^\alpha w_\rho\right|^\lambda} \frac{d}{dt}\left|\nabla u_w\right|^2 dx\,dy$$
$$=\frac{1}{2}\frac{d}{dt}\int_\Omega \frac{\left|w_\rho\right|^\beta}{\left(M_\rho^w\right)^\beta} \frac{1}{1+\left|\nabla^\alpha w_\rho\right|^\lambda} \left|\nabla u_w\right|^2 dx\,dy - \frac{1}{2}\int_\Omega \frac{d}{dt}\left(\frac{\left|w_\rho\right|^\beta}{\left(M_\rho^w\right)^\beta} \frac{1}{1+\left|\nabla^\alpha w_\rho\right|^\lambda}\right)\left|\nabla u_w\right|^2 dx\,dy.$$

Therefore, by using the inequality (3.11), we deduce that

$$\int_\Omega \frac{\left|w_\rho\right|^\beta}{\left(M_\rho^w\right)^\beta} \frac{1}{1+\left|\nabla^\alpha w_\rho\right|^\lambda} \nabla u_w \cdot \nabla\left(\frac{\partial u_w}{\partial t}\right) dx\,dy$$
$$\geq \frac{1}{2}\frac{d}{dt}\int_\Omega \frac{\left|w_\rho\right|^\beta}{\left(M_\rho^w\right)^\beta} \frac{1}{1+\left|\nabla^\alpha w_\rho\right|^\lambda} \left|\nabla u_w\right|^2 dx\,dy - \frac{\zeta}{2}\|\nabla u_w\|^2_{L^2(\Omega)}. \tag{3.22}$$

Combining (3.20) and (3.22), we obtain

$$\frac{1}{2}\left\|\frac{\partial u_w}{\partial t}\right\|^2_{L^2(\Omega)} + \frac{1}{2}\frac{d}{dt}\int_\Omega \frac{|w_\rho|^\beta}{\left(M_\rho^w\right)^\beta}\frac{1}{1+\left|\nabla^\alpha w_\rho\right|^\lambda}|\nabla u_w|^2\,dx\,dy$$
$$\leq \gamma^2\,\|u_0\|^2_{\mathcal{H}^1(\Omega)} + \gamma^2\ell^2|\Omega| + \frac{\zeta}{2}\,\|\nabla u_w\|^2_{L^2(\Omega)}.$$

Noting in (3.10) that $0 < \psi \leq \frac{|w_\rho|^\beta}{\left(M_\rho^w\right)^\beta}\frac{1}{1+\left|\nabla^\alpha w_\rho\right|^\lambda}$ gives the following:

$$\psi\,\|\nabla u_w\|^2_{L^2(\Omega)} \leq \int_\Omega \frac{|w_\rho|^\beta}{\left(M_\rho^w\right)^\beta}\frac{1}{1+\left|\nabla^\alpha w_\rho\right|^\lambda}|\nabla u_w|^2\,dx\,dy,$$

which implies that:

$$\|\nabla u_w\|^2_{L^2(\Omega)} \leq \frac{1}{\psi}\int_\Omega \frac{|w_\rho|^\beta}{\left(M_\rho^w\right)^\beta}\frac{1}{1+\left|\nabla^\alpha w_\rho\right|^\lambda}|\nabla u_w|^2\,dx\,dy. \tag{3.23}$$

Applying (3.23) and substituting $C_0 = \gamma^2\,\|u_0\|^2_{\mathcal{H}^1(\Omega)} + \gamma^2\ell^2|\Omega|$, it follows that:

$$\frac{1}{2}\left\|\frac{\partial u_w}{\partial t}\right\|^2_{L^2(\Omega)} + \frac{1}{2}\frac{d}{dt}\int_\Omega \frac{|w_\rho|^\beta}{\left(M_\rho^w\right)^\beta}\frac{1}{1+\left|\nabla^\alpha w_\rho\right|^\lambda}|\nabla u_w|^2\,dx\,dy$$
$$\leq C_0 + \frac{C_1}{2}\int_\Omega \frac{|w_\rho|^\beta}{\left(M_\rho^w\right)^\beta}\frac{1}{1+\left|\nabla^\alpha w_\rho\right|^\lambda}|\nabla u_w|^2\,dx\,dy, \tag{3.24}$$

where $C_1 = \dfrac{\zeta}{\psi}$.

It is evident that

$$\frac{d}{dt}\int_\Omega \frac{|w_\rho|^\beta}{\left(M_\rho^w\right)^\beta}\frac{1}{1+\left|\nabla^\alpha w_\rho\right|^\lambda}|\nabla u_w|^2\,dx\,dy$$
$$\leq 2C_0 + C_1\int_\Omega \frac{|w_\rho|^\beta}{\left(M_\rho^w\right)^\beta}\frac{1}{1+\left|\nabla^\alpha w_\rho\right|^\lambda}|\nabla u_w|^2\,dx\,dy.$$

Employing Gronwall's lemma, we derive:

$$\int_\Omega \frac{\left|w_\rho(x,y,t)\right|^\beta}{\left(M_\rho^w\right)^\beta}\frac{1}{1+\left|\nabla^\alpha w_\rho(x,y,t)\right|^\lambda}\left|\nabla u_w(x,y,t)\right|^2\,dx\,dy \leq e^{C_1 t}(C_2 + 2C_0 t),$$

for a.e. $t \in (0, T]$, where

$$C_2 = \int_{\Omega} \frac{\left|w_\rho(x,y,0)\right|^{\beta}}{\left(M_\rho^w\right)^{\beta}} \frac{1}{1 + \left|\nabla^\alpha w_\rho(x,y,0)\right|^{\lambda}} \left|\nabla u_w(x,y,0)\right|^2 dx\, dy.$$

From (3.23), we have

$$\|\nabla u_w\|^2_{L^2(\Omega)} \leq \frac{1}{\psi} e^{C_1 T}(C_2 + 2C_0 T). \tag{3.25}$$

Furthermore, from (3.24), we can deduce that

$$\begin{aligned} &\frac{1}{2}\left\|\frac{\partial u_w}{\partial t}\right\|^2_{L^2(\Omega)} + \frac{1}{2}\frac{d}{dt}\int_{\Omega} \frac{\left|w_\rho\right|^{\beta}}{\left(M_\rho^w\right)^{\beta}} \frac{1}{1 + \left|\nabla^\alpha w_\rho\right|^{\lambda}} |\nabla u_w|^2 dx\, dy \\ &\leq C_0 + \frac{C_1}{2} e^{C_1 T}(C_2 + 2C_0 T). \end{aligned} \tag{3.26}$$

By integrating (3.26) over $(0, t)$, we get to that

$$\begin{aligned} &\int_0^t \left\|\frac{\partial u_w}{\partial \tau}\right\|^2_{L^2(\Omega)} d\tau + \int_{\Omega} \frac{\left|w(x,y,t)_\rho\right|^{\beta}}{\left(M_\rho^w\right)^{\beta}} \frac{1}{1 + \left|\nabla^\alpha w(x,y,t)_\rho\right|^{\lambda}} \left|\nabla u_w(x,y,t)\right|^2 dx\, dy \\ &\leq \left(2C_0 + C_1 e^{C_1 T}(C_2 + 2C_0 T)\right) t + C_2, \end{aligned}$$

for a.e $t \in (0, T]$.

We see that:

$$\int_0^t \left\|\frac{\partial u_w}{\partial \tau}\right\|^2_{L^2(\Omega)} d\tau \leq \left(2C_0 + C_1 e^{C_1 T}(C_2 + 2C_0 T)\right) T + C_2. \tag{3.27}$$

According to $u_w(x,y,t) = u_w(x,y,0) + \int_0^t \frac{\partial u_w}{\partial \tau} d\tau$, inequalities (1.15), and (3.27), we have

$$\begin{aligned} \|u_w\|^2_{L^2(\Omega)} &\leq 2\,\|u_0\|^2_{\mathcal{H}^1(\Omega)} + 2T \int_0^t \left\|\frac{\partial u_w(\tau)}{\partial \tau}\right\|^2_{L^2(\Omega)} d\tau \\ &\leq 2\,\|u_0\|^2_{\mathcal{H}^1(\Omega)} + 2T^2\left(2C_0 + C_1 e^{C_1 t}(C_2 + 2C_0 t)\right) + C_2 T. \end{aligned} \tag{3.28}$$

From (3.28) and (3.25), it follows that

$$\|u_w\|_{L^\infty(0,T;\mathcal{H}^1(\Omega))} \leq \kappa_2. \tag{3.29}$$

iii): Multiplying (3.7) by $\varphi \in \mathcal{H}^1(\Omega)$ where $\|\varphi\|_{\mathcal{H}^1(\Omega)} \leq 1$, applying Cauchy-Schwarz's inequality, and combining (3.20) and (3.29), we acquire that:

$$\left|\left\langle \frac{\partial u_w}{\partial t}, \varphi \right\rangle\right| = \left| \int_\Omega \frac{\left|w_\rho\right|^\beta}{\left(M_\rho^w\right)^\beta} \frac{1}{1+\left|\nabla^\alpha w_\rho\right|^\lambda} \nabla u_w \cdot \nabla \varphi \, dx\, dy + \gamma \int_\Omega (u_0 - u_w)\, \varphi \, dx\, dy \right|$$
$$\leq \left(\left| \frac{\left|w_\rho\right|^\beta}{\left(M_\rho^w\right)^\beta} \frac{1}{1+\left|\nabla^\alpha w_\rho\right|^\lambda} \right| \|\nabla u_w\|_{L^2(\Omega)} + \gamma \|u_0 - u_w\|_{L^2(\Omega)} \right) \|\varphi\|_{\mathcal{H}^1(\Omega)}$$
$$\leq \left(\kappa_2 + \sqrt{2}\gamma \|u_0\|_{\mathcal{H}^1(\Omega)} + \sqrt{2|\Omega|}\gamma \ell\right) \|\varphi\|_{\mathcal{H}^1(\Omega)} .$$

Consequently, we obtain

$$\left\| \frac{\partial u_w}{\partial t} \right\|_{(\mathcal{H}^1(\Omega))'} \leq \kappa_0 + \sqrt{2}\gamma \|u_0\|_{\mathcal{H}^1(\Omega)} , \tag{3.30}$$

where $\kappa_0 = \kappa_2 + \sqrt{2|\Omega|}\gamma \ell$.

In addition, by squaring (3.30) and integrating over $(0, T)$, we get to that:

$$\int_0^T \left\| \frac{\partial u_w}{\partial t} \right\|^2_{(\mathcal{H}^1(\Omega))'} dt \leq \kappa_3 .$$

The proof is complete. □

Existence of a weak solution

Theorem 3.1. *Assuming that $u_0 \in \mathcal{H}^1(\Omega)$ and that (3.4) holds, the problem defined by (3.1)-(3.3) admits a weak solution $v \in W(0, T)$.*

Proof. We now establish the existence of a weak solution to the underlying problem using Schauder fixed-point theorem. To this end, we introduce the subset $\bar{W}$ of $W(0, T)$, defined by:

$$\bar{W} = \left\{ \begin{array}{l} w \in W(0,T); \|w\|_{L^\infty(0,T;\mathcal{H}^1(\Omega))} \leq \kappa_2, \|w\|_{L^\infty(0,T;L^2(\Omega))} \leq \|u_0\|_{L^2(\Omega)} , \left\| \frac{\partial w}{\partial t} \right\|_{L^2(0,T;(\mathcal{H}^1(\Omega))')} \leq \kappa_3, \\ 0 < m \leq w(x, y, t) \leq \ell \text{ for a.e. } (x, y, t) \in \Omega \times (0, T), w(0) = u_0 \end{array} \right\} .$$

Furthermore, it can be shown that $\bar{W}$ is a nonempty and convex subset of $W(0, T)$. Since the functions in $\bar{W}$ satisfy uniform bounds, the set is bounded in $W(0, T)$ and is also weakly closed. As $W(0, T)$ is a reflexive Banach space, the Banach-Alaoglu theorem [43] ensures that $\bar{W}$ is weakly compact in $W(0, T)$. Moreover, by the Eberlein-Smulaian theorem [24], weak compactness and weak sequential compactness are equivalent in Banach spaces. Therefore, $\bar{W}$ is weakly sequential compact in $W(0,T)$. Subsequently, we define the next mapping:

$$Q : \bar{W} \to \bar{W}$$

$$w \mapsto u_w.$$

To apply Schauder's fixed-point theorem, we must prove that the mapping $Q : w \mapsto u_w$ is weakly continuous from $\bar{W}$ into $\bar{W}$. Consider a sequence w_j in $\bar{W}$ that weakly converges to some w in $\bar{W}$, and let $u_j = Q(w_j)$. Our objective is to demonstrate that $Q(w_j) := u_j$ weakly converges to $Q(w) := u_w$. By applying lemma 3.2 and using classical results of compact inclusion in Sobolev spaces [2], we can extract sub-sequences of w_j and u_j (still denoted by w_j and u_j), hence we obtain:

$$w_j \to w \text{ in } L^2((0,T);L^2(\Omega)) \text{ and a.e. on } \Omega \times (0,T), \tag{3.31}$$

$$\mathcal{K}_\rho * w_j \to \mathcal{K}_\rho * w \text{ in } L^2((0,T);L^2(\Omega)) \text{ and a.e. on } \Omega \times (0,T), \tag{3.32}$$

$$\left|\mathcal{K}_\rho * w_j\right|^\beta \to \left|\mathcal{K}_\rho * w\right|^\beta \text{ in } L^2((0,T);L^2(\Omega)) \text{ and a.e. on } \Omega \times (0,T), \tag{3.33}$$

$$\frac{\left|(w_j)_\rho\right|^\beta}{\left(M_\rho^{w_j}\right)^\beta} \to \frac{\left|w_\rho\right|^\beta}{\left(M_\rho^{w}\right)^\beta} \text{ in } L^2((0,T);L^2(\Omega)) \text{ and a.e. on } \Omega \times (0,T), \tag{3.34}$$

$${}^C\mathcal{D}_x^\alpha (w_j)_\rho \to {}^C\mathcal{D}_x^\alpha w_\rho, {}^C\mathcal{D}_y^\alpha (w_j)_\rho \to {}^C\mathcal{D}_y^\alpha w_\rho \text{ in } L^2((0,T);L^2(\Omega)) \tag{3.35}$$

and a.e. on $\Omega \times (0,T)$,

$$\left|\nabla^\alpha (w_j)_\rho\right|^\lambda \to \left|\nabla^\alpha w_\rho\right|^\lambda \text{ in } L^2((0,T);L^2(\Omega)) \text{ and a.e. on } \Omega \times (0,T), \tag{3.36}$$

$$\frac{1}{1+\left|\nabla^\alpha (w_j)_\rho\right|^\lambda} \to \frac{1}{1+\left|\nabla^\alpha w_\rho\right|^\lambda} \text{ in } L^2((0,T);L^2(\Omega)) \text{ and a.e. on } \Omega \times (0,T), \tag{3.37}$$

$$u_j \to u \text{ weakly in } L^\infty((0,T);\mathcal{H}^1(\Omega)), \tag{3.38}$$

$$\frac{\partial u_j}{\partial t} \to \frac{\partial u}{\partial t} \text{ weakly in } L^2((0,T);(\mathcal{H}^1(\Omega))'), \tag{3.39}$$

$$u_j \to u \text{ in } L^2((0,T);L^2(\Omega)) \text{ and a.e. on } \Omega \times (0,T), \tag{3.40}$$

$$\nabla u_j \to \nabla u \text{ weakly in } L^\infty((0,T);L^2(\Omega)), \tag{3.41}$$

$$u_j(0) \to u(0) \text{ in } L^2(\Omega). \tag{3.42}$$

The (3.33), (3.34), and (3.37) are acquired by applying the dominated convergence theorem [10].

Since u_j is the weak solution of (3.7) associated with w_j, we have, for almost every $t \in (0,T]$, and

$\varphi \in \mathcal{H}^1(\Omega)$:

$$\int_\Omega \frac{\partial v_j}{\partial t}\,\varphi\,dx\,dy + \int_\Omega \frac{\left|(w_j)_\rho\right|^\beta}{(M^{w_j})^\beta}\frac{1}{1+\left|\nabla^\alpha (w_j)_\rho\right|^\lambda}\nabla u_j.\nabla\varphi\,dx\,dy = \gamma\int_\Omega \left(u_j(0)-u_j\right)\varphi\,dx\,dy. \tag{3.43}$$

Integrating (3.43) over $(0,T)$ yields

$$\begin{aligned}&\int_0^T\int_\Omega \frac{\partial v_j}{\partial t}\,\varphi\,dx\,dy\,dt + \int_0^T\int_\Omega \frac{\left|(w_j)_\rho\right|^\beta}{(M^{w_j})^\beta}\frac{1}{1+\left|\nabla^\alpha (w_j)_\rho\right|^\lambda}\nabla u_j.\nabla\varphi\,dx\,dy\,dt\\&= \gamma\int_0^T\int_\Omega \left(u_j(0)-u_j\right)\varphi\,dx\,dy\,dt.\end{aligned} \tag{3.44}$$

From (3.39), we have

$$\int_0^T\int_\Omega \frac{\partial u_j}{\partial t}\,\varphi\,dx\,dy\,dt \to \int_0^T\int_\Omega \frac{\partial u}{\partial t}\,\varphi\,dx\,dy\,dt, \quad \text{as } j\to\infty.$$

Examining the second term in (3.44)

$$\begin{aligned}&\left|\int_0^T\int_\Omega \frac{\left|(w_j)_\rho\right|^\beta}{\left(M_\rho^{(w_j)}\right)^\beta}\frac{1}{1+\left|\nabla^\alpha (w_j)_\rho\right|^\lambda}\nabla u_j\cdot\nabla\varphi\,dx\,dy\,dt - \int_0^T\int_\Omega \frac{\left|w_\rho\right|^\beta}{\left(M_\rho^{w}\right)^\beta}\frac{1}{1+\left|\nabla^\alpha w_\rho\right|^\lambda}\nabla u\cdot\nabla\varphi\,dx\,dy\,dt\right|\\&\le \int_0^T\int_\Omega\left|\frac{\left|(w_j)_\rho\right|^\beta}{\left(M_\rho^{w_j}\right)^\beta}\frac{1}{1+\left|\nabla^\alpha (w_j)_\rho\right|^\lambda} - \frac{\left|w_\rho\right|^\beta}{\left(M_\rho^{w}\right)^\beta}\frac{1}{1+\left|\nabla^\alpha w_\rho\right|^\lambda}\right||\nabla u|\left|\nabla\varphi\right|\,dx\,dy\,dt\\&+\left|\int_0^T\int_\Omega \frac{\left|(w_j)_\rho\right|^\beta}{\left(M_\rho^{w_j}\right)^\beta}\frac{1}{1+\left|\nabla^\alpha (w_j)_\rho\right|^\lambda}\nabla(u_j-u)\cdot\nabla\varphi\,dx\,dy\,dt\right|.\end{aligned}$$

According to 3.12, we deduce, as $j\to\infty$

$$\begin{aligned}&\int_0^T\int_\Omega\left|\frac{\left|(w_j)_\rho\right|^\beta}{(M^{w_j})^\beta}\frac{1}{1+\left|\nabla^\alpha (w_j)_\rho\right|^\lambda} - \frac{\left|w_\rho\right|^\beta}{\left(M_\rho^{w}\right)^\beta}\frac{1}{1+\left|\nabla^\alpha w_\rho\right|^\lambda}\right||\nabla u|\left|\nabla\varphi\right|\,dx\,dy\,dt\\&\le C\int_0^T\int_\Omega \left\|w_j-w\right\|_{L^2(\Omega)}|\nabla u|\left|\nabla\varphi\right|\,dx\,dy\,dt\\&\le C(\varphi)\left\|w_j-w\right\|_{L^2(\Omega)}\|\nabla u\|_{L^2((0,T);L^2(\Omega))}\to 0,\end{aligned}$$

and also, as $j\to\infty$,

$$\left|\int_0^T\int_\Omega \frac{\left|(w_j)_\rho\right|^\beta}{\left(M_\rho^{w_j}\right)^\beta}\frac{1}{1+\left|\nabla^\alpha (w_j)_\rho\right|^\lambda}\nabla(u_j-u)\cdot\nabla\varphi\,dx\,dy\,dt\right|\to 0.$$

Through (3.40) and (3.42), we obtain

$$\int_0^T \int_\Omega \left(u_j(0) - u_j\right) \varphi \, dx \, dy \, dt \to \int_0^T \int_\Omega (u_0 - u) \, \varphi \, dx \, dy \, dt.$$

Letting $j \to \infty$ in (3.44) implies that

$$\int_0^T \int_\Omega \frac{\partial u}{\partial t} \varphi \, dx \, dy \, dt + \int_0^T \int_\Omega \frac{\left|w_\rho\right|^\beta}{\left(M_\rho^w\right)^\beta} \frac{1}{1 + \left|\nabla^\alpha w_\rho\right|^\lambda} \nabla u . \nabla \varphi \, dx \, dy \, dt = \gamma \int_0^T \int_\Omega (u_0 - u) \, \varphi \, dx \, dy \, dt.$$

Therefore, by the arbitrariness of $\varphi \in \mathcal{H}^1(\Omega)$, we get for a.e $t \in (0, T]$

$$\int_\Omega \frac{\partial v}{\partial t} \varphi \, dx \, dy + \int_\Omega \frac{\left|w_\rho\right|^\beta}{\left(M_\rho^w\right)^\beta} \frac{1}{1 + \left|\nabla^\alpha w_\rho\right|^\lambda} \nabla u . \nabla \varphi \, dx \, dy = \gamma \int_\Omega (u_0 - u) \, \varphi \, dx \, dy.$$

Hence, it follows that

$$u = u_w = Q(w).$$

Furthermore, given the uniqueness of the solution to problem (3.7), the whole sequence $u_j = Q(w_j)$ converge weakly in $\bar{W}$ to $u = Q(w)$. This confirms that Q is weakly continuous.

Therefore, by Schauder's fixed-point theorem, there exists $w \in \bar{W}$ such that

$$w = Q(w) = u_w.$$

Consequently, the existence of the weak solution u_w to the problem (3.1)-(3.3), is proved. □

Uniqueness of the weak solution

Theorem 3.2. *Assuming that u is a weak solution to (3.1)-(3.3), then this solution is unique.*

Proof. Let u_1, u_2 be tow weak solutions of (3.1)-(3.3). Then for a.e $t \in (0, T)$, we have

$$\begin{cases} \dfrac{\partial u_i}{\partial t} = \operatorname{div}\left(\dfrac{\left|(u_i)_\rho\right|^\beta}{\left(M_\rho^{u_i}\right)^\beta} \dfrac{1}{1 + \left|\nabla^\alpha (u_i)_\rho\right|^\lambda} \nabla u_i \right) + \gamma \left(u_0 - u_i\right) & \Omega \times (0, T), \\ u_i(x, y, 0) = u_0(x, y), & \Omega, \\ \nabla v_i . \vec{n} = 0, & \text{on } \partial\Omega \times (0, T). \end{cases} \tag{3.45}$$

Such that $i = 1, 2$.

Denote $\bar{u} = u_1 - u_2$. Then we can get:

$$\frac{\partial \bar{u}}{\partial t} - \operatorname{div}\left(\frac{\left|(u_1)_\rho\right|^\beta}{\left(M_\rho^{u_1}\right)^\beta}\frac{1}{1+\left|\nabla^\alpha (u_1)_\rho\right|^\lambda}\nabla \bar{u}\right)$$
$$= \operatorname{div}\left(\left(\frac{\left|(u_1)_\rho\right|^\beta}{\left(M_\rho^{u_1}\right)^\beta}\frac{1}{1+\left|\nabla^\alpha (u_1)_\rho\right|^\lambda} - \frac{\left|(u_2)_\rho\right|^\beta}{\left(M_\rho^{u_2}\right)^\beta}\frac{1}{1+\left|\nabla^\alpha (u_2)_\rho\right|^\lambda}\right)\nabla u_2\right) - \gamma\,\bar{u} \qquad \text{in}\,\Omega\times(0,T)\,, \tag{3.46}$$

with initial condition:

$$\bar{u}(x,y,0) = 0\ \Omega, \tag{3.47}$$

and Neumann boundary condition:

$$\nabla\bar{u}.\vec{n} = 0,\ \text{ on}\,\partial\Omega\times(0,T)\,. \tag{3.48}$$

Multiplying (3.46) by $\bar{u}$, and integrating over Ω, we obtain:

$$\int_\Omega \frac{\partial \bar{u}}{\partial t}\,\bar{u}\,dx\,dy - \int_\Omega \operatorname{div}\left(\frac{\left|(u_1)_\rho\right|^\beta}{\left(M_\rho^{u_1}\right)^\beta}\frac{1}{1+\left|\nabla^\alpha (u_1)_\rho\right|^\lambda}\nabla \bar{u}\right)\bar{u}\,dx\,dy$$
$$= \int_\Omega \operatorname{div}\left(\left(\frac{\left|(u_1)_\rho\right|^\beta}{\left(M_\rho^{u_1}\right)^\beta}\frac{1}{1+\left|\nabla^\alpha (u_1)_\rho\right|^\lambda} - \frac{\left|(u_2)_\rho\right|^\beta}{\left(M_\rho^{u_2}\right)^\beta}\frac{1}{1+\left|\nabla^\alpha (u_2)_\rho\right|^\lambda}\right)\nabla u_2\right)\bar{u}\,dx\,dy - \gamma\int_\Omega |\bar{u}|^2\,dx\,dy.$$

By applying the integration by parts formula, we have:

$$\frac{1}{2}\frac{d}{dt}\int_\Omega |\bar{u}|^2\,dx\,dy + \int_\Omega \frac{\left|(u_1)_\rho\right|^\beta}{\left(M_\rho^{u_1}\right)^\beta}\frac{1}{1+\left|\nabla^\alpha (u_1)_\rho\right|^\lambda}|\nabla\bar{u}|^2\,dx\,dy - \int_{\partial\Omega}\left(\frac{\left|(u_1)_\rho\right|^\beta}{\left(M_\rho^{u_1}\right)^\beta}\frac{1}{1+\left|\nabla^\alpha (u_1)_\rho\right|^\lambda}\nabla\bar{u}.\vec{n}\right)\bar{u}\,ds$$
$$= -\int_\Omega \left(\frac{\left|(u_1)_\rho\right|^\beta}{\left(M_\rho^{u_1}\right)^\beta}\frac{1}{1+\left|\nabla^\alpha (u_1)_\rho\right|^\lambda} - \frac{\left|(u_2)_\rho\right|^\beta}{\left(M_\rho^{u_2}\right)^\beta}\frac{1}{1+\left|\nabla^\alpha (u_2)_\rho\right|^\lambda}\right)\nabla u_2.\nabla\bar{u}\,dx\,dy$$
$$+ \int_{\partial\Omega}\left(\left(\frac{\left|(u_1)_\rho\right|^\beta}{\left(M_\rho^{u_1}\right)^\beta}\frac{1}{1+\left|\nabla^\alpha (u_1)_\rho\right|^\lambda} - \frac{\left|(u_2)_\rho\right|^\beta}{\left(M_\rho^{u_2}\right)^\beta}\frac{1}{1+\left|\nabla^\alpha (u_2)_\rho\right|^\lambda}\right)\nabla u_2.\vec{n}\right)\bar{u}\,ds - \gamma\int_\Omega |\bar{u}|^2\,dx\,dy.$$

Using the homogeneous Neumann boundary conditions stated in (3.45) and (3.48), we obtain:

$$\frac{1}{2}\frac{d}{dt}\int_\Omega |\bar{u}|^2\,dx\,dy + \int_\Omega \frac{\left|(u_1)_\rho\right|^\beta}{\left(M_\rho^{u_1}\right)^\beta}\frac{1}{1+\left|\nabla^\alpha (u_1)_\rho\right|^\lambda}|\nabla\bar{u}|^2\,dx\,dy$$
$$= -\int_\Omega \left(\frac{\left|(u_1)_\rho\right|^\beta}{\left(M_\rho^{u_1}\right)^\beta}\frac{1}{1+\left|\nabla^\alpha (u_1)_\rho\right|^\lambda} - \frac{\left|(u_2)_\rho\right|^\beta}{\left(M_\rho^{u_2}\right)^\beta}\frac{1}{1+\left|\nabla^\alpha (u_2)_\rho\right|^\lambda}\right)\nabla u_2.\nabla\bar{u}\,dx\,dy - \gamma\int_\Omega |\bar{u}|^2\,dx\,dy. \tag{3.49}$$

In view of proof to (3.10), there exists a constant $\psi_1 > 0$, such that:

$$\psi_1 \le \frac{\left|(u_1(x,y,t))_\rho\right|^\beta}{\left(M_\rho^{u_1}\right)^\beta} \frac{1}{1+\left|\nabla^\alpha (u_1(x,y,t))_\rho\right|^\lambda} \le 1, \quad \text{for a.e. } (x,y,t) \in \Omega \times (0,T).$$

Furthermore, according to (3.12) we find

$$\left\| \frac{\left|(u_1)_\rho\right|^\beta}{\left(M_\rho^{u_1}\right)^\beta} \frac{1}{1+\left|\nabla^\alpha (u_1)_\rho\right|^\lambda} - \frac{\left|(u_2)_\rho\right|^\beta}{\left(M_\rho^{u_2}\right)^\beta} \frac{1}{1+\left|\nabla^\alpha (u_2)_\rho\right|^\lambda} \right\|_{L^\infty(\Omega)} \le C \|\bar{u}\|_{L^2(\Omega)}, \tag{3.50}$$

where C is a positive constant.

Therefore, by substituting the estimate (3.50) into (3.49), we get

$$\frac{1}{2}\frac{d}{dt} \|\bar{u}\|^2_{L^2(\Omega)} + \psi_1 \|\nabla \bar{u}\|^2_{L^2(\Omega)} \le C \|\bar{u}\|_{L^2(\Omega)} \|\nabla u_2\|_{L^2(\Omega)} \|\nabla \bar{u}\|_{L^2(\Omega)} - \gamma \|\bar{u}\|^2_{L^2(\Omega)}.$$

By applying the Young's inequality

$$\mu.\nu \le \frac{\psi_1 \mu^2}{2} + \frac{\nu^2}{2\psi_1}, \quad \mu, \nu, \psi_1 \in \mathbb{R}^+.$$

We conclude that:

$$\frac{1}{2}\frac{d}{dt} \|\bar{u}\|^2_{L^2(\Omega)} + \psi_1 \|\nabla \bar{u}\|^2_{L^2(\Omega)} \le \frac{C^2}{2\psi_1} \|\bar{u}\|^2_{L^2(\Omega)} \|\nabla u_2\|^2_{L^2(\Omega)} + \frac{\psi_1}{2} \|\nabla \bar{u}\|^2_{L^2(\Omega)} - \gamma \|\bar{u}\|^2_{L^2(\Omega)},$$

which implies

$$\frac{d}{dt} \|\bar{u}\|^2_{L^2(\Omega)} \le \left(\frac{C^2}{\psi_1} \|\nabla u_2\|^2_{L^2(\Omega)} - 2\gamma \right) \|\bar{u}\|^2_{L^2(\Omega)}.$$

Since, $\bar{u}(0) = 0$, applying Gronwall's inequality yields

$$\|\bar{u}(t)\|^2_{L^2(\Omega)} \le 0.$$

In other words, $u_1 = u_2$. □

Remark 3.1. *(**Boundedness of the weak solution**). According to theorem 3.1, the weak solution of problem (3.1)-(3.3) belongs to $\bar{\mathbb{W}}$ and $w = Q(w) = u_w$ is the fixed point of (3.1)-(3.3). Thus, u_w is also in $\bar{\mathbb{W}}$. Given the uniqueness of the solution, we conclude that the unique weak solution $v = u_w$ satisfies the extremum principle:*

$$0 < m \leq u(x, y, t) \leq \ell \text{ for a.e. } (x, y, t) \in \Omega \times (0, T),$$

such that:

$$0 < m := \operatorname{ess} \inf_{x,y \in \Omega} u_0(x, y) \text{ and } \ell := \operatorname{ess} \sup_{x,y \in \Omega} u_0(x, y) < \infty.$$

The obtained extremum principle ensures that the weak solution remains uniformly bounded between the infimum and supermum of the initial data throughout the entire evolution. In particular, the solution preserves its positivity and does not exceed the upper bound determined by the initial condition. This property plays a fundamental role in the qualitative analysis of the model, as it prevents the occurrence of nonphysical behaviors such as negativity or blow-up. Moreover, it provides uniform a priori bounds that are crucial for establishing further results concerning the stability, and regularity of the solution.

3.4 Numerical implementation

This section is devoted to the numerical implementation of the proposed Caputo-based nonlinear diffusion model with the inclusion of a gray-level indicator.

The numerical scheme follows the same semi-implicit additive operator splitting (AOS) approach introduced in Chapter 2, ensuring computational efficiency and stability. The main difference in this model is the incorporation of the gray-level indicator into the diffusion coefficient, which allows the diffusion to adapt locally to the image intensity while maintaining the global nonlocal effects of the Caputo derivative. All other aspects of the finite difference discretization remain as in the previous chapter.

The main steps of the implementation are summarized in Algorithm 2.

Algorithm 2 AOS algorithm with diffusivity based on gray-level indicator and the Caputo derivative

Input: Original image U^0, time step Δt, number of iterations N_t, parameters α, ρ, β, λ, η
Initialize: $U^n := U^0$
for $n = 1$ to N_t **do**
  Compute $\tilde{U} := U^n + \eta\,\Delta t\,(U^0 - U^n)$
  Regularization: Compute the smoothed version using convolution $v := \mathcal{K}_\rho * U^n$
  Compute the diffusivity:

- **Compute gray-level indicator:**
  1. $\mathcal{M} := \max|v|$
  2. $G_{Indicator} := \dfrac{|v|^\beta}{(\mathcal{M})^\beta}$
- Approximate the fractional gradient $\nabla^\alpha v$ using the Caputo fractional derivative (Section 2.5.3)
- Compute the diffusivity function $\hbar := \left(G_{Indicator} \cdot \dfrac{1}{1 + |\nabla^\alpha v|^\lambda}\right)$ at each pixel

  Solve 1D system in x-direction:

$$R := (2I - 4\Delta t\, O_x)^{-1}\tilde{U}$$

  Solve tridiagonal system using Thomas algorithm
  Solve 1D system in y-direction:

$$P := (2I - 4\Delta t\, O_y)^{-1}\tilde{U}$$

  Solve tridiagonal system using Thomas algorithm
  Combine results:

$$U^{n+1} := R + P$$

end for
Output: U^{n+1}

3.5 Conclusion

This chapter has introduced and rigorously analyzed a nonlinear diffusion model for image denoising, in which the diffusion coefficient depends on the image gradient, gray-level information, and fractional-order derivatives in the sense of Caputo. The interplay between the Caputo fractional derivative and gray-level adaptation allows the model to effectively balance noise suppression with the preservation of essential structural details. Additionally, the incorporation of a Gaussian kernel improves the model's robustness and facilitates the derivation of key analytical properties.

A thorough theoretical investigation of the underlying nonlinear diffusion equation has been carried out. Using Schauder's fixed-point theorem, we established the existence and uniqueness of the weak solution and derived a priori estimates ensuring their boundedness. These results confirm the well-posedness of the proposed model and provide a solid mathematical foundation for its further study.

On the numerical side, the semi-implicit AOS scheme was adapted to this formulation, with the gray-level indicator incorporated into the diffusion coefficient. The resulting algorithm offers an efficient and stable implementation, complementing the theoretical findings and supporting the practical applicability of the model in image denoising.

CHAPTER 4

WEAK SOLUTION OF A SPATIAL FRACTIONAL NONLINEAR DIFFUSION EQUATION: EXISTENCE AND UNIQUENESS

The results presented in this chapter are based on the findings reported in [11].

4.1 Introduction

In this chapter, we focus on the theoretical study of a spatial fractional nonlinear diffusion equation. The proposed model is a parabolic PDE that interpolates between the second- and fourth-order nonlinear diffusion equations. In this model, the integer-order spatial derivatives in the Perona-Malik diffusion equation are replaced by fractional-order Caputo derivatives. The model is also inspired by the Catte-Lions-Morel model, where a Gaussian kernel function is used to regularize the diffusion coefficient, thereby enhancing well-posedness from a theoretical perspective and improving robustness in image denoising. Furthermore, we incorporate the fidelity term, as presented in [7], into this model.

The structure of this paper is outlined as follows. In section 4.2, we present some basic results and definitions of fractional calculus, and fractional-order Sobolev space. In section 4.3, we propose a fractional-order diffusion model. In section 4.4, we study the existence and uniqueness of weak solution of our proposed model. Section 4.5, provides the conclusion, constituting the final part in this paper.

4.2 Preliminaries and definitions

This section introduces the fractional calculus and the associated function spaces.

The fractional gradient of order α of $\mathcal{K}_\rho$ is defined as follows:

$$\nabla^\alpha \mathcal{K}_\rho(x,y) = \left({}^C\mathcal{D}_x^\alpha \mathcal{K}_\rho(x,y), {}^C\mathcal{D}_y^\alpha \mathcal{K}_\rho(x,y)\right),$$

and the magnitude of the fractional gradient is given by:

$$\left|\nabla^{\alpha}\mathcal{K}_{\rho}(x,y)\right| = \sqrt{({}^{C}\mathcal{D}_x^{\alpha}\mathcal{K}_{\rho}(x,y))^2 + ({}^{C}\mathcal{D}_y^{\alpha}\mathcal{K}_{\rho}(x,y))^2},$$

where ${}^{C}\mathcal{D}_x^{\alpha}\mathcal{K}_{\rho}(x,y)$ represents the fractional derivative of order α of $\mathcal{K}_{\rho}(x,y)$ with respect to the variable x, and ${}^{C}\mathcal{D}_y^{\alpha}\mathcal{K}_{\rho}(x,y)$ represents the fractional derivative of order α of $\mathcal{K}_{\rho}(x,y)$ with respect to the variable y.

From (1.12), we obtain:

$$\begin{aligned}
{}^{C}\mathcal{D}_x^{\alpha}\mathcal{K}_{\rho}(x,y) &= \frac{1}{\Gamma(2-\alpha)}\int_0^x (x-\eta)^{1-\alpha}\,\frac{\partial^2\mathcal{K}_{\rho}(\eta,y)}{\partial\eta^2}\,d\eta, \quad 1<\alpha<2\\
&= \frac{1}{\Gamma(3-\alpha)}\left(x^{2-\alpha}\,\frac{\partial^2\mathcal{K}_{\rho}(0,y)}{\partial\eta^2} + \int_0^x (x-\eta)^{2-\alpha}\frac{\partial^3\mathcal{K}_{\rho}(\eta,y)}{\partial\eta^3}\,d\eta\right),
\end{aligned}$$

and

$$\begin{aligned}
{}^{C}\mathcal{D}_y^{\alpha}\mathcal{K}_{\rho}(x,y) &= \frac{1}{\Gamma(2-\alpha)}\int_0^y (y-\eta)^{1-\alpha}\,\frac{\partial^2\mathcal{K}_{\rho}(x,\eta)}{\partial\eta^2}\,d\eta, \quad 1<\alpha<2\\
&= \frac{1}{\Gamma(3-\alpha)}\left(y^{2-\alpha}\,\frac{\partial^2\mathcal{K}_{\rho}(x,0)}{\partial\eta^2} + \int_0^y (y-\eta)^{2-\alpha}\frac{\partial^3\mathcal{K}_{\rho}(x,\eta)}{\partial\eta^3}\,d\eta\right).
\end{aligned}$$

It should be noted that the kernel $(x-\eta)^{2-\alpha}$ belongs to $L^1(0,+\infty)$ locally.

Lemma 4.1. *Let $\Omega\subset\mathbb{R}^2$, $u\in L^2(\Omega)$, and $v\in L^2(\Omega)$. Then there exists a constant C_{ρ} such that:*

$$\left\|(\nabla^{\alpha}\mathcal{K}_{\rho}) * u\right\|_{L^{\infty}(\Omega)} \leq C_{\rho}\,\|u\|_{L^2(\Omega)}\,. \tag{4.1}$$

Furthermore, there exists a constant K such that:

$$\left\|h(\left|(\nabla^{\alpha}\mathcal{K}_{\rho}) * u\right|) - h(\left|(\nabla^{\alpha}\mathcal{K}_{\rho}) * v\right|)\right\|_{L^{\infty}(\Omega)} \leq K\,\|u-v\|_{L^2(\Omega)}\,, \tag{4.2}$$

where h is a non-negative, smooth, Lipschitz, and decreasing function.

Proof. By convolution property, we have:

$$\begin{aligned}
\left|(\nabla^{\alpha}\mathcal{K}_{\rho}) * u\right| &\leq \int_{\Omega}\left|(\nabla^{\alpha}\mathcal{K}_{\rho})(x_1-y_1,x_2-y_2)\,u(y_1,y_2)\right|dy_1\,dy_2\\
&= \int_{\Omega}\left|(\nabla^{\alpha}\mathcal{K}_{\rho})(x_1-y_1,x_2-y_2)\right|\cdot\left|u(y_1,y_2)\right|dy_1\,dy_2.
\end{aligned}$$

Since $u \in L^2(\Omega)$, it follows from the above inequality that:

$$\left\|(\nabla^\alpha \mathcal{K}_\rho) * u\right\|_{L^\infty(\Omega)} \leq C_\rho \|u\|_{L^2(\Omega)} .$$

Moreover, since h and $(\nabla^\alpha \mathcal{K}_\rho) * u$ are smooth, it follows that $h(\left|(\nabla^\alpha \mathcal{K}_\rho) * u\right|)$ is smooth. Indeed,

$$\begin{aligned}
\left\|h(\left|(\nabla^\alpha \mathcal{K}_\rho) * u\right|) - h(\left|(\nabla^\alpha \mathcal{K}_\rho) * v\right|)\right\|_{L^\infty(\Omega)} &\leq C \left\|\left|(\nabla^\alpha \mathcal{K}_\rho) * u\right| - \left|(\nabla^\alpha \mathcal{K}_\rho) * v\right|\right\|_{L^\infty(\Omega)} \\
&\leq C \left\|\left|(\nabla^\alpha \mathcal{K}_\rho) * u - (\nabla^\alpha \mathcal{K}_\rho) * v\right|\right\|_{L^\infty(\Omega)} \\
&= C \left\|\left|(\nabla^\alpha \mathcal{K}_\rho) * (u - v)\right|\right\|_{L^\infty(\Omega)} \\
&\leq C \left\|C_\rho \|u - v\|_{L^2(\Omega)}\right\|_{L^\infty(\Omega)} \\
&\leq C\, C_\rho \|u - v\|_{L^2(\Omega)} \\
&= K \|u - v\|_{L^2(\Omega)} ,
\end{aligned}$$

where $K = CC_\rho$. The proof is complete. □

4.3 The proposed model

In our proposed model, we replace the integer-order spatial derivatives in the Perona-Malik (PM) equation with fractional-order Caputo derivatives. This modification transforms the equation into a parabolic partial differential equation that interpolates between the second- and fourth-order nonlinear diffusion equations. To regularize the diffusion coefficient and enhance the theoretical well-posedness and robustness in image denoising, inspired by [19], we incorporate a Gaussian kernel into the diffusivity function. Additionally, we introduce the fidelity term $H(u_0, u) = \int_\Omega \left(\log u + \dfrac{u_0}{u}\right) dx_1\, dx_2$, as presented in [7]. Consequently, the source term in the diffusion equation, defined as:

$$h(u_0, u) = \frac{u_0 - u}{u^2},$$

plays a significant role in influencing the denoising process. The proposed model is introduced in the following part.

4.3.1 Formulation of the proposed model

Consider $\Omega \subset \mathbb{R}^2$ as a bounded domain with $\partial\Omega$ as its boundary, and let u_0 be the initial condition, which represents the noisy image in image processing .

For $1 < \alpha < 2$, $\beta > 0$, $\gamma > 0$, and $u_\rho = \mathcal{K}_\rho * u$, the fractional gradient of order α is given by: $\nabla^\alpha u = \left({}^C\mathcal{D}_x^\alpha u, {}^C\mathcal{D}_y^\alpha u\right)$, $|\nabla^\alpha u| = \sqrt{|{}^C\mathcal{D}_x^\alpha u|^2 + \left|{}^C\mathcal{D}_y^\alpha u\right|^2}$, and
$\operatorname{div}^\alpha (v_1(x,y), v_2(x,y)) = {}^C\mathcal{D}_x^\alpha (v_1(x,y)) + {}^C\mathcal{D}_y^\alpha (v_2(x,y))$.

The fractional-order diffusion model is then formulated as:

$$\frac{\partial u}{\partial t} = \operatorname{div}^\alpha\left(\frac{1}{1+\left|\nabla^\alpha u_\rho\right|^\beta}\nabla^\alpha u\right) + \gamma\frac{u_0 - u}{u^2}, \qquad \text{in } \Omega \times (0,T), \tag{4.3}$$

$$u(x,y,0) = u_0(x,y), \qquad \text{in } \Omega, \tag{4.4}$$

$$\nabla^\alpha u.\vec{n} = 0, \qquad \text{on } \partial\Omega \times (0,T), \tag{4.5}$$

where $\vec{n}$ denotes the unit outward normal to $\partial\Omega$.

4.4 Existence and uniqueness

In this section, we prove the existence and uniqueness of the weak solution of the proposed model (4.3)-(4.5). Since the problem (4.3)-(4.5) is nonlinear, we first consider the linearized problem, and then use Schauder's fixed point Theorem to establish the existence of a weak solution. Without loss of generality, we assume $\gamma = 1$ in (4.3).

We introduce the Hilbert space:

$$W(0,T) = \left\{ w \in L^2(0,T;\mathcal{H}^\alpha(\Omega)), \frac{dw}{dt} \in L^2\left(0,T;(\mathcal{H}^\alpha(\Omega))'\right)\right\},$$

with the norm:

$$\|w\|_W = \|w\|_{L^2(0,T;\mathcal{H}^\alpha(\Omega))} + \left\|\frac{\partial w}{\partial t}\right\|_{L^2(0,T;(\mathcal{H}^\alpha(\Omega))')}.$$

Definition 4.1. We say that a function u is a weak solution of (4.3)-(4.5) if there exists $u \in W(0,T)$ such that

$$\left\langle \frac{\partial u}{\partial t}, \varphi \right\rangle + \int_\Omega \left(\frac{1}{1+\left|\nabla^\alpha u_\rho\right|^\beta}\nabla^\alpha u.\nabla^\alpha \varphi\right) dx\,dy = \int_\Omega \left(\frac{u_0 - u}{u^2}\right)\varphi\,dx\,dy,$$

$$u(x,y,0) = u_0(x,y), \quad \text{in } \Omega,$$

for a.e. $t \in (0,T)$ and all $\varphi \in \mathcal{H}^\alpha(\Omega)$.

Next, we assume that the initial data $u_0 \in \mathcal{H}^\alpha(\Omega)$ satisfies:

$$0 < I := \operatorname{ess} \inf_{x,y\in\Omega} u_0(x,y) \text{ and } M := \operatorname{ess} \sup_{x,y\in\Omega} u_0(x,y) < \infty. \tag{4.6}$$

For any positive constant $N > 0$, we define:

$$W_N = \left\{ \begin{array}{l} w \in W(0,T) \cap L^\infty(0,T;L^2(\Omega)) : I \leq w(x,y,t) \leq M, \text{ a.e in } \Omega \times (0,T) \\ \\ \|w\|_{L^\infty(0,T;L^2(\Omega))} \leq \|u_0\|_{L^2(\Omega)}, \left\|\dfrac{\partial w}{\partial t}\right\|_{L^2(0,T;L^2(\Omega))} \leq N \|u_0\|_{\mathcal{H}^\alpha(\Omega)} \end{array} \right\}.$$

Let $w \in W_N$. We consider the following linear problem P_w:

$$\frac{\partial u_w}{\partial t} = \operatorname{div}^\alpha (h_w \nabla^\alpha u_w) + \frac{u_0 - u_w}{w^2}, \qquad \text{in } \Omega \times (0,T), \tag{4.7}$$

$$u_w(x,y,0) = u_0(x,y), \qquad \text{in } \Omega, \tag{4.8}$$

$$\nabla^\alpha u_w.\vec{n} = 0, \qquad \text{on } \partial\Omega \times (0,T), \tag{4.9}$$

where the function h_w is given by:

$$h_w(x,y,t) := \frac{1}{1 + \left|\nabla^\alpha w_\rho\right|^\beta}, \quad \text{with } w_\rho = w * \mathcal{K}_\rho.$$

Lemma 4.2. *Let u_w be a weak solution of the problem P_w, then*

$$0 < I \leq u_w(x,y,t) \leq M \text{ for a.e. } (x,y,t) \in \Omega \times (0,T).$$

Proof. We define $(u_w - M)_+ = \max\{0, u_w - M\}$.

By multiplying equation (4.7) by $(u_w - M)_+$ and then integrating over Ω, we obtain:

$$\frac{1}{2}\frac{d}{dt}\int_\Omega |(u_w - M)_+|^2\, dx\, dy = \int_\Omega \operatorname{div}^\alpha (h_w \nabla^\alpha u_w)(u_w - M)_+ dx\, dy + \int_\Omega \left(\frac{u_0 - u_w}{w^2}\right)(u_w - M)_+\, dx\, dy,$$

which yields

$$\frac{1}{2}\frac{d}{dt}\int_\Omega |(u_w - M)_+|^2\, dx\, dy = -\int_{\{u_w \geq M\}} h_w \nabla^\alpha u_w \cdot \nabla^\alpha u_w dx\, dy + \int_{\{u_w \geq M\}} \left(\frac{u_0 - u_w}{w^2}\right)(u_w - M)_+\, dx\, dy,$$

this implies that

$$\frac{1}{2}\frac{d}{dt}\int_\Omega |(u_w - M)_+|^2\, dx\, dy + \int_{\{u_w \geq M\}} h_w |\nabla^\alpha u_w|^2\, dx\, dy + \int_{\{u_w \geq M\}} \left(\frac{u_w - u_0}{w^2}\right)(u_w - M)_+\, dx\, dy = 0.$$

Observe that, $h_w > 0$ and $(u_w - u_0)(u_w - M)_+ \geq 0$,

thus, we have

$$\frac{d}{dt}\int_\Omega |(u_w - M)_+|^2\, dx\, dy \leq 0.$$

Since $u_0 \le M$, it follows that:

$$\int_\Omega |(u_w - M)_+|^2 \, dx \, dy \le \int_\Omega |(u_0 - M)_+|^2 \, dx \, dy \le 0.$$

Therefore, $u_w \le M$ for a.e. $(x_1, x_2, t) \in \Omega \times (0, T)$.

Similarly, we define $(u_w - I)_- = \min\{0, u_w - I\}$. By multiplying equation (4.7) by$(u_w - I)_-$ and then integrating over Ω, we deduce that $0 < I \le u_w(x, y, t)$ for a.e. $(x, y, t) \in \Omega \times (0, T)$. $\square$

Lemma 4.3. *The following inequalities are satisfied:*

1. $0 < \kappa \le h_w \le 1$,

2. $\left|\dfrac{\partial h_w}{\partial t}\right| \le C_0$,

where the positive constant C_0 *depends only on* $\mathcal{K}_\rho$,u_0,N,I,M, *and* β.

Proof. 1. Let $w \in W_N$. By convolution property, we have:

$$\begin{aligned}\left|\nabla^\alpha w_\rho\right| &\le \left|(\nabla^\alpha \mathcal{K}_\rho) * w\right| \\ &\le C_\rho \, ||w||_{L^2(\Omega)} \\ &\le C_\rho N \, ||u_0||_{\mathcal{H}^\alpha(\Omega)}\end{aligned}$$

$$1 \le 1 + \left|\nabla^\alpha w_\rho\right|^\beta \le 1 + C_\rho^\beta N^\beta \, ||u_0||^\beta_{\mathcal{H}^\alpha(\Omega)}$$
$$\frac{1}{1 + C_\rho^\beta N^\beta \, ||u_0||^\beta_{\mathcal{H}^\alpha(\Omega)}} \le \frac{1}{1 + \left|\nabla^\alpha w_\rho\right|^\beta} \le 1.$$

Now, we set

$$\kappa = \frac{1}{1 + C_\rho^\beta N^\beta \, ||u_0||^\beta_{\mathcal{H}^\alpha}}.$$

Therefore, $0 < \kappa \le h_w \le 1$.

2. Observe that:

$$\begin{aligned}\left|\frac{\partial h_w}{\partial t}\right| &= \left|\frac{\frac{\partial}{\partial t}(\nabla^\alpha w_\rho)^\beta}{(1 + \left|\nabla^\alpha w_\rho\right|^\beta)^2}\right| \\ &\le \beta C_\rho^{\beta-1} N^{\beta-1} \, ||u_0||^{\beta-1}_{\mathcal{H}^\alpha(\Omega)} \left|\nabla^\alpha \mathcal{K}_\rho * \frac{\partial w}{\partial t}\right| \\ &\le \beta C_\rho^\beta N^\beta \, ||u_0||^\beta_{\mathcal{H}^\alpha(\Omega)} \\ &\le C_0.\end{aligned}$$

This completes the proof of Lemma. $\square$

By using Lemma 4.3, we can apply the classical Galerkin method [26] to prove that the linearized problem (4.7))-(4.9) has a unique weak solution $u_w \in W(0,T)$.

Lemma 4.4. *The unique weak solution $u_w \in W(0,T)$ of the linearized problem (4.7) with (4.9) and the initial condition (4.8), fulfills the estimates:*

1. $\|u_w\|_{L^\infty(0,T;L^2(\Omega))} \leq \|u_0\|_{L^2(\Omega)} + C_1$,

2. $\|u_w\|_{L^\infty(0,T;\mathcal{H}^\alpha(\Omega))} \leq C_2$,

3. $\int_0^T \left\|\frac{\partial u_w}{\partial t}\right\|^2_{(\mathcal{H}^\alpha(\Omega))'} dt \leq C_3$,

where the constants $C_1 > 0$, $C_2 > 0$, and $C_3 > 0$ only depend on $\|u_0\|_{\mathcal{H}^\alpha(\Omega)}$, $\mathcal{K}_\rho, \kappa, I, M, N$, and β.

Proof. 1. Multiplying equation (4.7) by u_w and integrating by parts over Ω, we obtain:

$$\int_\Omega \frac{\partial u_w}{\partial t}\, u_w\, dx\, dy = \int_\Omega \mathrm{div}^\alpha \left(h_w \nabla^\alpha u_w\right) u_w\, dx\, dy + \int_\Omega \left(\frac{u_0 - u_w}{w^2}\right) u_w\, dx\, dy,$$
$$\frac{1}{2}\frac{d}{dt}\int_\Omega |u_w|^2\, dx\, dy + \int_\Omega h_w\, |\nabla^\alpha u_w|^2\, dx\, dy = \int_\Omega \left(\frac{u_0 - u_w}{w^2}\right) u_w\, dx\, dy.$$

Using Young's inequality and Lemma 4.3 (1), we find:

$$\frac{1}{2}\frac{d}{dt}\int_\Omega |u_w|^2\, dx\, dy + \kappa \int_\Omega |\nabla^\alpha u_w|^2\, dx\, dy \leq \frac{1}{2}\left\|\frac{u_0 - u_w}{w^2}\right\|^2_{L^2(\Omega)} + \frac{1}{2}\|u_w\|^2_{L^2(\Omega)}.$$

Since $w \in W_N$ and by Lemma 4.2, we have:

$$\begin{aligned} \left\|\frac{u_0 - u_w}{w^2}\right\|^2_{L^2(\Omega)} &\leq \frac{1}{I^4}\|u_0 - u_w\|^2_{L^2(\Omega)} \\ &\leq \frac{2}{I^4}\left(\|u_0\|^2_{\mathcal{H}^\alpha(\Omega)} + \|u_w\|^2_{L^2(\Omega)}\right) \\ &\leq \frac{2}{I^4}\|u_0\|^2_{\mathcal{H}^\alpha(\Omega)} + \frac{2}{I^4}M^2|\Omega|. \end{aligned} \tag{4.10}$$

According to inequality (4.10), we obtain:

$$\begin{aligned} \frac{1}{2}\frac{d}{dt}\int_\Omega |u_w|^2\, dx\, dy + \kappa \int_\Omega |\nabla^\alpha u_w|^2\, dx\, dy &\leq \frac{1}{I^4}\|u_0\|^2_{\mathcal{H}^\alpha(\Omega)} + \frac{1}{I^4}M^2|\Omega| + \frac{M^2}{2}|\Omega|, \\ &= C, \end{aligned}$$

integrating the last inequality with respect to the time variable, we find that:

$$\frac{1}{2}\int_0^t \frac{d}{ds}\|u_w\|^2_{L^2(\Omega)}\, ds + \kappa \int_0^t \int_\Omega |\nabla^\alpha u_w|^2\, dx\, dy\, ds \leq Ct,$$

therefore, for a.e. $t \in (0, T]$,

$$\frac{1}{2}\|u_w(t)\|^2_{L^2(\Omega)} + \kappa \int_0^t \int_\Omega |\nabla^\alpha u_w|^2 \, dx\, dy\, ds \;\leq\; CT + \frac{1}{2}\|u_0\|^2_{L^2(\Omega)},$$

we conclude that

$$\|u_w\|_{L^\infty(0,T;L^2(\Omega))} \;\leq\; \|u_0\|_{L^2(\Omega)} + C_1,$$

where $C_1 = 2CT$.

2. Multiplying equation (4.7) by $\dfrac{\partial u_w}{\partial t}$ and integrating over Ω,

$$\int_\Omega \left|\frac{\partial u_w}{\partial t}\right|^2 dx\, dy = \int_\Omega \operatorname{div}^\alpha (h_w \nabla^\alpha u_w)\, \frac{\partial u_w}{\partial t}\, dx\, dy + \int_\Omega \left(\frac{u_0 - u_w}{w^2}\right) \frac{\partial u_w}{\partial t}\, dx\, dy.$$

By integrating by parts and applying Young's inequality, we arrive at the following:

$$\int_\Omega \left|\frac{\partial u_w}{\partial t}\right|^2 dx\, dy + \int_\Omega h_w \nabla^\alpha u_w \cdot \nabla^\alpha \left(\frac{\partial u_w}{\partial t}\right) dx\, dy \leq \frac{1}{2}\left\|\frac{u_0 - u_w}{w^2}\right\|^2_{L^2(\Omega)} + \frac{1}{2}\left\|\frac{\partial u_w}{\partial t}\right\|^2_{L^2(\Omega)}.$$

Applying the integration by parts formula, we obtain the result:

$$\begin{aligned}
\int_\Omega h_w \nabla^\alpha u_w \cdot \nabla^\alpha \left(\frac{\partial u_w}{\partial t}\right) dx\, dy &= \int_\Omega h_w \nabla^\alpha u_w \cdot \frac{\partial}{\partial t}(\nabla^\alpha u_w)\, dx\, dy \\
&= \frac{1}{2}\int_\Omega h_w \frac{d}{dt}|\nabla^\alpha u_w|^2\, dx\, dy \\
&= \frac{1}{2}\frac{d}{dt}\int_\Omega h_w |\nabla^\alpha u_w|^2\, dx\, dy - \frac{1}{2}\int_\Omega \frac{dh_w}{dt}|\nabla^\alpha u_w|^2\, dx\, dy.
\end{aligned}$$

Then, using Lemma 4.3 (2), we deduce that:

$$\int_\Omega h_w \nabla^\alpha u_w \cdot \nabla^\alpha \left(\frac{\partial u_w}{\partial t}\right) dx\, dy \geq \frac{1}{2}\frac{d}{dt}\int_\Omega h_w |\nabla^\alpha u_w|^2\, dx\, dy - \frac{C_0}{2}\|\nabla^\alpha u_w\|^2_{L^2(\Omega)}. \tag{4.11}$$

By combining (4.10) and (4.11), we obtain:

$$\frac{1}{2}\left\|\frac{\partial u_w}{\partial t}\right\|^2_{L^2(\Omega)} + \frac{1}{2}\frac{d}{dt}\int_\Omega h_w |\nabla^\alpha u_w|^2\, dx\, dy \;\leq\; \frac{1}{l^4}\|u_0\|^2_{\mathcal{H}^\alpha(\Omega)} + \frac{1}{l^4}M^2|\Omega| + \frac{C_0}{2}\|\nabla^\alpha u_w\|^2_{L^2(\Omega)}.$$

Noting that $0 < \kappa \leq h_w$ in Lemma 4.3, which implies that:

$$\kappa\, \|\nabla^\alpha u_w\|^2_{L^2(\Omega)} \;\leq\; \int_\Omega h_w |\nabla^\alpha u_w|^2\, dx\, dy,$$

thus,

$$\|\nabla^\alpha u_w\|^2_{L^2(\Omega)} \;\leq\; \frac{1}{\kappa}\int_\Omega h_w |\nabla^\alpha u_w|^2\, dx\, dy. \tag{4.12}$$

From (4.12), we have:

$$\frac{1}{2}\left\|\frac{\partial u_w}{\partial t}\right\|^2_{L^2(\Omega)} + \frac{1}{2}\frac{d}{dt}\int_\Omega h_w\,|\nabla^\alpha u_w|^2\,dx\,dy \;\le\; C + \frac{K_1}{2}\int_\Omega h_w\,|\nabla^\alpha u_w|^2\,dx\,dy, \tag{4.13}$$

where $K_1 = \dfrac{C_0}{\kappa}$, we observe that:

$$\frac{d}{dt}\int_\Omega h_w\,|\nabla^\alpha u_w|^2\,dx\,dy \;\le\; 2C + K_1\int_\Omega h_w\,|\nabla^\alpha u_w|^2\,dx\,dy.$$

By applying Gronwall's Lemma, we obtain:

$$\int_\Omega h_w(x,y,t)\left|\nabla^\alpha u_w(x,y,t)\right|^2 dx\,dy \;\le\; e^{K_1 t}(K_2 + 2Ct),$$

for a.e. $t \in (0,T]$, where $K_2 = \int_\Omega h_w(x,y,0)\left|\nabla^\alpha u_w(x,y,0)\right|^2 dx_1\,dx_2$.

From inequality (4.12), we conclude:

$$\|\nabla^\alpha u_w\|^2_{L^2(\Omega)} \;\le\; \frac{1}{\kappa}e^{K_1 T}(K_2 + 2CT). \tag{4.14}$$

Furthermore, from (4.13) it follows that:

$$\frac{1}{2}\left\|\frac{\partial u_w}{\partial t}\right\|^2_{L^2(\Omega)} + \frac{1}{2}\frac{d}{dt}\int_\Omega h_w\,|\nabla^\alpha u_w|^2\,dx\,dy \;\le\; C + \frac{K_1}{2}e^{K_1 T}(K_2 + 2CT). \tag{4.15}$$

Integrating (4.15) over $(0,t)$, we reach the result that:

$$\int_0^t \left\|\frac{\partial u_w}{\partial s}\right\|^2_{L^2(\Omega)} ds + \int_\Omega h_w(x,y,t)\left|\nabla^\alpha u_w(x,y,t)\right|^2 dx\,dy \;\le\; \left(2C + K_1 e^{K_1 T}(K_2 + 2CT)\right)t + K_2,$$

for a.e $t \in (0,T]$.

Note that

$$\int_0^t \left\|\frac{\partial u_w}{\partial s}\right\|^2_{L^2(\Omega)} ds \;\le\; \left(2C + K_1 e^{K_1 T}(K_2 + 2CT)\right)T + K_2. \tag{4.16}$$

Combining $u_w(x,y,t) = u_w(x,y,0) + \int_0^t \frac{\partial u_w}{\partial s}ds$, inequality (1.15), and (4.16), we find that:

$$\begin{aligned}\|u_w\|^2_{L^2(\Omega)} &\le 2\,\|u_0\|^2_{\mathcal{H}^\alpha(\Omega)} + 2T\int_0^t \left\|\tfrac{\partial u_w(s)}{\partial s}\right\|^2_{L^2(\Omega)} ds\\ &\le 2\,\|u_0\|^2_{\mathcal{H}^\alpha(\Omega)} + 2T^2\left(2C + K_1 e^{K_1 t}(K_2 + 2Ct)\right) + K_2 T.\end{aligned} \tag{4.17}$$

From (4.17) and (4.14), we conclude that:

$$\|u_w\|_{L^\infty(0,T;\mathcal{H}^\alpha(\Omega))} \;\le\; C_2. \tag{4.18}$$

3. Multiplying (4.7) by $\varphi \in \mathcal{H}^\alpha(\Omega)$ with $\|\varphi\|_{\mathcal{H}^\alpha(\Omega)} \leq 1$, and applying the Cauchy-Schwarz's inequality along with (4.10) and (4.18), we obtain:

$$\begin{aligned}\left|\left\langle \frac{\partial u_w}{\partial t}, \varphi \right\rangle\right| &= \left| \int_\Omega h_w \nabla^\alpha u_w \cdot \nabla^\alpha \varphi \, dx\, dy + \int_\Omega \left(\frac{u_0 - u_w}{u_w^2} \right) \varphi \, dx\, dy \right| \\ &\leq \left(|h_w| \, \|\nabla^\alpha u_w\|_{L^2(\Omega)} + \left\| \frac{u_0 - u_w}{w^2} \right\|_{L^2(\Omega)} \right) \|\varphi\|_{\mathcal{H}^\alpha(\Omega)} \\ &\leq \left(C_2 + \sqrt{\frac{2}{I^4}} \|u_0\|_{\mathcal{H}^\alpha(\Omega)} + \sqrt{\frac{2|\Omega|}{I^4}} M \right) \|\varphi\|_{\mathcal{H}^\alpha(\Omega)} .\end{aligned}$$

Therefore, we have:

$$\left\| \frac{\partial u_w}{\partial t} \right\|_{(\mathcal{H}^\alpha(\Omega))'} \leq C + \sqrt{\frac{2}{I^4}} \|u_0\|_{\mathcal{H}^\alpha(\Omega)} .$$

Furthermore, by taking the square of both sides of the above inequality and then integrating over $(0, T)$, it follows that:

$$\int_0^T \left\| \frac{\partial u_w}{\partial t} \right\|^2_{(\mathcal{H}^\alpha(\Omega))'} dt \leq C_3.$$

□

Theorem 4.1. *Let $u_0 \in \mathcal{H}^\alpha(\Omega)$ and (4.6) hold, then the problem (4.3)-(4.5) has a weak solution $u \in W(0,T)$.*

Proof. From Lemma 4.4, we introduce the subspace W_0 of $W(0,T)$ defined by:

$$\bar{W} = \left\{ \begin{array}{l} w \in W(0,T); \|w\|_{L^\infty(0,T;\mathcal{H}^\alpha(\Omega))} \leq C_2, \|w\|_{L^\infty(0,T;L^2(\Omega))} \leq \|u_0\|_{L^2(\Omega)}, \left\| \frac{\partial w}{\partial t} \right\|_{L^2(0,T;(\mathcal{H}^\alpha(\Omega))')} \leq C_3, \\ 0 < I \leq w(x,y,t) \leq M \text{ for a.e. } (x,y,t) \in \Omega \times (0,T), w(0) = u_0 \end{array} \right\}.$$

Moreover, it can be proved that $\bar{W}$ is a nonempty, convex, and weakly compact subset of $W(0,T)$. Subsequently, we construct the following mapping:

$$\begin{aligned} Q : & \bar{W} \to \bar{W} \\ & w \mapsto u_w. \end{aligned}$$

To apply Schauder's fixed-point Theorem, we need to show that the mapping $Q : w \mapsto u_w$ is weakly continuous from $\bar{W}$ into $\bar{W}$. Let w_j be a sequence that weakly converges to some w in W_0 and let $u_j = Q(w_j)$. Our goal is to prove that $Q(w_j) := u_j$ weakly converges to $Q(w) := u_w$. By

Lemma 4.4, we can apply classical results of compact inclusion in Sobolev spaces [2] to extract the sub-sequences of w_j and u_j (still denoted by w_j and u_j), we have:

$$w_j \to w \text{ in } L^2((0,T);L^2(\Omega)) \text{ and a.e. on } \Omega\times(0,T), \tag{4.19}$$

$$\nabla^\alpha \mathcal{K}_\rho * w_j \to \nabla^\alpha \mathcal{K}_\rho * w \text{ in } L^2((0,T);L^2(\Omega)) \text{ and a.e. on } \Omega\times(0,T), \tag{4.20}$$

$$\frac{1}{1+\left|\nabla^\alpha (w_j)_\rho\right|^\beta} \to \frac{1}{1+\left|\nabla^\alpha w_\rho\right|^\beta} \text{ in } L^2((0,T);L^2(\Omega)) \text{ and a.e. on } \Omega\times(0,T), \tag{4.21}$$

$$\frac{1}{w_j^2} \to \frac{1}{w^2} \text{ in } L^2((0,T);L^2(\Omega)) \text{ and a.e. on } \Omega\times(0,T), \tag{4.22}$$

$$u_j \to u \text{ weakly in } L^\infty((0,T);\mathcal{H}^\alpha(\Omega)), \tag{4.23}$$

$$\frac{\partial u_j}{\partial t} \to \frac{\partial u}{\partial t} \text{ weakly in } L^2((0,T);(\mathcal{H}^\alpha(\Omega))'), \tag{4.24}$$

$$u_j \to u \text{ in } L^2((0,T);L^2(\Omega)) \text{ and a.e. on } \Omega\times(0,T), \tag{4.25}$$

$$\nabla^\alpha u_j \to \nabla^\alpha u \text{ weakly in } L^\infty((0,T);L^2(\Omega)), \tag{4.26}$$

$$u_j(0) \to u(0) \text{ in } L^2(\Omega). \tag{4.27}$$

The (4.21) and (4.22) are obtained by applying Dominated Convergence Theorem [10].

The aforementioned convergence allows us to pass to the limit in the problem P_{w_j} and obtain $u = Q(w)$.

Considering u_j is the weak solution of (4.7) associated to w_j, we have, for a.e $t \in (0,T]$, and $\varphi \in \mathcal{H}^\alpha(\Omega)$:

$$\int_\Omega \frac{\partial u_j}{\partial t}\varphi\,dx\,dy + \int_\Omega h_{w_j}\nabla^\alpha u_j.\nabla^\alpha\varphi\,dx\,dy = \int_\Omega \left(\frac{u_j(0)-u_j}{w_j^2}\right)\varphi\,dx\,dy. \tag{4.28}$$

The integral from 0 to T of (4.28) equals:

$$\int_0^T\int_\Omega \frac{\partial u_j}{\partial t}\varphi\,dx\,dy\,dt + \int_0^T\int_\Omega h_{w_j}\nabla^\alpha u_j.\nabla^\alpha\varphi\,dx\,dy\,dt = \int_0^T\int_\Omega \left(\frac{u_j(0)-u_j}{w_j^2}\right)\varphi\,dx\,dy\,dt. \tag{4.29}$$

From (4.24), we obtain the following:

$$\int_0^T\int_\Omega \frac{\partial u_j}{\partial t}\varphi\,dx\,dy\,dt \to \int_0^T\int_\Omega \frac{\partial u}{\partial t}\varphi\,dx\,dy\,dt, \quad \text{as } j\to\infty.$$

Considering the second term in equation (4.29),

$$\begin{aligned}
&\left|\int_0^T\int_\Omega h_{w_j}\nabla^\alpha u_j\nabla^\alpha\varphi\,dx\,dy\,dt-\int_0^T\int_\Omega h_w\nabla^\alpha u\nabla^\alpha\varphi\,dx\,dy\,dt\right|\\
&\leq\int_0^T\int_\Omega\left|h_{w_j}-h_w\right||\nabla^\alpha u|\left|\nabla^\alpha\varphi\right|\,dx\,dy\,dt+\left|\int_0^T\int_\Omega h_{w_j}\nabla^\alpha(u_j-u)\nabla^\alpha\varphi\,dx\,dy\,dt\right|\\
&=A+B.
\end{aligned}$$

According to Lemma 4.1, we conclude that, as $j\to\infty$,

$$\begin{aligned}
A&\leq C\int_0^T\int_\Omega\left\|w_j-w\right\|_{L^2(\Omega)}|\nabla^\alpha u|\left|\nabla^\alpha\varphi\right|\,dx\,dy\,dt\\
&\leq C(\varphi)\left\|w_j-w\right\|_{L^2(\Omega)}\|\nabla^\alpha u\|_{L^2((0,T);L^2(\Omega))}\to 0.
\end{aligned}$$

Also, as $j\to\infty$, $B\to 0$.

From (4.22), (4.25), and (4.27), we have:

$$\int_0^T\int_\Omega\left(\frac{u_j(0)-u_j}{w_j^2}\right)\varphi\,dx\,dy\,dt\to\int_0^T\int_\Omega\left(\frac{u_0-u}{w^2}\right)\varphi\,dx\,dy\,dt.$$

Allowing $j\to\infty$ in (4.29) yields:

$$\int_0^T\int_\Omega\frac{\partial u}{\partial t}\varphi\,dx_1\,dx_2\,dt+\int_0^T\int_\Omega h_w\nabla^\alpha u.\nabla^\alpha\varphi\,dx\,dy\,dt=\int_0^T\int_\Omega\left(\frac{u_0-u}{w^2}\right)\varphi\,dx_1\,dx_2\,dt.$$

Hence, by the arbitrariness of $\varphi\in\mathcal{H}^\alpha(\Omega)$, we obtain for a.e $t\in(0,T]$,

$$\int_\Omega\frac{\partial u}{\partial t}\varphi\,dx\,dy+\int_\Omega h_w\nabla^\alpha u.\nabla^\alpha\varphi\,dx\,dy=\int_\Omega\left(\frac{u_0-u}{w^2}\right)\varphi\,dx\,dy.$$

This implies that

$$u=u_w=Q(w).$$

Furthermore, since the solution of problem (4.7) is unique, the whole sequence $u_j=Q(w_j)$ converges weakly in W_0 to $u=E(w)$. Hence Q, is weakly continuous.

Consequently, by Schauder's fixed-point Theorem, there exists $w\in W_0$ such that

$$w=E(w)=u_w.$$

Thus, the existence of the weak solution u_w to the problem (4.3)-(4.5) is proved. □

Theorem 4.2. *Let u be a weak solution of (4.3)-(4.5), then the solution u is unique.*

Proof. Let u_1 and u_2 be two weak solutions of (4.3)-(4.5), we have for almost every $t \in (0,T)$,

$$\begin{cases} \dfrac{\partial u_i}{\partial t} = \operatorname{div}^\alpha\left(\dfrac{\nabla^\alpha u_i}{1+\left|\nabla^\alpha (u_i)_\rho\right|^\beta}\right) + \dfrac{u_0 - u_i}{u_i^2} & \Omega \times (0,T)\,, \\ u_i(x,y,0) = u_0(x,y), & \Omega, \\ \nabla^\alpha u_i.\vec{n} = 0, & \text{on } \partial\Omega \times (0,T)\,. \end{cases} \tag{4.30}$$

Where $i = 1,2$, denote $\overline{u} = u_1 - u_2$. Then, we obtain:

$$\frac{\partial \overline{u}}{\partial t} - \operatorname{div}^\alpha(h_{u_1}\nabla^\alpha \overline{u}) = \operatorname{div}^\alpha((h_{u_1} - h_{u_2})\nabla^\alpha u_2) + \acute{u} \qquad \text{in } \Omega \times (0,T)\,, \tag{4.31}$$

$$\overline{u}(x,y,0) = 0 \qquad \Omega, \tag{4.32}$$

$$\nabla^\alpha \overline{u}.\vec{n} = 0, \qquad \text{on } \partial\Omega \times (0,T)\,, \tag{4.33}$$

where $\acute{u} = \dfrac{-u_0\overline{u}(u_1+u_2)}{u_1^2u_2^2} + \dfrac{\overline{u}}{u_1u_2}$.
Now, multiplying (4.31) by $\overline{u}$ and integrating over Ω, we find:

$$\begin{aligned} &\int_\Omega \frac{\partial \overline{u}}{\partial t}\,\overline{u}\,dx\,dy - \int_\Omega \operatorname{div}^\alpha(h_{u_1}(\nabla^\alpha \overline{u})\overline{u}\,dx\,dy \\ &= \int_\Omega \operatorname{div}^\alpha((h_{u_1} - h_{u_2})\nabla^\alpha u_2)\overline{u}\,dx\,dy + \int_\Omega \frac{\left|\overline{u}\right|^2}{u_1u_2} - \frac{u_0(u_1+u_2)\left|\overline{u}\right|^2}{u_1^2u_2^2}dx\,dy. \end{aligned}$$

By applying the integration by parts formula, we obtain:

$$\begin{aligned} &\frac{1}{2}\frac{d}{dt}\int_\Omega \left|\overline{u}\right|^2 dx_1\,dx_2 + \int_\Omega h_{u_1}\left|\nabla^\alpha \overline{u}\right|^2 dx\,dy \\ &= -\int_\Omega (h_{u_1} - h_{u_2})\nabla^\alpha u_2.\nabla^\alpha \overline{u}\,dx\,dy + \int_\Omega \frac{\left|\overline{u}\right|^2}{u_1u_2}dx\,dy - \int_\Omega \frac{u_0(u_1+u_2)\left|\overline{u}\right|^2}{u_1^2u_2^2}dx\,dy. \end{aligned}$$

Noting that $\dfrac{1}{u_1u_2} \leq \dfrac{1}{I^2}$ and $\dfrac{u_0(u_1+u_2)}{u_1^2u_2^2} \leq \dfrac{2M^2}{I^4}$, using these inequalities in the above equality, we get:

$$\begin{aligned} &\frac{1}{2}\frac{d}{dt}\int_\Omega \left|\overline{u}\right|^2 dx\,dy + \int_\Omega h_{u_1}\left|\nabla^\alpha \overline{u}\right|^2 dx\,dy \\ &\leq -\int_\Omega (h_{u_1} - h_{u_2})\nabla^\alpha u_2.\nabla^\alpha \overline{u}dx\,dy + \left(\frac{2M^2}{I^4} + \frac{1}{I^2}\right)\int_\Omega \left|\overline{u}\right|^2 dx\,dy. \end{aligned} \tag{4.34}$$

As seen in the the proof of Lemma 4.3, there exists a positive constant $\kappa_1 > 0$, where:

$$\kappa_1 \leq h_{u_1}(x,y,t) \leq 1, \quad \text{for a.e. } (x,y,t) \in \Omega \times (0,T).$$

Moreover, since (4.2), we have:

$$\left\|h_{u_1} - h_{u_2}\right\|_{L^\infty(\Omega)} \leq C \left\|\overline{u}\right\|_{L^2(\Omega)},$$

where C is a positive constant. Thus, using the above estimates in (4.34), we get:

$$\frac{1}{2}\frac{d}{dt}\left\|\overline{u}\right\|^2_{L^2(\Omega)} + \kappa_1 \left\|\nabla^\alpha \overline{u}\right\|^2_{L^2(\Omega)} \leq C\left\|\overline{u}\right\|_{L^2(\Omega)} \|\nabla^\alpha u_2\|_{L^2(\Omega)} \left\|\nabla^\alpha \overline{u}\right\|_{L^2(\Omega)} + \left(\frac{2M^2}{I^4} + \frac{1}{I^2}\right)\left\|\overline{u}\right\|^2_{L^2(\Omega)}.$$

By using Young's inequality,

$$a.b \leq \frac{\kappa_1 a^2}{2} + \frac{b^2}{2\kappa_1}, \quad a, b, \kappa_1 \in \mathbb{R}^+,$$

we derive the following:

$$\frac{1}{2}\frac{d}{dt}\left\|\overline{u}\right\|^2_{L^2(\Omega)} + \kappa_1 \left\|\nabla^\alpha \overline{u}\right\|^2_{L^2(\Omega)} \leq \frac{C^2}{2\kappa_1}\left\|\overline{u}\right\|^2_{L^2(\Omega)} \|\nabla^\alpha u_2\|^2_{L^2(\Omega)} + \frac{\kappa_1}{2}\left\|\nabla^\alpha \overline{u}\right\|^2_{L^2(\Omega)} + \left(\frac{2M^2}{I^4} + \frac{1}{I^2}\right)\left\|\overline{u}\right\|^2_{L^2(\Omega)},$$

from which we deduce that:

$$\frac{d}{dt}\left\|\overline{u}\right\|^2_{L^2(\Omega)} \leq \left(\frac{C^2}{\kappa_1}\|\nabla^\alpha u_2\|^2_{L^2(\Omega)} + \frac{4M^2}{I^4} + \frac{2}{I^2}\right)\left\|\overline{u}\right\|^2_{L^2(\Omega)},$$

since $\overline{u}(0) = 0$, applying Gronwall's inequality yields:

$$\left\|\overline{u}(t)\right\|^2_{L^2(\Omega)} \leq 0.$$

Therefore, we conclude that $u_1 = u_2$. □

Remark 4.1. *Through Theorem 4.1, the weak solution of (4.3)-(4.5) is in W_0, and $w = E(w) = u_w$ is the fixed point of (4.3)-(4.5). Therefore, u_w is also in W_0. With the uniqueness of the solution, we deduce that the unique weak solution $u = u_w$ satisfies the extremum principle:*

$$0 < I \leq u(x, y, t) \leq M \text{ for a.e. } (x, y, t) \in \Omega \times (0, T), \tag{4.35}$$

where

$$0 < I := \operatorname{ess}\inf_{x_1, x_2 \in \Omega} u_0(x, y) \text{ and } M := \operatorname{ess}\sup_{x, y \in \Omega} u_0(x, y) < \infty.$$

4.5 Conclusion

In this chapter, we introduced a nonlinear fractional-order diffusion model based on Caputo fractional derivatives. This model is applicable to image processing, effectively reducing noise while preserving edges and structural features. By incorporating spatial fractional derivatives, the model leverages the strengths of both second- and fourth-order diffusion equations. The existence and uniqueness of the weak solution were established using Schauder's fixed-point theorem.

CHAPTER 5

FRACTIONAL GRADIENT-BASED NONLINEAR TELEGRAPH DIFFUSION MODEL FOR IMAGE RESTORATION

The results presented in this chapter are based on the findings reported in [14].

5.1 Introduction

Building on the previous chapters, which mainly addressed parabolic PDE-based models for image denoising, we note that, to our knowledge, most researchers have also predominantly focused on such approaches. However, several studies have indicated that hyperbolic PDE-based methods are more effective for edge detection and provide superior image enhancement compared to parabolic PDEs [6]. In [40], the authors regarded the image as an elastic sheet in a damping environment and introduced an extension of the diffusion equation, known as the telegraph-diffusion equation (TDE). The term 'telegraph' originates from the telegraphers' equation, as discussed in [60].

In this chapter, we propose a novel model that integrates the nonlinear telegraph diffusion equation with fractional-order derivatives in the diffusivity function. The primary objective is to apply this model to image denoising, effectively addressing various types of noise (additive, multiplicative and impulse noise) while preserving essential image features such as edges and textures. The proposed model is formulated as follows:

$$\frac{\partial^2 u}{\partial t^2} + \lambda \frac{\partial u}{\partial t} = \operatorname{div}\left(\hbar\left(\left|\nabla^\alpha u_\rho\right|\right)\nabla u\right) + \gamma\,(u_0 - u)\,, \qquad \text{in}\,\Omega\times(0,T)\,, \tag{5.1}$$

$$u(x,y,0) = u_0(x,y),\ \frac{\partial u(x,y,0)}{\partial t} = 0, \qquad \text{in}\,\Omega, \tag{5.2}$$

$$\nabla u.\vec{n} = 0, \qquad \text{on}\,\partial\Omega\times(0,T)\,. \tag{5.3}$$

In this context, Ω is a bounded domain of $\mathbb{R}^2$, and u_0 represent the original image, where $0 < \alpha < 1$, $\lambda > 0$, and $\gamma > 0$.

Given $u_\rho = \mathcal{K}_\rho * u$, where "$*$" denotes convolution operator.

$\left|\nabla^\alpha u_\rho\right| = \sqrt{\left|{}^{CF}\mathcal{D}_x^\alpha u_\rho\right|^2 + \left|{}^{CF}\mathcal{D}_y^\alpha u_\rho\right|^2}$, where ${}^{CF}\mathcal{D}_x^\alpha u_\rho$ represents the Caputo-Fabrizio fractional derivative of order α of v_ρ with respect to the variable x, and ${}^{CF}\mathcal{D}_y^\alpha u_\rho$ represents the Caputo-Fabrizio fractional derivative of order α of v_ρ with respect to the variable y.

$\vec{n}$ is the unit outer normal vector along $\partial\Omega$.

$\hbar$ is a positive, decreasing function that satisfies the following conditions:

1.
$$\hbar(0) = 1,$$

2.
$$\lim_{s \to +\infty} \hbar(s) = 0.$$

Our proposed model offers the following advantages:

- The telegraph diffusion equation is a parabolic-hyperbolic partial differential equation (PDE) that can be understood as an interpolation between the diffusion and wave equation. This equation combines the characteristics of both diffusion and wave propagation. Compared to other diffusion-based methods, the telegraph diffusion equation more effectively preserves edges and details.

- The function $\hbar$ is an edge-controlled diffusion function that preserves essential features while smoothing out unwanted signals. Moreover, the fractional derivative operator exhibits a non-local property; unlike traditional derivatives, it depends on the behavior of the entire function rather than just nearby values, allowing for enhanced feature preservation.

- The use of Gaussian convolution in the proposed model offers several advantages. Not only does it enhance robustness in denoising, but it also contributes to the theoretical well-posedness of the model.

- The term $\gamma\,(u_0 - u)$ represents the source term associated with fidelity control [44], where γ regulates the balance between maintaining fidelity to the original image and applying nonlinear diffusion for noise reduction.

We begin our analysis by establishing the existence, uniqueness, and boundedness of the weak solution using Schauder's fixed point theorem, thereby providing a rigorous mathematical foundation. This is followed by the numerical implementation, which employs semi-implicit finite difference schemes based on the additive operator splitting (AOS) method [54]. This method ensures computational efficiency and unconditional stability. To evaluate the effectiveness of the proposed approach, we perform a comparative analysis with the classical telegraph model. The results highlight the advantages of incorporating fractional-order derivatives in the diffusivity function, particularly in improving noise reduction and preserving image quality.

The reminder of this chapter is organized as follows. In section 5.2, we investigate the existence and uniqueness of the weak solution for the proposed model. Section 5.3 outlines the numerical schemes developed for the model. Section 5.4 presents the experimental results to assess the model's performance. Finally, section 5.5 concludes the study by summarizing the key findings.

5.2 Theoretical framework and analysis

In this section, we establish the existence and uniqueness of the weak solution to the proposed model (5.1)-(5.3). To address the nonlinear nature of the problem, we first analyze its linearized form. Subsequently, we apply Schauder's fixed-point theorem to prove the existence of a weak solution. The associated space is defined as follows:

$$W(0,T) = \left\{ w \in L^2(0,T;\mathcal{H}^1(\Omega)),\ \frac{\partial w}{\partial t} \in L^2\left(0,T;L^2(\Omega)\right),\ \frac{\partial^2 w}{\partial t^2} \in L^2\left(0,T;(\mathcal{H}^1(\Omega))'\right) \right\}.$$

It is evident that $W(0,T)$ constitutes a Hilbert space endowed with the norm:

$$\|w\|_W = \|w\|_{L^2(0,T;\mathcal{H}^1(\Omega))} + \left\|\frac{\partial w}{\partial t}\right\|_{L^2\left(0,T;L^2(\Omega)\right)} + \left\|\frac{\partial^2 w}{\partial t^2}\right\|_{L^2\left(0,T;(\mathcal{H}^1(\Omega))'\right)}.$$

Definition 5.1. (**Weak solution**). A function u is said to be a weak solution of (5.1)-(5.3) if $u \in W(0,T)$ satisfies the following:

$$\left\langle \frac{\partial^2 u}{\partial t^2}, \varphi \right\rangle + \int_\Omega \left(\lambda\, \frac{\partial u}{\partial t}\, \varphi + \hbar\left(\left|\nabla^\alpha u_\rho\right|\right) \nabla u . \nabla \varphi \right) dx\, dy = \gamma \int_\Omega (u_0 - u)\, \varphi\, dx\, dy,$$

$$u(x,y,0) = u_0(x,y),\ \ \frac{\partial u(x,y,0)}{\partial t} = 0, \quad \text{in}\ \Omega,$$

for a.e. $t \in (0,T)$ and all $\varphi \in \mathcal{H}^1(\Omega)$.

We assume that the initial value $u_0 \in \mathcal{H}^1(\Omega)$ satisfies the following conditions:

$$0 < \eta := \operatorname{ess}\inf_{x,y\in\Omega} u_0(x,y) \text{ and } \ell := \operatorname{ess}\sup_{x,y\in\Omega} u_0(x,y) < \infty. \tag{5.4}$$

The space Ψ is defined as follows:

$$\Psi = \left\{ \quad w \in W(0,T) \cap L^\infty(0,T;L^2(\Omega)) : \eta \leq w(x,y,t) \leq \ell, \text{ a.e in } \Omega \times (0,T) \right\}.$$

For every $w \in \Psi$,

$$\|w\|_{L^\infty(0,T;\mathcal{H}^1(\Omega))} + \left\|\frac{\partial w}{\partial t}\right\|_{L^\infty(0,T;L^2(\Omega))} \leq C \|u_0\|_{\mathcal{H}^1(\Omega)}. \tag{5.5}$$

Formulation of the linearized problem

The linearized problem is formulated as follows:

$$\frac{\partial^2 u_w}{\partial t^2} + \lambda \frac{\partial u_w}{\partial t} = \operatorname{div}\left(\hbar\left(\left|\nabla^\alpha w_\rho\right|\right)\nabla u_w\right) + \gamma\left(u_0 - u_w\right), \qquad \text{in } \Omega \times (0,T), \tag{5.6}$$

$$u_w(x,y,0) = v_0(x,y), \quad \frac{\partial u_w(x,y,0)}{\partial t} = 0, \qquad \text{in } \Omega, \tag{5.7}$$

$$\nabla u_w.\vec{n} = 0, \qquad \text{on } \partial\Omega \times (0,T). \tag{5.8}$$

Lemma 5.1. *The following inequalities hold:*

$$\nu \leq \hbar\left(\left|\nabla^\alpha w_\rho\right|\right) \leq 1, \tag{5.9}$$

$$\left|\frac{\partial \hbar\left(\left|\nabla^\alpha w_\rho\right|\right)}{\partial t}\right| \leq \mu, \tag{5.10}$$

a.e. $t \in (0,T)$, *for any* $(x,y) \in \Omega$, *where the positive constant* μ, *depends only on* $\mathcal{K}_\rho$ *and* u_0.

Proof. See Proof 2.4.1. □

By using (5.9) and (5.10), we can apply the classical Galerkin method [26] to prove that the linearized problem (5.6)-(5.8) has a unique weak solution $u_w \in W(0,T)$.

Lemma 5.2. *Let* u_w *be a weak solution of the problem (5.6)-(5.8). Then*

$$0 < \eta \leq u_w(x,y,t) \leq \ell \text{ for a.e. } (x,y,t) \in \Omega \times (0,T). \tag{5.11}$$

Proof. We define $(u_w - \ell)_+$ as $(u_w - \ell)_+ = \max\{0, u_w - \ell\}$.

Integrating the equation (5.6) with respect the time variable, to get

$$\int_0^t \frac{\partial^2 u_w}{\partial s^2} ds + \lambda \int_0^t \frac{\partial u_w}{\partial s} ds = \int_0^t \operatorname{div}\left(\hbar\left(\left|\nabla^\alpha w_\rho\right|\right)\nabla u_w\right) ds + \gamma \int_0^t (u_0 - u_w)\, ds,$$

using (5.7), this implies that:

$$\frac{\partial u_w}{\partial t} + \lambda\left(u_w - u_0\right) = \int_0^t \operatorname{div}\left(\hbar\left(\left|\nabla^\alpha w_\rho\right|\right)\nabla u_w\right) ds + \gamma \int_0^t \left(u_0 - u_w\right) ds, \tag{5.12}$$

multiplying the equation (5.12) by $(u_w - \ell)_+$ and then integrating over Ω, we obtain that

$$\begin{aligned}&\int_\Omega \frac{\partial u_w}{\partial t}(u_w - \ell)_+ dx\,dy + \lambda \int_\Omega (u_w - u_0)(u_w - \ell)_+ dx\,dy \\ &= \int_0^t \int_\Omega \operatorname{div}\left(\hbar\left(\left|\nabla^\alpha w_\rho\right|\right)\nabla u_w\right)(u_w - \ell)_+ dx\,dy\,ds + \gamma \int_0^t \int_\Omega (u_0 - u_w)\left(u_w - \ell\right)_+ \,dx\,dy\,ds,\end{aligned}$$

using integrating by part formula and (5.8), we have:

$$\begin{aligned}&\frac{1}{2}\frac{d}{dt}\int_\Omega |(u_w - \ell)_+|^2\, dx\,dy + \lambda \int_\Omega (u_w - u_0)(u_w - \ell)_+ dx\,dy \\ &= -\int_0^t \int_{\{u_w \geq \ell\}} \hbar\left(\left|\nabla^\alpha w_\rho\right|\right)\nabla u_w \cdot \nabla u_w\, dx\,dy\,ds + \gamma \int_0^t \int_{\{u_w \geq \ell\}} (u_0 - u_w)\left(u_w - \ell\right)_+ dx\,dy\,ds,\end{aligned}$$

this is equivalent to the following:

$$\begin{aligned}&\frac{1}{2}\frac{d}{dt}\int_\Omega |(u_w - \ell)_+|^2\, dx\,dy + \lambda \int_\Omega (u_w - u_0)(u_w - \ell)_+ dx\,dy + \int_0^t \int_{\{u_w \geq \ell\}} \hbar\left(\left|\nabla^\alpha w_\rho\right|\right)|\nabla u_w|^2\, dx\,dy\,ds \\ &+ \gamma \int_0^t \int_{\{u_w \geq \ell\}} (u_w - u_0)\left(u_w - \ell\right)_+ \,dx\,dy\,ds = 0.\end{aligned}$$

Noting that $\hbar\left(\left|\nabla^\alpha w_\rho\right|\right) > 0$ and $(u_w - u_0)(u_w - \ell)_+ \geq 0$,

consequently, we have

$$\frac{d}{dt}\int_\Omega |(u_w - \ell)_+|^2\, dx\,dy \leq 0.$$

Because of $u_0 \leq \ell$, we obtain

$$\int_\Omega |(u_w - \ell)_+|^2\, dx\,dy \leq \int_\Omega |(u_0 - \ell)_+|^2\, dx\,dy \leq 0.$$

As a result,

$$u_w(x, y, t) \leq \ell \quad \text{for a.e. } (x, y, t) \in \Omega \times (0, T).$$

In the same way, we define $(u_w-\eta)_-$ as $(u_w-\eta)_- = \min\{0, u_w-\eta\}$, multiplying the equation (5.12) by $(u_w-\eta)_-$ and then integrating over Ω, we find:

$$0 < \eta \le u_w(x,y,t) \;\text{ for a.e. }\; (x,y,t) \in \Omega \times (0,T).$$

$\square$

Lemma 5.3. *The linearized problem (5.6)-(5.8) has a unique weak solution $u_w \in W(0,T)$ that satisfies the given estimates:*

$$\|u_w\|_{L^\infty(0,T;\mathcal{H}^1\Omega))} + \left\|\frac{\partial u_w}{\partial t}\right\|_{L^\infty(0,T;L^2(\Omega))} \le K_1, \tag{5.13}$$

$$\int_0^T \left\|\frac{\partial^2 u_w}{\partial t^2}\right\|^2_{(\mathcal{H}^1(\Omega))'} dt \le K_2, \tag{5.14}$$

where the constants K_1, and K_2 are positive and depend on $\|u_0\|_{\mathcal{H}^1(\Omega)}, \mathcal{K}_\rho, \nu, \eta$, and ℓ.

Proof. • Multiplying the equation (5.6) by $\dfrac{\partial u_w}{\partial t}$ and integrating by parts on Ω yields

$$\frac{1}{2}\frac{d}{dt}\left\|\frac{\partial u_w}{\partial t}\right\|^2_{L^2(\Omega)} + \lambda\left\|\frac{\partial u_w}{\partial t}\right\|^2_{L^2(\Omega)} + \int_\Omega \hbar\left(\left|\nabla^\alpha w_\rho\right|\right)\nabla u_w \cdot \nabla\left(\frac{\partial u_w}{\partial t}\right) dx\,dy = \gamma\int_\Omega (u_0-u_w)\frac{\partial u_w}{\partial t} dx\,dy.$$

According to Young's inequality, we get that:

$$\begin{aligned}&\frac{1}{2}\frac{d}{dt}\left\|\frac{\partial u_w}{\partial t}\right\|^2_{L^2(\Omega)} + \lambda\left\|\frac{\partial u_w}{\partial t}\right\|^2_{L^2(\Omega)} + \int_\Omega \hbar\left(\left|\nabla^\alpha w_\rho\right|\right)\nabla u_w \cdot \nabla\left(\frac{\partial u_w}{\partial t}\right) dx\,dy\\ &\le \frac{\gamma^2}{2}\|u_0-u_w\|^2_{L^2(\Omega)} + \frac{1}{2}\left\|\frac{\partial u_w}{\partial t}\right\|^2_{L^2(\Omega)}.\end{aligned}$$

Noting that:

$$\begin{aligned}\int_\Omega \hbar\left(\left|\nabla^\alpha w_\rho\right|\right)\nabla u_w \cdot \nabla\left(\frac{\partial u_w}{\partial t}\right) dx\,dy &= \int_\Omega \hbar\left(\left|\nabla^\alpha w_\rho\right|\right)\nabla u_w \cdot \frac{\partial}{\partial t}(\nabla u_w)\,dx\,dy\\ &= \frac{1}{2}\int_\Omega \hbar\left(\left|\nabla^\alpha w_\rho\right|\right)\frac{d}{dt}|\nabla u_w|^2\,dx\,dy.\end{aligned}$$

On the other hand, we have also

$$\begin{aligned}&\frac{1}{2}\int_\Omega \hbar\left(\left|\nabla^\alpha w_\rho\right|\right)\frac{d}{dt}|\nabla u_w|^2\,dx\,dy\\ &= \frac{1}{2}\frac{d}{dt}\int_\Omega \hbar\left(\left|\nabla^\alpha w_\rho\right|\right)|\nabla u_w|^2\,dx\,dy - \frac{1}{2}\int_\Omega \frac{d\hbar\left(\left|\nabla^\alpha w_\rho\right|\right)}{dt}|\nabla u_w|^2\,dx\,dy.\end{aligned}$$

Therefore, by using the inequality (5.10), we conclude that

$$\int_{\Omega} \hbar\left(\left|\nabla^{\alpha} w_{\rho}\right|\right) \nabla u_{w} \cdot \nabla\left(\frac{\partial u_{w}}{\partial t}\right) dx\, dy \geq \frac{1}{2} \frac{d}{dt} \int_{\Omega} \hbar\left(\left|\nabla^{\alpha} w_{\rho}\right|\right) |\nabla u_{w}|^{2}\, dx\, dy - \frac{\mu}{2} \|\nabla u_{w}\|_{L^{2}(\Omega)}^{2}. \tag{5.15}$$

According to (5.15), we observe that

$$\frac{d}{dt}\left(\left\|\frac{\partial u_{w}}{\partial t}\right\|_{L^{2}(\Omega)}^{2} + \int_{\Omega} \hbar\left(\left|\nabla^{\alpha} w_{\rho}\right|\right) |\nabla u_{w}|^{2}\, dx\, dy\right) \leq \gamma^{2} \|u_{0} - u_{w}\|_{L^{2}(\Omega)}^{2} + \left\|\frac{\partial u_{w}}{\partial t}\right\|_{L^{2}(\Omega)}^{2} + \mu \|\nabla u_{w}\|_{L^{2}(\Omega)}^{2}.$$

By using Lemma 5.2, we obtain

$$\begin{aligned} \|u_{0} - u_{w}\|_{L^{2}(\Omega)}^{2} &\leq 2\left(\|u_{0}\|_{\mathcal{H}^{1}(\Omega)}^{2} + \|u_{w}\|_{L^{2}(\Omega)}^{2}\right) \\ &\leq 2 \|u_{0}\|_{\mathcal{H}^{1}(\Omega)}^{2} + 2\ell^{2} |\Omega|. \end{aligned} \tag{5.16}$$

By (5.16), we obtain:

$$\begin{aligned} &\frac{d}{dt}\left(\left\|\frac{\partial u_{w}}{\partial t}\right\|_{L^{2}(\Omega)}^{2} + \int_{\Omega} \hbar\left(\left|\nabla^{\alpha} w_{\rho}\right|\right) |\nabla u_{w}|^{2}\, dx\, dy\right) \\ &\leq 2\gamma^{2} \|u_{0}\|_{\mathcal{H}^{1}(\Omega)}^{2} + 2\gamma^{2}\ell^{2} |\Omega| + \left\|\frac{\partial u_{w}}{\partial t}\right\|_{L^{2}(\Omega)}^{2} + \mu \|\nabla u_{w}\|_{L^{2}(\Omega)}^{2}. \end{aligned}$$

Observing in (5.9) that $0 < \nu \leq \hbar\left(\left|\nabla^{\alpha} w_{\rho}\right|\right)$ gives the following:

$$\nu \|\nabla u_{w}\|_{L^{2}(\Omega)}^{2} \leq \int_{\Omega} \hbar\left(\left|\nabla^{\alpha} w_{\rho}\right|\right) |\nabla u_{w}|^{2}\, dx\, dy.$$

Which implies

$$\|\nabla u_{w}\|_{L^{2}(\Omega)}^{2} \leq \frac{1}{\nu} \int_{\Omega} \hbar\left(\left|\nabla^{\alpha} w_{\rho}\right|\right) |\nabla u_{w}|^{2}\, dx\, dy. \tag{5.17}$$

Using (5.17) and substituting $C_{0} = 2\gamma^{2} \|u_{0}\|_{\mathcal{H}^{1}(\Omega)}^{2} + 2\gamma^{2}\ell^{2} |\Omega|$, we have:

$$\begin{aligned} &\frac{d}{dt}\left(\left\|\frac{\partial u_{w}}{\partial t}\right\|_{L^{2}(\Omega)}^{2} + \int_{\Omega} \hbar\left(\left|\nabla^{\alpha} w_{\rho}\right|\right) |\nabla u_{w}|^{2}\, dx\, dy\right) \\ &\leq C_{0} + C_{1}\left(\left\|\frac{\partial u_{w}}{\partial t}\right\|_{L^{2}(\Omega)}^{2} + \int_{\Omega} \hbar\left(\left|\nabla^{\alpha} w_{\rho}\right|\right) |\nabla u_{w}|^{2}\, dx\, dy\right), \end{aligned} \tag{5.18}$$

where $C_{1} = \max\left\{1, \frac{\mu}{\nu}\right\}$.

Through the use of Gronwall's lemma, we obtain

$$\left\|\frac{\partial u_{w}(t)}{\partial t}\right\|_{L^{2}(\Omega)}^{2} + \int_{\Omega} \hbar\left(\left|\nabla^{\alpha} w_{\rho}(x, y, t)\right|\right) |\nabla u_{w}|^{2}\, dx\, dy \leq e^{C_{1}t}(C_{2} + C_{0}t),$$

for a.e. $t \in (0, T]$, where

$$C_{2} = \left\|\frac{\partial u_{w}(0)}{\partial t}\right\|_{L^{2}(\Omega)}^{2} + \int_{\Omega} \hbar\left(\left|\nabla^{\alpha} w_{\rho}(x, y, 0)\right|\right) \left|\nabla u_{w}(x, y, 0)\right|^{2}\, dx\, dy.$$

With the inequality (5.17), we have

$$\|\nabla u_w\|^2_{L^2(\Omega)} \leq \frac{1}{\nu} e^{C_1 T}(C_2 + C_0 T). \tag{5.19}$$

Therefore, for a.e. $t \in (0, T]$,

$$\left\|\frac{\partial u_w}{\partial t}\right\|^2_{L^2(\Omega)} + \|\nabla u_w\|^2_{L^2(\Omega)} \leq K e^{C_1 t}(C_2 + C_0 t), \tag{5.20}$$

where $K = \max\left\{1, \dfrac{1}{\nu}\right\}$.

According to $u_w(x, y, t) = u_w(x, y, 0) + \int_0^t \frac{\partial u_w}{\partial \tau} d\tau$, inequalities (1.15), and (5.20), we have

$$\begin{aligned}\|u_w\|^2_{L^2(\Omega)} &\leq 2\,\|u_0\|^2_{\mathcal{H}^1(\Omega)} + 2T \int_0^t \left\|\frac{\partial u_w(\tau)}{\partial \tau}\right\|^2_{L^2(\Omega)} d\tau \\ &\leq 2\,\|u_0\|^2_{\mathcal{H}^1(\Omega)} + 2T^2 K e^{C_1 T}(C_2 + C_0 T).\end{aligned} \tag{5.21}$$

From (5.20) and (5.21), it follows that

$$\|u_w\|_{L^\infty(0,T;\mathcal{H}^1(\Omega))} + \left\|\frac{\partial u_w}{\partial t}\right\|_{L^\infty(0,T;L^2(\Omega))} \leq K_1. \tag{5.22}$$

- Multiplying (5.6) by $\varphi \in \mathcal{H}^1(\Omega)$ where $\|\varphi\|_{\mathcal{H}^1(\Omega)} \leq 1$, applying Cauchy-Schwarz's inequality, and combining (5.16) and (5.22), we acquire that:

$$\begin{aligned}\left|\left\langle \frac{\partial^2 u_w}{\partial t^2}, \varphi\right\rangle\right| &= \left|\lambda \int_\Omega \frac{\partial u_w}{\partial t}\,\varphi\, dx\, dy + \int_\Omega \hbar\left(\left|\nabla^\alpha w_\rho\right|\right) \nabla u_w \cdot \nabla\varphi\, dx\, dy + \gamma \int_\Omega (u_0 - u_w)\,\varphi\, dx\, dy\right| \\ &\leq \left(\lambda \left\|\frac{\partial u_w}{\partial t}\right\|_{L^2(\Omega)} + \left|\hbar\left(\left|\nabla^\alpha w_\rho\right|\right)\right| \|\nabla u_w\|_{L^2(\Omega)} + \gamma\,\|u_0 - u_w\|_{L^2(\Omega)}\right) \|\varphi\|_{\mathcal{H}^1(\Omega)} \\ &\leq \left((\lambda + 1)\,K_1 + \sqrt{2}\gamma\,\|u_0\|_{\mathcal{H}^1(\Omega)} + \sqrt{2\,|\Omega|}\gamma\ell\right) \|\varphi\|_{\mathcal{H}^1(\Omega)}\,.\end{aligned}$$

Consequently, we find

$$\left\|\frac{\partial^2 u_w}{\partial t^2}\right\|_{(\mathcal{H}^1(\Omega))'} \leq K_0 + \sqrt{2}\gamma\,\|u_0\|_{\mathcal{H}^1(\Omega)}\,. \tag{5.23}$$

Where $K_0 = (\lambda + 1)\,K_1 + \sqrt{2\,|\Omega|}\gamma\ell$.

Additionally, by squaring (5.23) and integrating over $(0, T)$, we obtain:

$$\int_0^T \left\|\frac{\partial^2 u_w}{\partial t^2}\right\|^2_{(\mathcal{H}^1(\Omega))'} dt \leq K_2.$$

The proof is complete. □

Theorem 5.1. *(**Existence of weak solution**). Assuming that $u_0 \in \mathcal{H}^1(\Omega)$ and that (5.4) is satisfied, the problem described by (5.1)-(5.3) admits a weak solution $v \in W(0,T)$.*

Proof. We now establish the existence of a weak solution to the underlying problem using Schauder fixed-point theorem. To this end, we introduce the subset $\bar{W}$ of $W(0,T)$, defined by:

$$\bar{W} = \left\{ \begin{array}{l} w \in W(0,T); \|w\|_{L^2(0,T;\mathcal{H}^1(\Omega))} + \left\|\dfrac{\partial w}{\partial t}\right\|_{L^2(0,T;L^2(\Omega))} \leq K_1, \left\|\dfrac{\partial^2 w}{\partial t^2}\right\|_{L^2(0,T;(\mathcal{H}^1(\Omega))')} \leq K_2 \\ 0 < \eta \leq w(x,y,t) \leq \ell \text{ for a.e. } (x,y,t) \in \Omega \times (0,T), w(0) = u_0, \dfrac{\partial w(0)}{\partial t} = 0 \end{array} \right\}.$$

In addition, it can be proved that $\bar{W}$ is a non-empty, convex, and weakly compact subset of $W(0,T)$. Following this, we define the subsequent mapping:

$$\begin{aligned} Q :& \bar{W} \to \bar{W} \\ & w \mapsto u_w. \end{aligned}$$

To apply Schauder's fixed-point theorem, it is necessary to prove that the mapping $Q : w \mapsto u_w$ is weakly continuous from $\bar{W}$ into $\bar{W}$. Consider a sequence w_j in $\bar{W}$ that weakly converges to some w in $\bar{W}$, and let $u_j = Q(w_j)$. Our goal is to demonstrate that $Q(w_j) := u_j$ weakly converges to $Q(w) := u_w$. By lemma 5.3, we can use the classical results concerning compact inclusion in Sobolev spaces [2], which allows us to extract sub-sequences from both w_j and u_j (still denoted by w_j and u_j). Thus, we have:

$$w_j \to w \text{ in } L^2((0,T);L^2(\Omega)) \text{ and a.e. on } \Omega \times (0,T), \tag{5.24}$$

$$\nabla^\alpha (w_j)_\rho \to \nabla^\alpha w_\rho \text{ in } L^2((0,T);L^2(\Omega)) \text{ and a.e. on } \Omega \times (0,T), \tag{5.25}$$

$$\hbar\left(\left|\nabla^\alpha (w_j)_\rho\right|\right) \to \hbar\left(\left|\nabla^\alpha w_\rho\right|\right) \text{ in } L^2((0,T);L^2(\Omega)) \text{ and a.e. on } \Omega \times (0,T), \tag{5.26}$$

$$u_j \to u \text{ weakly in } L^2((0,T);\mathcal{H}^1(\Omega)), \tag{5.27}$$

$$\frac{\partial u_j}{\partial t} \to \frac{\partial u}{\partial t} \text{ weakly in } L^2((0,T);L^2(\Omega)), \tag{5.28}$$

$$\frac{\partial^2 u_j}{\partial t^2} \to \frac{\partial^2 u}{\partial t^2} \text{ weakly in } L^2((0,T);(\mathcal{H}^1(\Omega))'), \tag{5.29}$$

$$u_j \to u \text{ in } L^2((0,T);L^2(\Omega)) \text{ and a.e. on } \Omega \times (0,T), \tag{5.30}$$

$$\nabla u_j \to \nabla u \text{ weakly in } L^2((0,T);L^2(\Omega)), \tag{5.31}$$

$$u_j(0) \to u(0) \text{ in } L^2(\Omega), \tag{5.32}$$

$$\frac{\partial u_j(0)}{\partial t} \to 0 \text{ in } (\mathcal{H}^1(\Omega))'. \tag{5.33}$$

The result in (5.26) is obtained by applying the dominated convergence theorem [10].

Given that u_j is the weak solution of (5.6) associated with w_j, it follows that, for almost every $t \in (0,T]$, and for any $\varphi \in \mathcal{H}^1(\Omega)$, the following holds:

$$\int_\Omega \frac{\partial^2 u_j}{\partial t^2}\varphi\, dx\, dy + \lambda \int_\Omega \frac{\partial u_j}{\partial t}\varphi\, dx\, dy + \int_\Omega \hbar\left(\left|\nabla^\alpha (w_j)_\rho\right|\right)\nabla u_j \cdot \nabla\varphi\, dx\, dy = \gamma \int_\Omega \left(u_j(0) - u_j\right)\varphi\, dx\, dy. \tag{5.34}$$

By integrating equation (5.34) over the interval $(0,T)$, we obtain the resulting formula:

$$\begin{aligned}&\int_0^T \int_\Omega \frac{\partial^2 u_j}{\partial t^2}\varphi\, dx\, dy\, dt + \lambda \int_0^T \int_\Omega \frac{\partial u_j}{\partial t}\varphi\, dx\, dy\, dt \int_0^T \int_\Omega \hbar\left(\left|\nabla^\alpha (w_j)_\rho\right|\right)\nabla u_j \cdot \nabla\varphi\, dx\, dy\, dt\\ &= \gamma \int_0^T \int_\Omega \left(u_j(0) - u_j\right)\varphi\, dx\, dy\, dt.\end{aligned} \tag{5.35}$$

From (5.28)-(5.29), we get

$$\int_0^T \int_\Omega \frac{\partial^2 u_j}{\partial t^2}\varphi\, dx\, dy\, dt \to \int_0^T \int_\Omega \frac{\partial^2 u}{\partial t^2}\varphi\, dx\, dy\, dt, \quad \text{as } j \to \infty,$$

$$\lambda \int_0^T \int_\Omega \frac{\partial u_j}{\partial t}\varphi\, dx\, dy\, dt \to \lambda \int_0^T \int_\Omega \frac{\partial u}{\partial t}\varphi\, dx\, dy\, dt, \quad \text{as } j \to \infty.$$

Examining the third term in (5.35)

$$
\begin{aligned}
&\left|\int_0^T\int_\Omega \hbar\left(\left|\nabla^\alpha (w_\jmath)_\rho\right|\right)\nabla u_\jmath\cdot\nabla\varphi\,dx\,dy\,dt-\int_0^T\int_\Omega \hbar\left(\left|\nabla^\alpha w_\rho\right|\right)\nabla u\cdot\nabla\varphi\,dx\,dy\,dt\right|\\
&\leq \int_0^T\int_\Omega \left|\hbar\left(\left|\nabla^\alpha (w_\jmath)_\rho\right|\right)-\hbar\left(\left|\nabla^\alpha w_\rho\right|\right)\right||\nabla u|\left|\nabla\varphi\right|\,dx\,dy\,dt\\
&+\left|\int_0^T\int_\Omega \hbar\left(\left|\nabla^\alpha (w_\jmath)_\rho\right|\right)\nabla(u_\jmath-u)\cdot\nabla\varphi\,dx\,dy\,dt\right|.
\end{aligned}
$$

Based on claim 2.1, we infer that, as $\jmath\to\infty$

$$
\begin{aligned}
&\int_0^T\int_\Omega \left|\hbar\left(\left|\nabla^\alpha (w_\jmath)_\rho\right|\right)-\hbar\left(\left|\nabla^\alpha w_\rho\right|\right)\right||\nabla u|\left|\nabla\varphi\right|\,dx\,dy\,dt\\
&\leq C\int_0^T\int_\Omega \left\|w_\jmath-w\right\|_{L^2(\Omega)}|\nabla u|\left|\nabla\varphi\right|\,dx\,dy\,dt\\
&\leq C(\varphi)\left\|w_\jmath-w\right\|_{L^2(\Omega)}\|\nabla u\|_{L^2((0,T);L^2(\Omega))}\to 0.
\end{aligned}
$$

Additionally, as $\jmath\to\infty$,

$$
\left|\int_0^T\int_\Omega \hbar\left(\left|\nabla^\alpha (w_\jmath)_\rho\right|\right)\nabla(u_\jmath-u)\cdot\nabla\varphi\,dx\,dy\,dt\right|\to 0.
$$

From (5.30) and (5.32), we have

$$
\gamma\int_0^T\int_\Omega \left(u_\jmath(0)-u_\jmath\right)\varphi\,dx\,dy\,dt\to\gamma\int_0^T\int_\Omega (u_0-u)\,\varphi\,dx\,dy\,dt.
$$

Taking the limit as $\jmath\to\infty$ in equation (5.35) leads to the conclusion that

$$
\begin{aligned}
&\int_0^T\int_\Omega \frac{\partial^2 u}{\partial t^2}\varphi\,dx\,dy\,dt+\lambda\int_0^T\int_\Omega \frac{\partial u}{\partial t}\varphi\,dx\,dy\,dt+\int_0^T\int_\Omega \hbar\left(\left|\nabla^\alpha w_\rho\right|\right)\nabla u.\nabla\varphi\,dx\,dy\,dt\\
&=\gamma\int_0^T\int_\Omega (u_0-u)\,\varphi\,dx\,dy\,dt.
\end{aligned}
$$

Consequently, due to the arbitrariness of $\varphi\in\mathcal{H}^1(\Omega)$, we obtain for a.e $t\in(0,T]$

$$
\int_\Omega \frac{\partial^2 u}{\partial t^2}\varphi\,dx\,dy+\lambda\int_\Omega \frac{\partial u}{\partial t}\varphi\,dx\,dy+\int_\Omega \hbar\left(\left|\nabla^\alpha w_\rho\right|\right)\nabla u.\nabla\varphi\,dx\,dy=\gamma\int_\Omega (u_0-u)\,\varphi\,dx\,dy.
$$

As a result, it can be concluded that

$$u = u_w = Q(w).$$

Moreover, considering the uniqueness of the solution to problem (5.6), the whole sequence $u_j = Q(w_j)$ converge weakly in $\bar{W}$ to $u = Q(w)$. This demonstrates that the mapping Q is weakly continuous.

Thus, according to Schauder's fixed-point theorem, there exists $w \in \bar{W}$ such that

$$w = Q(w) = u_w.$$

Therefore, the existence of the weak solution u_w to the problem (5.1)-(5.3) is proved. □

Theorem 5.2. *(**Uniqueness of weak solution**). Given that u is a weak solution to (5.1)-(5.3), it follows that u is unique.*

Proof. Let u_1, u_2 be tow weak solutions of (5.1)-(5.3). Then for almost every $t \in (0,T)$, we have

$$\begin{cases} \dfrac{\partial^2 u_i}{\partial t^2} + \lambda \dfrac{\partial u_i}{\partial t} = \operatorname{div}\left(\hbar\left(\left|\nabla^\alpha (u_i)_\rho\right|\right)\nabla v\right) + \gamma\,(u_0 - u_i)\,, & \Omega\times(0,T)\,, \\ u_i(x,y,0) = u_0(x,y),\ \dfrac{\partial u_i(x,y,0)}{\partial t} = 0, & \Omega, \\ \nabla u_i.\vec{n} = 0, & \partial\Omega\times(0,T)\,. \end{cases} \tag{5.36}$$

Where $i = 1,2$.

Set $\bar{u} = u_1 - u_2$. Then we have:

$$\frac{\partial^2 \bar{u}}{\partial t^2} + \lambda\frac{\partial \bar{u}}{\partial t} - \operatorname{div}(\hbar\left(\left|\nabla^\alpha (u_1)_\rho\right|\right)\nabla\bar{u}) = \operatorname{div}((\hbar\left(\left|\nabla^\alpha (u_1)_\rho\right|\right) - \hbar\left(\left|\nabla^\alpha (u_2)_\rho\right|\right))\nabla u_2) - \gamma\,\bar{u}, \quad \Omega\times(0,T)\,, \tag{5.37}$$

$$\bar{u}(x,y,0) = 0,\ \frac{\partial \bar{u}(x,y,0)}{\partial t} = 0, \quad \Omega, \tag{5.38}$$

$$\nabla\bar{u}.\vec{n} = 0, \quad \partial\Omega\times(0,T)\,. \tag{5.39}$$

It is sufficient to demonstrate that $\bar{u} = 0$. To confirm this, fix $0 < \eta < T$, and set for $i = 1,2$,

$$\vartheta_i(.,t) = \begin{cases} \int_t^\eta u_i(.,\tau)d\tau, & 0 < t \le \eta, \\ 0 & \eta \le t < T. \end{cases} \tag{5.40}$$

Then, $\vartheta_i(.,t) \in \mathcal{H}^1(\Omega)$ for $t \in (0,T)$. Define $\vartheta = \vartheta_1 - \vartheta_2$. It can be verified that $\vartheta(.,\eta) = 0$. By multiplying both sides of equation (5.37) by ϑ, integrating over $\Omega\times(0,\eta)$ and applying the integration by parts formula, we get:

$$\begin{aligned}
&\int_0^\eta \int_\Omega \left(-\frac{\partial \bar{u}}{\partial t}\frac{\partial \vartheta}{\partial t} - \lambda\, \bar{u}\frac{\partial \vartheta}{\partial t} + \hbar\left(\left|\nabla^\alpha (u_1)_\rho\right|\right)\nabla \bar{u}\cdot\nabla\vartheta \right) dx\,dy\,dt \\
&= -\int_0^\eta \int_\Omega (\hbar\left(\left|\nabla^\alpha (u_1)_\rho\right|\right) - \hbar\left(\left|\nabla^\alpha (u_2)_\rho\right|\right))\nabla u_2\cdot\nabla\vartheta\, dx\,dy\,dt - \gamma\int_0^\eta\int_\Omega \bar{u}\,\vartheta\, dx\,dy\,dt.
\end{aligned}$$

Since

$$\frac{\partial \vartheta}{\partial t} = -\bar{u} \ \text{ for } \ 0<t<T. \tag{5.41}$$

The above equality becomes

$$\begin{aligned}
&\frac{1}{2}\int_0^\eta\int_\Omega \frac{\partial}{\partial t}|\bar{u}|^2\, dx\,dy\,dt + \lambda\int_0^\eta\int_\Omega |\bar{u}|^2\, dx\,dy\,dt - \int_0^\eta\int_\Omega \hbar\left(\left|\nabla^\alpha (u_1)_\rho\right|\right)\frac{\partial\nabla\vartheta}{\partial t}\cdot\nabla\vartheta dx\,dy\,dt \\
&= -\int_0^\eta \int_\Omega (\hbar\left(\left|\nabla^\alpha (u_1)_\rho\right|\right) - \hbar\left(\left|\nabla^\alpha (u_2)_\rho\right|\right))\nabla u_2\cdot\nabla\vartheta\, dx\,dy\,dt - \gamma\int_0^\eta\int_\Omega \bar{u}\,\vartheta\, dx\,dy\,dt.
\end{aligned}$$

By applying the Young's inequality, we obtain

$$\begin{aligned}
&\frac{1}{2}\int_0^\eta\int_\Omega \frac{\partial}{\partial t}|\bar{u}|^2\, dx\,dy\,dt + \lambda\int_0^\eta\int_\Omega |\bar{u}|^2\, dx\,dy\,dt - \int_0^\eta\int_\Omega \hbar\left(\left|\nabla^\alpha (u_1)_\rho\right|\right)\frac{\partial\nabla\vartheta}{\partial t}\cdot\nabla\vartheta\, dx\,dy\,dt \\
&\leq -\int_0^\eta \int_\Omega (\hbar\left(\left|\nabla^\alpha (u_1)_\rho\right|\right) - \hbar\left(\left|\nabla^\alpha (u_2)_\rho\right|\right))\nabla u_2\cdot\nabla\vartheta\, dx\,dy\,dt + \frac{\gamma^2}{2}\int_0^\eta\int_\Omega |\bar{u}|^2\, dx\,dy\,dt \\
&+ \frac{1}{2}\int_0^\eta\int_\Omega |\vartheta|^2\, dx\,dy\,dt.
\end{aligned}$$

Which implies

$$\begin{aligned}
&\frac{1}{2}\left\|\bar{u}(\eta)\right\|^2_{L^2(\Omega)} + \lambda\int_0^\eta \|\bar{u}\|^2_{L^2(\Omega)}\, dt - \int_0^\eta\int_\Omega \hbar\left(\left|\nabla^\alpha (u_1)_\rho\right|\right)\frac{\partial\nabla\vartheta}{\partial t}\cdot\nabla\vartheta\, dx\,dy\,dt \\
&\leq \int_0^\eta \left\|\hbar\left(\left|\nabla^\alpha (u_1)_\rho\right|\right) - \hbar\left(\left|\nabla^\alpha (u_2)_\rho\right|\right)\right\|_{L^\infty(\Omega)} \|\nabla u_2\|_{L^2(\Omega)}\, \|\nabla\vartheta\|_{L^2(\Omega)}\, dt + \frac{\gamma^2}{2}\int_0^\eta \|\bar{u}\|^2_{L^2(\Omega)}\, dt \\
&+ \frac{1}{2}\int_0^\eta \|\vartheta\|^2_{L^2(\Omega)}\, dt.
\end{aligned}$$

Noting that

$$\begin{aligned}
&\hbar\left(\left|\nabla^\alpha (u_1)_\rho\right|\right)\frac{\partial\nabla\vartheta}{\partial t}\cdot\nabla\vartheta = \frac{1}{2}\frac{\partial}{\partial t}\left(\hbar\left(\left|\nabla^\alpha (u_1)_\rho\right|\right)|\nabla\vartheta|^2\right) - \frac{1}{2}\frac{\partial\hbar\left(\left|\nabla^\alpha (u_1)_\rho\right|\right)}{\partial t}|\nabla\vartheta|^2, \\
&\nabla\vartheta(x,y,\eta) = 0,
\end{aligned}$$

with (5.38), we have

$$\begin{aligned}
&\frac{1}{2}\left\|\bar{u}(\eta)\right\|^2_{L^2(\Omega)} + \lambda\int_0^\eta \|\bar{u}\|^2_{L^2(\Omega)}\,dt + \frac{1}{2}\int_\Omega \hbar\left(\left|\nabla^\alpha(u_1(x,y,0))_\rho\right|\right)\left|\nabla\vartheta(x,y,0)\right|^2 dx\,dy\\
&\leq \left|-\frac{1}{2}\int_0^\eta\int_\Omega |\nabla\vartheta|^2\,\frac{\partial\hbar\left(\left|\nabla^\alpha(u_1)_\rho\right|\right)}{\partial t}dx\,dy\,dt\right|\\
&+\int_0^\eta \left\|\hbar\left(\left|\nabla^\alpha(u_1)_\rho\right|\right)-\hbar\left(\left|\nabla^\alpha(u_2)_\rho\right|\right)\right\|_{L^\infty(\Omega)}\|\nabla u_2\|_{L^2(\Omega)}\|\nabla\vartheta\|_{L^2(\Omega)}\,dt + \frac{\gamma^2}{2}\int_0^\eta \|\bar{u}\|^2_{L^2(\Omega)}\,dt\\
&+\frac{1}{2}\int_0^\eta \|\vartheta\|^2_{L^2(\Omega)}\,dt.
\end{aligned}$$

As seen in (5.9) and (5.10), there exists positive constants ν_1 and μ_1 such that:

$$\nu_1 \leq \hbar\left(\left|\nabla^\alpha(u_1)_\rho(x,y,t)\right|\right)\leq 1,\quad \left|\frac{\partial\hbar\left(\nabla^\alpha(u_1)_\rho(x,y,t)\right)}{\partial t}\right|\leq \mu_1,$$

for a.e. $(x,y,t)\in\Omega\times(0,T)$.

Moreover, according to (2.2) we deduce:

$$\left\|\hbar\left(\left|\nabla^\alpha(u_1)_\rho\right|\right)-\hbar\left(\left|\nabla^\alpha(u_2)_\rho\right|\right)\right\|_{L^\infty(\Omega)}\leq \bar{C}\,\|\bar{u}\|_{L^2(\Omega)}\,, \tag{5.42}$$

where $\bar{C}$ is a positive constant.

Thus, we arrive at the following inequality:

$$\begin{aligned}
&\frac{1}{2}\left\|\bar{u}(\eta)\right\|^2_{L^2(\Omega)} + \lambda\int_0^\eta \|\bar{u}\|^2_{L^2(\Omega)}\,dt + \frac{\nu_1}{2}\|\nabla\vartheta(0)\|^2_{L^2(\Omega)}\\
&\leq \frac{\mu_1}{2}\int_0^\eta \|\nabla\vartheta\|^2_{L^2(\Omega)}\,dt + \bar{C}\,\|u_2\|_{L^\infty(0,T;\mathcal{H}^1(\Omega))}\int_0^\eta \|\bar{u}\|_{L^2(\Omega)}\|\nabla\vartheta\|_{L^2(\Omega)}\,dt + \frac{\gamma^2}{2}\int_0^\eta\|\bar{u}\|^2_{L^2(\Omega)}\,dt\\
&+\frac{1}{2}\int_0^\eta\|\vartheta\|^2_{L^2(\Omega)}\,dt.
\end{aligned}$$

By using the Young inequality, we obtain

$$\frac{1}{2}\left\|\bar{u}(\eta)\right\|^2_{L^2(\Omega)} + \lambda\int_0^\eta \|\bar{u}\|^2_{L^2(\Omega)}\,dt + \frac{\nu_1}{2}\|\nabla\vartheta(0)\|^2_{L^2(\Omega)} \leq C\left(\int_0^\eta \|\bar{u}\|^2_{L^2(\Omega)}\,dt + \int_0^\eta \|\vartheta\|^2_{\mathcal{H}^1(\Omega)}\,dt\right). \tag{5.43}$$

From (5.40), it deduce that

$$\|\vartheta(0)\|^2_{L^2(\Omega)} = \left\|\int_0^\eta \bar{u}\,dt\right\|^2_{L^2(\Omega)} \leq T\int_0^\eta \|\bar{u}\|^2_{L^2(\Omega)}\,dt. \tag{5.44}$$

Utilizing (5.44) in (5.43), we conclude that

$$\frac{1}{2}\left\|\bar{u}(\eta)\right\|^2_{L^2(\Omega)} + \lambda\int_0^\eta \|\bar{u}\|^2_{L^2(\Omega)}\,dt + \frac{\nu_1}{2}\|\vartheta(0)\|^2_{\mathcal{H}^1(\Omega)} \leq C\left(\int_0^\eta \|\bar{u}\|^2_{L^2(\Omega)}\,dt + \int_0^\eta \|\vartheta\|^2_{\mathcal{H}^1(\Omega)}\,dt\right). \tag{5.45}$$

Now, we define:

$$\psi_i(.,t) = \int_0^t u_i(.,\tau)d\tau, \quad 0 < t < T,$$

and, $\psi = \psi_1 - \psi_2$.

Based on the above definition and by integrating the both sides of (5.41) over $(0,\eta)$, we observe that:

$$\vartheta(x,y,0) = \vartheta(x,y,\eta) + \int_0^\eta \bar{u}(x,y,t)dt = \int_0^\eta \bar{u}(x,y,t)dt = \psi(x,y,\eta),$$
$$\vartheta(x,y,t) = \psi(x,y,\eta) - \psi(x,y,t), \quad 0 < t \leq \eta.$$

Consequently, 5.45 implies

$$\frac{1}{2}\left\|\bar{u}(\eta)\right\|^2_{L^2(\Omega)} + \lambda\int_0^\eta \|\bar{u}\|^2_{L^2(\Omega)}\,dt + \frac{\nu_1}{2}\left\|\psi(\eta)\right\|^2_{\mathcal{H}^1(\Omega)} \leq C\left(\int_0^\eta \|\bar{u}\|^2_{L^2(\Omega)}\,dt + \int_0^\eta \left\|\psi(\eta) - \psi(t)\right\|^2_{\mathcal{H}^1(\Omega)}\,dt\right). \tag{5.46}$$

Take note that

$$\left\|\psi(\eta) - \psi(t)\right\|^2_{\mathcal{H}^1(\Omega)} \leq 2\left\|\psi(\eta)\right\|^2_{\mathcal{H}^1(\Omega)} + 2\left\|\psi(t)\right\|^2_{\mathcal{H}^1(\Omega)}. \tag{5.47}$$

Thus, (5.46) reduces to

$$\begin{aligned}&\frac{1}{2}\left\|\bar{u}(\eta)\right\|^2_{L^2(\Omega)} + \lambda\int_0^\eta \|\bar{u}\|^2_{L^2(\Omega)}\,dt + \frac{\nu_1}{2}\left\|\psi(\eta)\right\|^2_{\mathcal{H}^1(\Omega)}\\ &\leq C\int_0^\eta \|\bar{u}\|^2_{L^2(\Omega)}\,dt + 2C\eta\left\|\psi(\eta)\right\|^2_{\mathcal{H}^1(\Omega)} + 2C\int_0^\eta \left\|\psi(t)\right\|^2_{\mathcal{H}^1(\Omega)}\,dt.\end{aligned} \tag{5.48}$$

This implies

$$\begin{aligned}&\frac{1}{2}\left\|\bar{u}(\eta)\right\|^2_{L^2(\Omega)} + \lambda\int_0^\eta \|\bar{u}\|^2_{L^2(\Omega)}\,dt + \left(\frac{\nu_1}{2} - 2C\eta\right)\left\|\psi(\eta)\right\|^2_{\mathcal{H}^1(\Omega)}\\ &\leq C\int_0^\eta \|\bar{u}\|^2_{L^2(\Omega)}\,dt + 2C\int_0^\eta \left\|\psi\right\|^2_{\mathcal{H}^1(\Omega)}\,dt.\end{aligned} \tag{5.49}$$

There exists a sufficiently small T_1 such that

$$\frac{\nu_1}{2} - 2T_1C > 0.$$

For $0 < \eta \leq T_1$, (5.49) yields that

$$\left\|\bar{u}(\eta)\right\|^2_{L^2(\Omega)} + \left\|\psi(\eta)\right\|^2_{\mathcal{H}^1(\Omega)} \leq K\int_0^\eta \left(\|\bar{u}\|^2_{L^2(\Omega)} + \left\|\psi\right\|^2_{\mathcal{H}^1(\Omega)}\right)dt. \tag{5.50}$$

As a result, applying Gronwall's lemma implies that $\bar{u} \equiv 0$ on the interval $(0,T_1]$.

In the end, we apply the same procedure to the intervals $(T_1,2T_1]$, $(2T_1,3T_1]$, and so on, step by step, ultimately concluding that $u_1 = u_2$ on $(0,T)$. Consequently, we establish the uniqueness of the weak solution. □

Remark 5.1. *(**Boundedness of weak solution**). As stated in theorem 5.1, the weak solution to problem (5.1)-(5.3) belongs to $\bar{W}$ and $w = Q(w) = u_w$ represents the fixed point of the problem (5.1)-(5.3). Consequently, u_w is also an element of $\bar{W}$. Due to the uniqueness of the solution, it follows that the unique weak solution $v = u_w$ satisfies the extremum principle:*

$$0 < \eta \leq u(x, y, t) \leq \ell \text{ for a.e. } (x, y, t) \in \Omega \times (0, T).$$

Such that:

$$0 < \eta := \text{ess} \inf_{x,y \in \Omega} u_0(x, y) \text{ and } \ell := \text{ess} \sup_{x,y \in \Omega} u_0(x, y) < \infty.$$

5.3 Numerical implementation

In this section, to numerically solve the problem defined by (5.1)-(5.3), we construct a semi-implicit finite difference scheme based on the additive operator splitting (AOS) technique. Originally introduced by Weickert et al. [54] , this technique provides an efficient, reliable, and unconditionally stable scheme for nonlinear diffusion in image processing.

Assume a space grid size of $\Delta x = \Delta y = \Delta s$ and a time-step size of Δt. Denote $v_{i,j}^n = v(x_i, y_i, t_n)$ where $x_i = i\Delta s$, $0 \leq i \leq N$; $y_j = j\Delta s$, $0 \leq j \leq M$; $t_n = n\Delta t$, $n \geq 0$, where n is the number of iterations and $N \times M$ is the size of the image.

1). Discretize the Caputo-Fabrizio fractional derivatives. Based on definition (1.13), the discretization of these derivatives over the interval $[0, x_i]$ (analogously, $[0, y_j]$) is carried out using the forward finite difference scheme as follows:

$$^{CF}D_x^{\alpha}\, u(x_i, y_j, t_n) = \frac{1}{1-\alpha} \int_0^{x_i} e^{-\left(\frac{\alpha}{1-\alpha}\right)(x_i - s)} \frac{\partial}{\partial s} u(s, y_j, t_n) ds. \tag{5.51}$$

Equation (5.51) can be rewritten as:

$$^{CF}D_x^{\alpha}\, u(x_i, y_j, t_n) \approx \frac{1}{1-\alpha} \sum_{k=0}^{i-1} \left(\frac{u_{k+1,j}^n - u_{k,j}^n}{\Delta s} \right) \int_{x_k}^{x_{k+1}} e^{-\left(\frac{\alpha}{1-\alpha}\right)(x_i - s)} ds.$$

Using the space grid point $x_i = i\Delta s$ for $i = 0, 1, ...N$, and by integrating, we obtain:

$$
\begin{aligned}
{}^{CF}D_x^{\alpha}\, u_{i,j}^n &\approx \frac{1}{\alpha\,\Delta s}\sum_{k=0}^{i-1}\left(u_{k+1,j}^n - u_{k,j}^n\right)\left[e^{-\left(\frac{\alpha}{1-\alpha}\right)(i-(k+1))\Delta s} - e^{-\left(\frac{\alpha}{1-\alpha}\right)(i-k)\Delta s}\right]\\
&= \sum_{k=0}^{i-1}\Lambda_{\alpha,i,k}\left(u_{k+1,j}^n - u_{k,j}^n\right),
\end{aligned}
$$

where

$$
\Lambda_{\alpha,i,k} = \frac{1}{\alpha\,\Delta s}\left[e^{-\left(\frac{\alpha}{1-\alpha}\right)(i-(k+1))\Delta s} - e^{-\left(\frac{\alpha}{1-\alpha}\right)(i-k)\Delta s}\right].
$$

An analogue expression is obtained for ${}^{CF}D_y^{\alpha}\, u_{i,j}^n$,

$$
\begin{aligned}
{}^{CF}D_y^{\alpha}\, u_{i,j}^n &\approx \frac{1}{\alpha\,\Delta s}\sum_{k=0}^{j-1}\left(u_{i,k+1}^n - u_{i,k}^n\right)\left[e^{-\left(\frac{\alpha}{1-\alpha}\right)\left(j-(k+1)\right)\Delta s} - e^{-\left(\frac{\alpha}{1-\alpha}\right)\left(j-k\right)\Delta s}\right]\\
&= \sum_{k=0}^{j-1}\Lambda_{\alpha,j,k}\left(u_{i,k+1}^n - u_{i,k}^n\right).
\end{aligned}
$$

The discretization of the gradient magnitude is given by:

$$
\left|\nabla^{\alpha}u(x_i, y_j, t_n)\right| \approx \left|\nabla^{\alpha}u_{i,j}^n\right| = \sqrt{\left|{}^{CF}D_x^{\alpha}u_{i,j}^n\right|^2 + \left|{}^{CF}D_y^{\alpha}\, u_{i,j}^n\right|^2}.
$$

2). The Symmetric boundary conditions are given by:

$$
u_{0,j}^n = u_{1,j}^n,\ u_{N,j}^n = u_{N-1,j}^n,\ 0 \le j \le M,\ \ u_{i,0}^n = u_{i,1}^n,\ u_{i,M}^n = u_{i,M-1}^n,\ 0 \le i \le N. \tag{5.52}
$$

3). The derivative terms are approximated as follows:

$$
\begin{aligned}
&\frac{\partial^2 u_{i,j}^n}{\partial t^2} \approx \frac{u_{i,j}^{n+1} - 2u_{i,j}^n + u_{i,j}^{n-1}}{\Delta t^2},\quad \frac{\partial u_{i,j}^n}{\partial t} \approx \frac{u_{i,j}^{n+1} - u_{i,j}^{n-1}}{2\Delta t},\\
&\frac{\partial u_{i,j}^n}{\partial x} \approx \frac{u_{i+1/2,j}^n - v_{i-1/2,j}^n}{\Delta s},\quad \frac{\partial u_{i,j}^n}{\partial y} \approx \frac{u_{i,j+1/2}^n - u_{i,j-1/2}^n}{\Delta s}.
\end{aligned}
$$

4). The discrete form of the proposed model (5.1) is represented as:

$$
\frac{u_{i,j}^{n+1} - 2u_{i,j}^n + u_{i,j}^{n-1}}{\Delta t^2} + \lambda\frac{u_{i,j}^{n+1} - u_{i,j}^{n-1}}{2\Delta t} = \frac{\partial}{\partial x}\left(\hbar_{i,j}^n\frac{\partial u_{i,j}^{n+1}}{\partial x}\right) + \frac{\partial}{\partial y}\left(\hbar_{i,j}^n\frac{\partial u_{i,j}^{n+1}}{\partial y}\right) + \gamma\left(u_{i,j}^0 - u_{i,j}^{n+1}\right), \tag{5.53}
$$

with the initial conditions, the following are specified:

$$
u_{i,j}^0 = u_0(i\Delta s, j\Delta s), 0 \le i \le N, 0 \le j \le M; u_{i,j}^1 = u_{i,j}^0, 0 \le i \le N, 0 \le j \le M. \tag{5.54}
$$

Furthermore, the discretization of equation (5.53) leads to:

$$
\begin{aligned}
&-\frac{\Delta t^2}{\Delta s^2}\left(\hbar^n_{i+\frac{1}{2},j}u^{n+1}_{i+1,j}-\hbar^n_{i-\frac{1}{2},j}u^{n+1}_{i-1,j}\right)-\frac{\Delta t^2}{\Delta s^2}\left(\hbar^n_{i,j+\frac{1}{2}}u^{n+1}_{i,j+1}-\hbar^n_{i,j-\frac{1}{2}}u^{n+1}_{i,j-1}\right)\\
&+\left[1+\frac{\lambda\Delta t}{2}+\gamma\Delta t^2+\frac{\Delta t^2}{\Delta s^2}\left(\hbar^n_{i+\frac{1}{2},j}+\hbar^n_{i-\frac{1}{2},j}+\hbar^n_{i,j+\frac{1}{2}}+\hbar^n_{i,j-\frac{1}{2}}\right)\right]u^{n+1}_{i,j}\\
&=2u^n_{i,j}+\left(\frac{\lambda\Delta t}{2}-1\right)u^{n-1}_{i,j}+\gamma\Delta t^2u^0_{i,j},
\end{aligned}
\tag{5.55}
$$

where $\hbar^n_{i+\frac{1}{2},j}$, $\hbar^n_{i-\frac{1}{2},j}$, $\hbar^n_{i,j+\frac{1}{2}}$, and $\hbar^n_{i,j-\frac{1}{2}}$, are approximations of $\hbar\left(\left|\nabla^\alpha u_\rho(x_{i+\frac{1}{2}},y_j,t_n)\right|\right)$, $\hbar\left(\left|\nabla^\alpha u_\rho(x_{i-\frac{1}{2}},y_j,t_n)\right|\right)$, $\hbar\left(\left|\nabla^\alpha u_\rho(x_i,y_{j+\frac{1}{2}},t_n)\right|\right)$, and $\hbar\left(\left|\nabla^\alpha u_\rho(x_i,y_{j-\frac{1}{2}},t_n)\right|\right)$, respectively.
Equation (5.55) can be expressed in matrix-vector form as follows:

$$
\left(D-\Delta t^2\sum_{k=1}^{2}A_k\left(U^n\right)\right)U^{n+1}=\widetilde{U}^n,
\tag{5.56}
$$

where A_k represents the diffusive interaction in the k direction, u^n is the vector with entries $u^n_{i,j}$, and

$$
\begin{aligned}
D&=I+\frac{\lambda\Delta t}{2}+\gamma\,\Delta t^2,\\
\widetilde{U}^n&=2u^n+\left(\frac{\lambda\Delta t}{2}-I\right)U^{n-1}+\gamma\,\Delta t^2\,U^0.
\end{aligned}
$$

This scheme involves solving a linear system, which is why it is called semi-implicit scheme. The solution U^{n+1} is given by:

$$
U^{n+1}=\left(D-\Delta t^2\sum_{k=1}^{2}A_k\left(U^n\right)\right)^{-1}\widetilde{U}^n.
\tag{5.57}
$$

To compute U^{n+1}, the matrix $\left(D-\Delta t^2\sum_{k=1}^{2}A_k\left(U^n\right)\right)$ must be inverted. Typically, this matrix has a large bandwidth because all the equations for the updated pixel values U^{n+1} are coupled. Direct methods, such as Gaussian elimination, may fill zeros within the bandwidth, leading to immense storage and computational effort. Iterative methods, including Jacobi and Gauss-Seidel, also present challenges, as their convergence slows down significantly for large Δt due to the increased condition number of the system matrix. Despite the absolute stability of the semi-implicit scheme, it is often not much faster than the explicit one. To fully leverage the benefits of absolute stability, it is crucial to develop a more efficient approach where the computational effort is independent of the time step size.

Additive Operator Splitting schemes

To address the aforementioned issue, we propose a modification of the semi-implicit scheme (5.57), known as the additive operator splitting (AOS) scheme. This approach aims to decouple the system, allowing each row and column of pixels to be processed independently. To achieve this, equation (5.57) is reformulated as:

$$U^{n+1} = \left(\frac{1}{2} \sum_{k=1}^{2} \left[D - 2\Delta t^2 A_k (U^n) \right] \right)^{-1} \widetilde{U}^n. \tag{5.58}$$

We then consider the desired form:

$$U^{n+1} = \sum_{k=1}^{2} \left(\frac{1}{2} \left[D - 2\Delta t^2 A_k (U^n) \right] \right)^{-1} \widetilde{U}^n. \tag{5.59}$$

This formulation introduces an interesting decomposition of the system matrix. However, the right-hand sides of (5.58) and (5.59) are not equal. To ensure equality, we multiply the right-hand side of (5.59) by a scalar r.

$$r \sum_{k=1}^{2} \left(\frac{1}{2} \left[D - 2\Delta t^2 A_k (U^n) \right] \right)^{-1} \widetilde{U}^n = \left(\frac{1}{2} \sum_{k=1}^{2} \left[D - 2\Delta t^2 A_k (U^n) \right] \right)^{-1} \widetilde{U}^n.$$

Letting $B_k = [D - 2\Delta t^2 A_k (U^n)]$, this implies:

$$4rB^{-1} = B^{-1}.$$

Thus, we find:

$$r = \frac{1}{4}.$$

Substituting this result into (5.59) simplifies the equation to:

$$U^{n+1} = \frac{1}{4} \sum_{k=1}^{2} \left[\frac{1}{2} \left(D - 2\Delta t^2 A_k (U^n) \right) \right]^{-1} \widetilde{U}^n = \sum_{k=1}^{2} \left(2D - 4\Delta t^2 A_k (U^n) \right)^{-1} \widetilde{U}^n. \tag{5.60}$$

Further simplification of (5.60) yields:

$$U^{n+1} = \left(2D - 4\Delta t^2 A_x (U^n) \right)^{-1} \widetilde{U}^n + \left(2D - 4\Delta t^2 A_y (U^n) \right)^{-1} \widetilde{U}^n.$$

This derivation shows that the scheme in (5.60) is a modified version of the semi-implicit scheme, incorporating a one-dimensional semi-implicit approach in arbitrary dimensions. Since it follows an additive splitting, all coordinate axes are treated equivalently.

Introducing the notation $U = (2D - 4\Delta t^2 A_x (U^n))^{-1} \widetilde{U}^n$, and $W = \left(2D - 4\Delta t^2 A_y (U^n) \right)^{-1} \widetilde{U}^n$, the solution can be expressed as the sum of two components:

$$U^{n+1} = V^{n+1} + W^{n+1}. \tag{5.61}$$

The equations for V and W are given by:

$$\begin{cases} (2D - 4\Delta t^2 A_x(U^n))\, V^{n+1} = \widetilde{U}^n \\ \left(2D - 4\Delta t^2 A_y(U^n)\right) W^{n+1} = \widetilde{U}^n. \end{cases} \tag{5.62}$$

Since the differential operators A_x and A_y are analogous, we derive the finite difference equation for a single row of pixels; the corresponding equation for a column of pixels is equivalent. Consider a row containing $N+1$ pixels indexed from 0 to N.

We introduce the following notation:

$$\delta_i = \frac{4\Delta t^2}{\Delta s^2}\left(\hbar_{i-\frac{1}{2}}\right), \text{ and } \sigma_i = \frac{4\Delta t^2}{\Delta s^2}\left(\hbar_{i+\frac{1}{2}}\right).$$

The finite difference equation for U simplifies to:

$$-\delta_i V_{i-1}^{n+1} + (2 + \lambda\Delta t + 2\gamma\,\Delta t^2 + \delta_i + \sigma_i)V_i^{n+1} - \sigma_i V_{i+1}^{n+1} = \widetilde{U}_i^n. \tag{5.63}$$

At each time step, the numerical scheme involves solving an algebraic system where the matrix $(2D - 4\Delta t\, A_x(U^n))$ is irreducible, strictly diagonally dominant, and therefore invertible. Such systems can be efficiently solved using block-wise solvers, such as the Tri-diagonal Matrix Algorithm.

A similar finite difference equation applies to W in the y dimension, for $j = 0, 1, ...M$.

$$-\delta_j W_{j-1}^{n+1} + (2 + \lambda\Delta t + 2\gamma\,\Delta t^2 + \delta_j + \sigma_j)W_j^{n+1} - \sigma_j W_{j+1}^{n+1} = \widetilde{U}_j^n, \tag{5.64}$$

where

$$\delta_j = \frac{4\Delta t^2}{\Delta s^2}\left(\hbar_{j-\frac{1}{2}}\right), \text{ and } \sigma_j = \frac{4\Delta t^2}{\Delta s^2}\left(\hbar_{j+\frac{1}{2}}\right).$$

At the boundary nodes, Neumann boundary conditions are imposed:

$$V_0 = V_1\,,\, V_N = V_{N-1} \qquad \text{and} \qquad W_0 = W_1\,,\, W_M = W_{M-1}.$$

In addition to discretizing equations (5.1)-(5.3), it is necessary to establish a stopping criterion for the numerical simulation. The process begins with the initial value u_0 , and the discrete system is iteratively applied, producing a sequence of progressively smoother images $u(x, y, t)$; $t > 0$, which represents filtered versions of u_0. The noise reduction process terminates when the restored image achieves optimal PSNR (Peak Signal-to-Noise Ratio) and SSIM (Structural Similarity Index) values.

We summarize the numerical algorithm for the model (5.1)-(5.3) in Algorithm 3.

Algorithm 3 AOS algorithm for Telg with diffusivity based on the Caputo-Fabrizio derivative

Input: Original image U^0, time step Δt, number of iterations N_t, parameters α, ρ, λ, γ
Initialize: $U^n = U^{n-1} = U^0$

1: **for** $n = 1$ to N_t **do**
2: **Compute**
- $D := I + \dfrac{\lambda \Delta t}{2} + \gamma \Delta t^2$
- $\tilde{U} := 2U^n + \left(\dfrac{\lambda \Delta t}{2} - I\right) U^{n-1} + \gamma \Delta t^2 U^0$

3: **Regularization:** Compute the smoothed version using convolution $v := \mathcal{K}_\rho * U^n$
4: **Compute the diffusivity:**
- Approximate the fractional gradient $\nabla^\alpha u$ using the Caputo-Fabrizio fractional derivative (Section 2.5.2)
- Compute the diffusivity function $\hbar := \hbar(|\nabla^\alpha v|)$ at each pixel

5: **Solve 1D system in x-direction:**

$$V := (2D - 4\Delta t^2 A_x)^{-1} \tilde{U}$$

Solve tridiagonal system using Thomas algorithm
6: **Solve 1D system in y-direction:**

$$W := (2D - 4\Delta t^2 A_y)^{-1} \tilde{U}$$

Solve tridiagonal system using Thomas algorithm
7: **Combine results:**

$$V^{n+1} := U + W$$

8: **end for**
Output: V^{n+1}

5.4 Experimental findings and their interpretation

This section presents a series of numerical experiments conducted to evaluate the effectiveness of the proposed model (5.1)-(5.3). In all the experiments and for each image type, we applied our model using three different values of α to evaluate its performance under varying conditions. The results indicate a direct relationship between noise density and the optimal fractional order. Specifically, as the noise density increases, the optimal fractional order that yields the best performance also increases. This suggests that higher noise levels necessitate a higher fractional order to achieve optimal results. These values of α are consistent across all figures and tables, and their impact on the results is reflected in the corresponding PSNR and SSIM values.

These experiments were performed on a diverse set of gray scale images using the AOS method with $\Delta s = 1$, $\rho = 2.5$, $\lambda = 0.1$, and $\hbar(|\nabla^{\alpha} u_{\rho}|) = \dfrac{1}{1 + |\nabla^{\alpha} u_{\rho}|^2}$. The original test images used in these simulations are shown in Figure 5.1. The selected images vary in size: the Brain MRI (BMRI) in Figure 5.2 has dimensions of 225×225, while the ultrasound image in Figure 5.3 has dimensions of 976×735. Figure 5.4 includes the Circle image, and Figure 5.5 presents the Barbara image, both with dimensions of 256×256.

To assess the robustness and effectiveness of the proposed model, different types of noise including speckle noise, salt-and-pepper noise, and Gaussian noise were added at progressively increasing levels. The performance of the model was evaluated using two widely used image quality metrics: the peak signal-to-noise ratio (PSNR) and the structural similarity index (SSIM). Additionally, the proposed model was compared against the classical telegraph diffusion-based model [17] to highlight its effectiveness in image restoration under various noise types and densities.

Figure 5.2 presents a Brain MRI (BMRI) scan with three different speckle noise densities. The proposed model demonstrates superior performance in noise removal while preserving fine image details, compared to the classical telegraph diffusion-based model [17]. This is supported by the results in Table 5.1, where the PSNR and SSIM values highlight the superior performance of the proposed model in both objective quality metrics. Additionally, the visual quality of the image shows a significant improvement, with clearer details and fewer noise artifacts. Such improvements are especially crucial in medical imaging, where maintaining high image quality is essential for accurate diagnosis and treatment planning.

Figure 5.3 shows an ultrasound image with various speckle noise densities. This image was used to further validate the effectiveness of our proposed model in removing speckle noise. The results confirm the superiority of our model over the classical telegraph diffusion-based model [17], as evidenced by the visual quality of the image and the results presented in Table 5.2, where the PSNR and SSIM values demonstrate the superior performance of the proposed model in terms of both objective quality metrics.

Figure 5.4 displays a Circle image with salt-and-pepper noise, applied at various noise densities. This images was used to further evaluate the effectiveness of our proposed model in removing salt-and-pepper noise. The results show that our model outperforms the classical telegraph diffusion-based model [17], as evidenced by the visual quality of the image and the results in Table 5.3, where the PSNR and SSIM values highlight the model's ability to preserve image quality while effectively eliminating noise.

Figure 5.5 presents the Barbara image with Gaussian noise, applied at three different noise densities. This image was used to evaluate the effectiveness of our proposed model in removing Gaussian noise, which can introduce random variations in pixel values, thus degrading image quality. The results indicate that our model provides superior noise reduction compared to the classical telegraph diffusion-based model [17], as shown by the improved visual quality of the image and the values in Table 5.4. These values, including PSNR and SSIM, highlight the model's ability to preserve image details and fine structures while effectively removing noise.

Building on the previous analysis of the proposed model's performance across various noise types and image categories, the numerical experiments further confirm its effectiveness in removing speckle, salt and pepper, and Gaussian noise at varying densities. The results clearly demonstrate that the proposed model outperforms the classical telegraph diffusion-based model [17], as evidenced by both objective quality metrics (PSNR and SSIM) and noticeable improvements in visual quality. These findings underscore the model's ability to preserve critical image details while effectively reducing noise, positioning it as a promising solution for applications such as medical imaging, where image quality is essential for accurate diagnosis. Furthermore, the results highlight the crucial role of the fractional order parameter α, revealing a direct relationship between noise density and the optimal α value. Specifically, as the noise level increases, a higher α is required to achieve optimal performance, underscoring its significance in fine-tuning the model for different noise conditions.

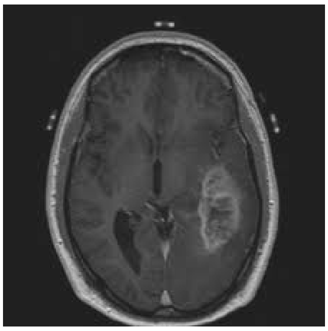

(a) BMRI

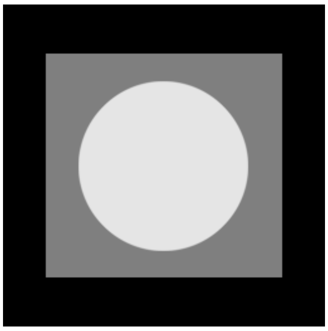

(b) Circle

(c) Barbara

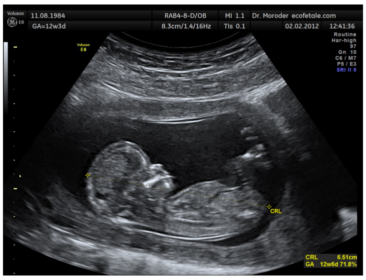

(d) Ultrasound

Figure 5.1: Original test images.

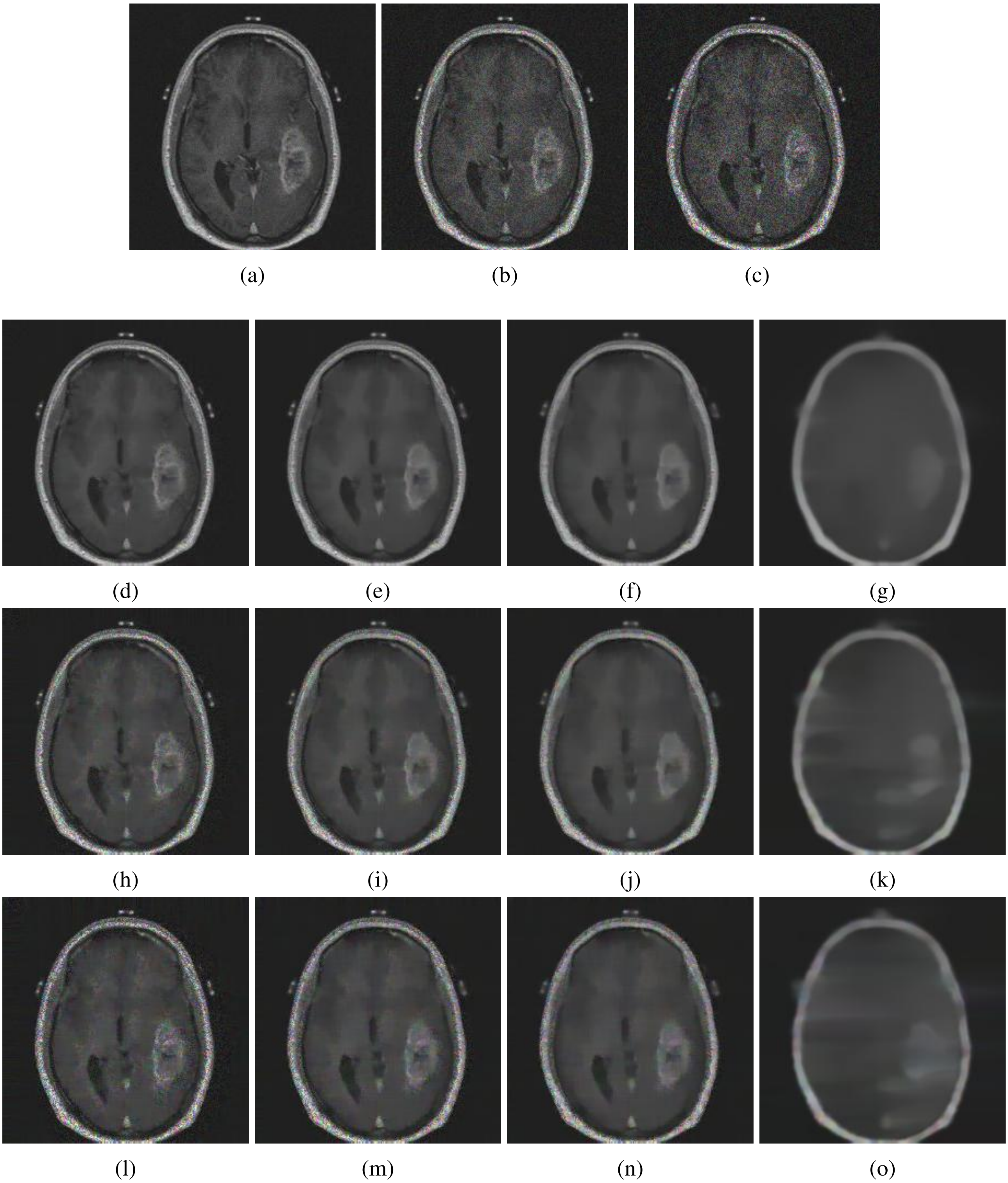

Figure 5.2: Comparison of denoising results for BMRI with varying noise levels after 6 iterations, using $\Delta t = 5.2$ and $\gamma = 0.01$. First row: (a-c) Noisy BMRI corrupted by speckle noise at levels of 0.01, 0.05, and 0.1, respectively. Second, third, and fourth rows: Filtered versions of images (a-c) using (5.1) and [17]. First, second, and third columns: Denoised images by (5.1) for $\alpha = 0.1, \alpha = 0.3$, and $\alpha = 0.5$, respectively. Fourth column: Denoised images by [17].

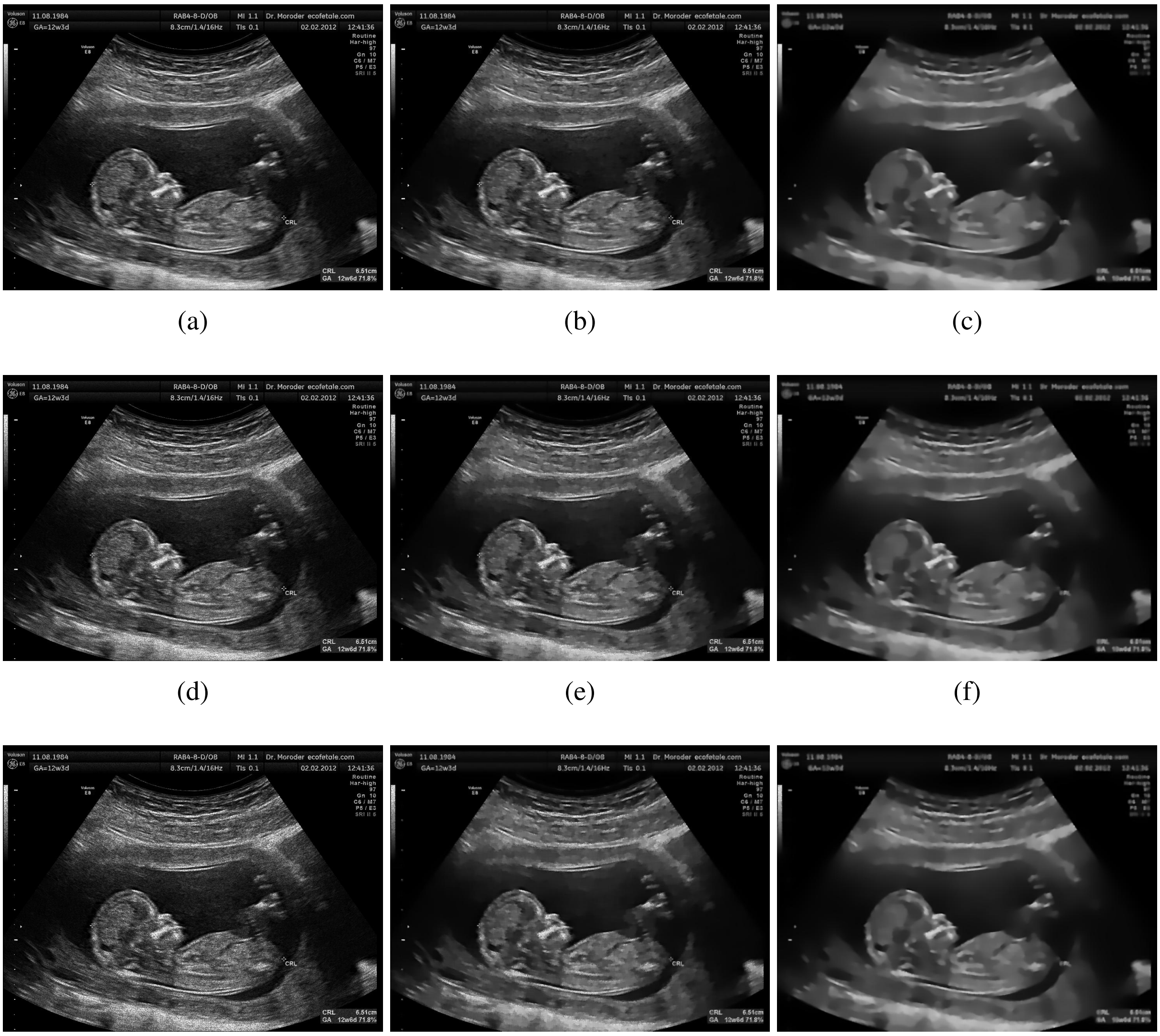

(a) (b) (c)

(d) (e) (f)

(g) (h) (i)

Figure 5.3: Comparison of denoising results for Ultrasound images with varying noise levels using $\gamma = 0.01$. (a,d,g): Noisy Ultrasound images corrupted by speckle noise with densities 0.01, 0.05, and 0.1, respectively. (b,e,h): Denoised images corresponding to (a,d,g) obtained using (5.1) for $\alpha = 0.1, \alpha = 0.3$, and $\alpha = 0.5$, respectively. (c,f,i): Denoised images corresponding to (a,d,g) obtained using [17].

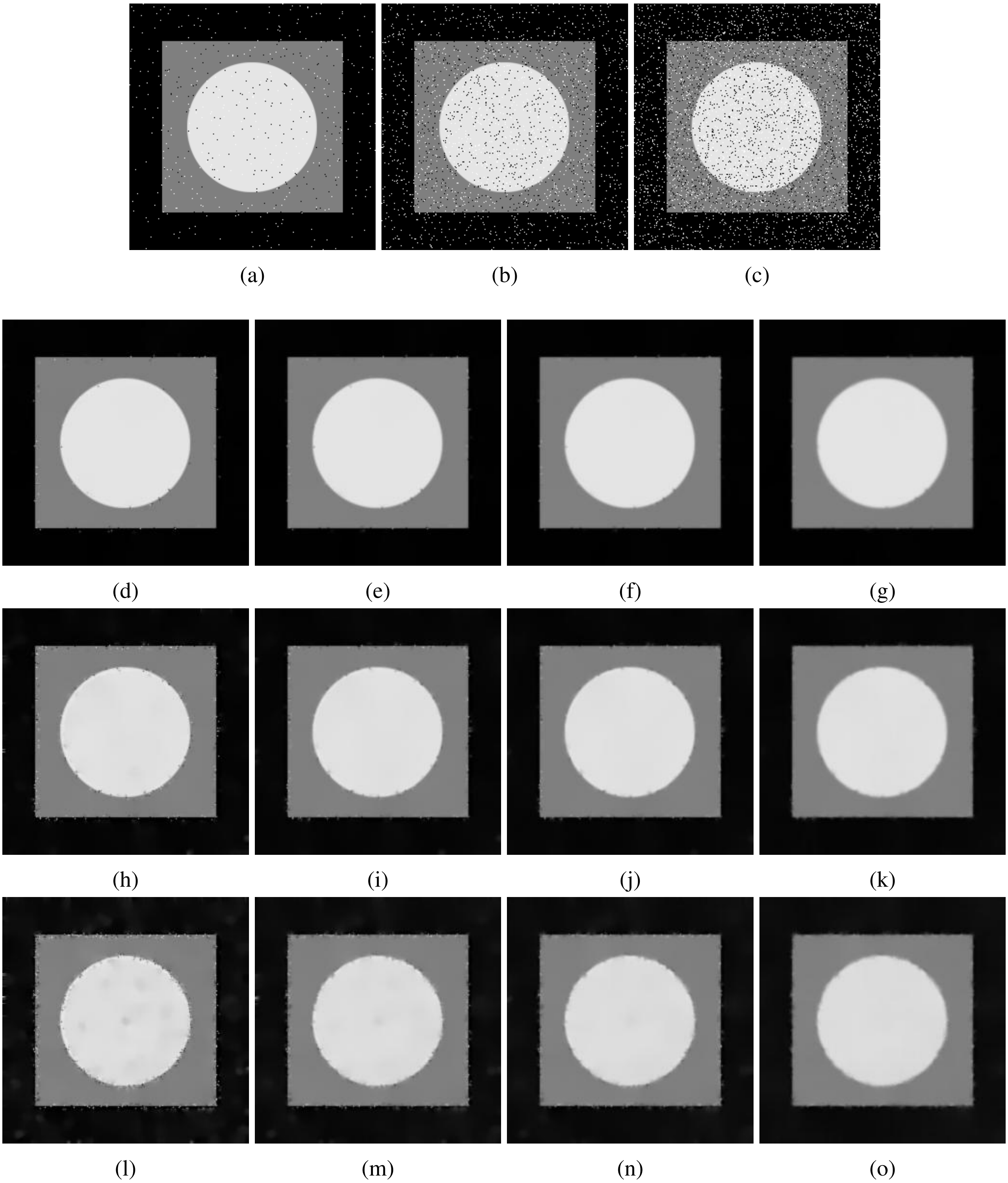

Figure 5.4: Comparison of denoising results for Circle images with varying noise levels after 6 iterations, using $\Delta t = 4$ and $\gamma = 0.001$. First row: (a-c) Noisy Circle images corrupted by salt-and-pepper noise at levels of 0.01, 0.05, and 0.1, respectively. Second, third, and fourth rows: Filtered versions of images (a-c) using (5.1) and [17]. First, second, and third columns: Denoised images by (5.1) for $\alpha = 0.5, \alpha = 0.7$, and $\alpha = 0.8$, respectively. Fourth column: Denoised images by [17].

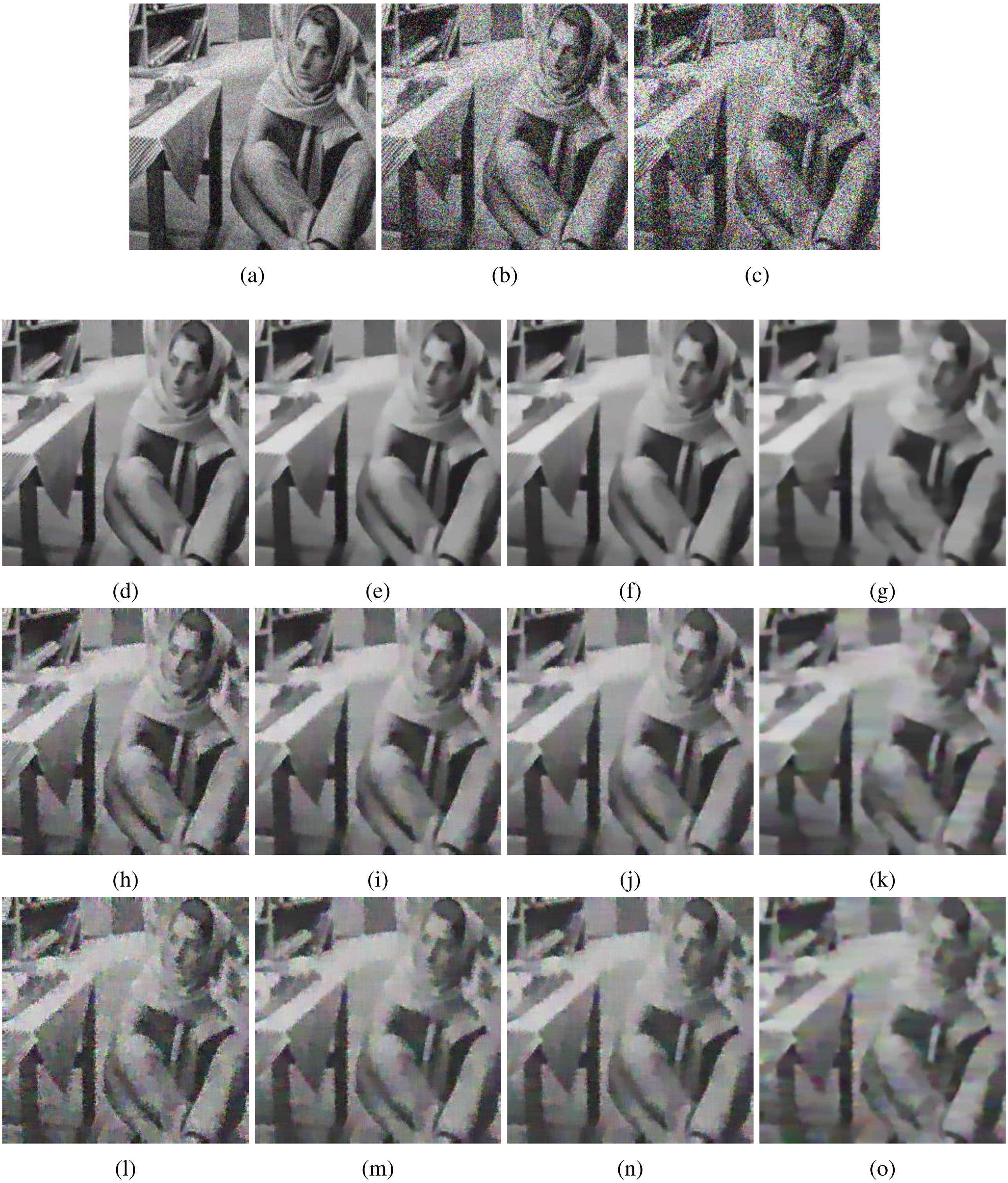

Figure 5.5: Comparison of denoising results for Barbara images with varying noise levels after 6 iterations, using $\Delta t = 4$ and $\gamma = 0.01$. First row: (a-c) Noisy Barbara images corrupted by Gaussian noise at levels of 0.01, 0.05, and 0.1, respectively. Second, third, and fourth rows: Filtered versions of images (a-c) using (5.1) and [17]. First, second, and third columns: Denoised images by (5.1) for $\alpha = 0.5, \alpha = 0.8$, and $\alpha = 0.9$, respectively. Fourth column: Denoised images by [17].

Image	Noise density	α Values						[17] model	
		$\alpha = 0.1$		$\alpha = 0.3$		$\alpha = 0.5$			
		PSNR	SSIM	PSNR	SSIM	PSNR	SSIM	PSNR	SSIM
BMRI	0.01	**36.04**	**0.95**	34.31	0.93	32.77	0.91	26.41	0.80
	0.05	31.17	0.90	**31.67**	**0.91**	31.43	0.90	25.99	0.79
	0.1	28.55	0.84	29.80	0.88	**30.25**	**0.88**	25.32	0.78

Table 5.1: Comparison of PSNR and SSIM for denoised images derived from noisy BMRI with varying levels of speckle noise.

Image	Noise density values					
Ultrasound	0.01		0.05		0.1	
	$\alpha = 0.1$	[17] model	$\alpha = 0.3$	[17] model	$\alpha = 0.5$	[17] model
PSNR	**30.42**	23.06	**27.76**	23.40	**26.63**	23.33
SSIM	**0.89**	0.59	**0.82**	0.61	**0.78**	0.61

Table 5.2: Comparison of PSNR and SSIM for denoised images derived from noisy Ultrasound images with varying levels of speckle noise.

Image	Noise density	α Values						[17] model	
		$\alpha = 0.5$		$\alpha = 0.7$		$\alpha = 0.8$			
		PSNR	SSIM	PSNR	SSIM	PSNR	SSIM	PSNR	SSIM
Circle	0.01	**35.81**	**0.89**	34.82	0.88	33.99	0.88	31.88	0.86
	0.05	30.34	0.61	**30.72**	**0.61**	30.47	0.60	29.47	0.59
	0.1	25.87	0.53	26.38	0.54	**26.41**	**0.54**	26.01	0.53

Table 5.3: Comparison of PSNR and SSIM for denoised images derived from noisy Circle images with varying levels of salt-and-pepper noise.

Image	Noise density	α Values						[17] model	
		$\alpha = 0.5$		$\alpha = 0.8$		$\alpha = 0.9$			
		PSNR	SSIM	PSNR	SSIM	PSNR	SSIM	PSNR	SSIM
Barbara	0.01	**26.99**	**0.76**	26.40	0.74	26.08	0.73	23.24	0.61
	0.05	23.32	0.59	**24.04**	**0.64**	24.02	0.64	22.14	0.54
	0.1	21.23	0.48	22.15	0.56	**22.20**	**0.57**	20.91	0.48

Table 5.4: Comparison of PSNR and SSIM for denoised images derived from noisy Barbara images with varying levels of Gaussian noise.

5.5 Conclusion

In this study, we proposed a novel nonlinear telegraph diffusion model that integrates fractional-order derivatives into the diffusivity function to enhance image denoising. We established a rigorous theoretical framework by proving the existence, uniqueness, and boundedness of the weak solution using Schauder's fixed-point theorem, ensuring the well-posedness of the model. From a numerical perspective, we employed an unconditionally stable semi-implicit finite difference schemes based on the additive operator splitting (AOS) technique, which has shown high efficiency in telegraph diffusion while maintaining computational feasibility.

Extensive experimental evaluations showed that the proposed model outperforms the classical telegraph diffusion approach in terms of noise removal, as well as edge and features preservation. The results, assessed using PSNR and SSIM, confirmed its effectiveness in restoring image quality across various types of noise while preserving fine structural details. Additionally, the findings reveal a direct relationship between the fractional order parameter α and noise characteristics, where the optimal choice of α varies according to noise density, ensuring enhanced denoising performance.

The improved denoising performance and structural preservation achieved by our model demonstrate its reliability for image processing applications. Its ability to reduce noise while maintaining essential usefulness in domains requiring high-quality image reconstruction, such as medical imaging and remote sensing.

General Conclusion

This thesis has presented a comprehensive study of fractional partial differential equation (FPDE) models for image restoration and denoising, combining rigorous theoretical analysis with efficient numerical implementations. The work has focused on nonlinear diffusion and telegraph diffusion models enhanced with fractional-order derivatives, considered either in the Caputo or Caputo-Fabrizio sense, to achieve a better balance between noise suppression and the preservation of structural image details.

From a theoretical perspective, the existence, uniqueness, and boundedness of weak solutions were established, ensuring the well-posedness of the proposed models. On the numerical side, semi-implicit additive operator splitting (AOS) schemes were developed, offering unconditional stability and computational efficiency. Comparative studies and extensive experiments, assessed through both visual inspection and quantitative metrics such as PSNR and SSIM, were conducted on images corrupted by different types of noise, including Gaussian, salt-and-pepper, and speckle noise. These experiments confirmed that the incorporation of fractional gradients, gray-level indicators, and fractional-order diffusivity enhances adaptability to local image features, improves denoising performance, and preserves edges and fine structures more effectively than classical models. In particular, the analysis confirmed a direct relationship between the fractional-order parameter α and noise characteristics, indicating that appropriately selecting α according to the noise level leads to improved denoising performance across varying noise densities.

Overall, the thesis provides a mathematically rigorous and computationally feasible framework for fractional PDE-based image denoising. The proposed models consistently demonstrate superior performance in terms of structural preservation, robustness to different types of noise, and computational efficiency, offering valuable tools for real-world applications in medical imaging, remote sensing, and other areas requiring high-quality image reconstruction.

Bibliography

[1] A. Abirami, P. Prakash, and Y.-K. Ma, *Variable-Order Fractional Diffusion Model-Based Medical Image Denoising.* Mathematical Problems in Engineering, 2021(1), 1-10, 2021.

[2] R.A. Adams, J.F. Fournier, *Sobolev Spaces*, second ed., Pure Appl. Math., vol. 140, Elsevier Academic Press, Amsterdam, 2003.

[3] L. Alvarez, P. L. Lions, and J. M. Morel, *Image selective smoothing and edge detection by nonlinear diffusion II.* SIAM Journal on Numerical Analysis, 29(3), 845-866, 1992.

[4] H. Amann. *Time-delayed Perona-Malik equations.* Acta Mathematica Universitatis Comenianae, 15-38, 2007.

[5] G. Asumu, M. Nchama, A.L Mecias, and M.R. Ricard, *Perona-Malik Model with Diffusion Coefficient Depending on Fractional Gradient via Caputo-Fabrizio Derivative.* Abstract and Applied Analysis. 2020, 1-15, 2020.

[6] A. Averbuch, B. Epstein, N.Rabin, and E. Turkel, *Edge-enhancement postprocessing using artificial dissipation.* IEEE Trans. Image Process. 15(6), 1486-1498, 2006.

[7] G. Aubert, and J. Aujol *A variational approach to removing multiplicative noise.* SIAM J. Appl. Math. 68, 925-946, 2008.

[8] G. Aubert, P. Kornprobst, *Mathematical problems in image processing: partial differential equations and the calculus of variations*, vol. 147. Springer Science and Business Media, 2006.

[9] J. Bai and X.-C. Feng, *Fractional-order anisotropic diffusion for image denoising.* IEEE Trans. Image Process, 16(10), 2492-2502, 2007.

[10] H. Brezis, *Functional analysis, Sobolev spaces and partial differential equations.* Springer Science and Business Media, 2010.

[11] I. Boudrissa, and N. Benhamidouche, *On the existence and uniqueness of the weak solution to spatial fractional nonlinear diffusion equation related to image processing.* MATHEMATICA SCANDINAVICA. 131(1), 83-103, 2025.

[12] I. Boudrissa, and N. Benhamidouche, *On the Well-Posedness of a Nonlinear Diffusion Equation With Gray-Level and Fractional Gradient Dependent Coefficients.* Mathematical Methods in the Applied Sciences. 48(18), 16495-16505, 2025.

[13] I. Boudrissa, R. Chouder, and N. Benhamidouche, *Fractional gradient-based nonlinear diffusion model for image denoising: theory and implementation.* Submitted.

[14] I. Boudrissa, R. Chouder, and N. Benhamidouche, *Fractional gradient-based nonlinear telegraph diffusion for image restoration.* Submitted.

[15] A. Buades, B. Coll, and J.M. Morel, *A non-local algorithm for image denoising.* IEEE Computer Vision and Pattern Recognition. 2, 60-65, 2005.

[16] E. Di Nezza, G. Palatucci, and E. Valdinoci, *Hitchhiker's guide to the fractional Sobolev spaces.* Bull. Sci. math. 136(5), 521-573, 2012.

[17] Y. Cao, J. Yin, Q. Liu, and M. Li, *A class of nonlinear parabolic-hyperbolic equations applied to image restoration.* Nonlinear Anal. Real World Appl. 11(1), 253-261, 2010.

[18] M. Caputo, and M. Fabrizio, *A new Definition of Fractional Derivative without Singular Kernel.* Progr. Fract. Differ. Appl., 1(2), 1-13, 2015.

[19] F. Catte, P. Lions, J. Morel and T. Coll, *Image Selective Smoothing and Edge Detection by Nonlinear Diffusion.* SIAM Journal on Numerical Analysis. 29(1), 182-193, 1992.

[20] R. A. Carmona and S. Zhong, *Adaptive smoothing respecting feature directions.* IEEE Trans. Image Process., 7(3), 353-358, 1998.

[21] A. Chauhan, S. Kumar, and Y. Karaca, *A New Fractional-order Derivative-based Nonlinear Anisotropic Diffusion Model for Biomedical Imaging.* CHAOS Theory and Applications, 5(3), 198-206, 2023.

[22] K. Chen, *Adaptive smoothing via contextual and local discontinuities.* IEEE Trans. Pattern Anal. Mach. Intell., 27(10), 1552-1567, 2005.

[23] E. Cuesta and J. Finat, *Image processing by means of a linear integro-differential equation.* IASTED, 438-442, 2003.

[24] J. Diestel, *Sequences and Series in Banach Spaces.* Springer, 1984.

[25] M. Elad, and M. Aharon, *Image denoising via sparse and redundant representations over learned dictionaries.* IEEE Transaction on Image Processing. 15(12), 3736-3745, 2006.

[26] L. C. Evans, *Partial Differential Equations.* American Mathematical Society, Vol. 19, pp.349-364, 1997.

[27] Y. Fujita, *Integro-differential equation which interpolates the heat equation and the wave equation.* Osaka Journal of Mathematics, 27, 319-327, 1990.

[28] Y. Fujita, *Integro-differential equation which interpolates the heat equation and the wave equation (II).* Osaka Journal of Mathematics 27, 797-804, 1990.

[29] R.C. Gonzalez, R.E. Woods, *Digital image processing.* 2nd ed., Prentice Hall, Englewood Cliffs, NJ, 2002.

[30] T. H. Gronwall, *Note on the derivatives with respect to a parameter of the solutions of a system of dierential equations.* Ann. Math. 20(4), 292-296, 1919.

[31] W. Jifara , F. Jiang , S. Rho , M. Cheng , S. Liu , *Medical image denoising using con- volutional neural network: a residual learning approach.* J. Supercomput. 75(2), 704-718, 2019.

[32] J. Hadamard, *Lectures on cauchys problem in linear partial differential equations.* Yale univ. Press. New Haven, 1953.

[33] V. Kamalaveni, R. A. Rajalakshmi, and K. A. Narayanankutty, *Image denoising using variations of Perona-Malik model with different edges stopping functions.* Procedia Computer Science, 58, 673-682, 2015.

[34] J. J. Koenderink, *The structure of images,* Biological Cybernetics, 1984.

[35] A. A. Kilbas, H. H. Srivastava, J. J. Trujillo, *Theory and Applications of Fractional Differential Equations.* Elsevier Science B.V, Amsterdam, 2006.

[36] M. Lysaker, A. Lundervold, and X.C. Tai, *Noise removal using fourth-order partial differential equation with application to medical magnetic resonance images in space and time.* IEEE Trans. Image Process 12(12), 1579-1590, 2003.

[37] S. Majee, R. Ray, A. Majee, *A gray level indicator-based regularized telegraph diffusion model: Application to image despeckling.* SIAMJ. Imaging Sci. 13(2), 844-870, 2020.

[38] R. Malladi and J. A. Sethian, *Image Processing: Flows under Min/ Max curvature and Mean Curvature.* Graphical Models and Image Processing. 58(2), 127-141,1996.

[39] P. Perona, and J. Malik, *Scale space and edge detection using anisotropic diffusion.* IEEE Trans. Pattern Anal. Mach. Intell., 12(7), 629-639, 1990.

[40] V. Ratner and Y.Y. Zeevi, *Image enhancement using elastic manifolds.* In Proceedings of the 14th International Conference on Image Analysis and Processing. 2007, ICIAP 2007, IEEE, 769- 774, 2007.

[41] J.G. Rosen, *The gradient projection method for nonlinear programming*, part II, nonlinear constraints. J. Soc. Ind. Appl. Math. 9(4), 514-532, 1961.

[42] G. Rosman, L. Dascal, A. Sidi, and R. Kimmel, *Efficient Beltrami image filtering via vector extrapolation methods.* SIAM J. Img. Sci. 2(3), 858-878, 2009.

[43] W. Rudin, *Functional Analysis,* 2nd ed. McGraw-Hill, 1991.

[44] L. I. Rudin, S. Osher, and E. Fatemi, *Nonlinear total variation based noise removal algorithms.* Physica D, 60(1-4), 259-268, 1992.

[45] X. Shan, J. Sun, Z. Guo, W. Yao, and Z. Zhou, *Fractional-order diffusion model for multiplicative noise removal in texture-rich images and its fast explicit diffusion solving.* BIT Numer. Math. 62(4), 1319-1354, 2022.

[46] M.R. Sidi Ammi , I. Jamiai, and D.F.M. Torres, *A finite element approximation for a class of Caputo time-fractional diffusion equations.* Computers and Mathematics with Applications, 78(5), 1334-1344, 2019.

[47] S. Singh and I. Singula, *Enhanced face matching technique-based Gabor Filter and PSO.* International Journal of Advanced Research in Computer Science and Software Engineering. 4(8), 1215-1220, 2014.

[48] V. Strela, *Denoising via block wiener filtering in wavelet domain.* in Proc. IEEE 3rd European Congress of Mathematics, Barcelona, Birkhauser Verlag. 619-625, 2001.

[49] G. A. Mboro-Nchama, A. L. Mecías and M. R. Ricard, *A New Version of Catte-Lions-Morel Model for Image Smoothing and Edge Detection.* Global Journal of Pure and Applied Mathematics, 16(6), 819-842, 2020.

[50] K. M. Owolabi, and A. Atangana, *Numerical Methods for Fractional Differentiation.* Springer Series in Computational Mathematics, vol 54, 2019.

[51] Z. Wang, and A. C. Bovik, *A universal image quality index.* IEEE Signal Processing Letters. 9(3), 81-84, 2002.

[52] Z. Wang, A.C. Bovik, H.R. Sheikh, E.P. Simoncelli, *Image quality assessment: from error visibility to structural similarity.* Image Processing, IEEE Transactions, 13(4), 600-612, 2004.

[53] J. Weickert. *Anisotropic di usion in image processing,*Teubner Stuttgart, 1998.

[54] J. Weickert, B.M. ter Haar Romeny and M.A. Viergever, *Efficient and reliable scheme for nonlinear diffusion filtering.* IEEE Trans on Image Processing, 7(3), 398-410, 1998.

[55] Y.-Q. Yang and C.-Y .Zhang, *Kernel based telegraph-diffusion equation for image noise removal.* Mathematical Problems in Engineering. 2014(1),283751, 2014.

[56] W. Yao, Z. Guo, J. Sun, B. Wu, and H. Gao, *Multiplicative noise removal for texture images based on adaptive anisotropic fractional diffusion equations.* Siam J. Imaging Sci. 12(2), 839-873, 2019.

[57] A. Yezzi, *Modified curvature motion for image smoothing and enhancement.* IEEE Transactions on Image Processing. 7(3), 345-352, 1998.

[58] Y.L. You, M. Kaveh, *Fourth-order partial differential equation for noise removal.* IEEE Trans. Image Process. 9(10), 1723-1730, 2000.

[59] J. Yuan and J. Wang, *Perona-Malik model with a new diffusion coefficient for image denoising.* International Journal of Image and Graphics, 16(2), 2016.

[60] E. Zauderer, *Partial Differential Equations of Applied Mathematics.* John Wiley and Sons: New York, NY, USA, 2011.

[61] W. Zhang, J. Li, and Y. Yang, *Spatial fractional telegraph equation for image structure preserving denoising.* Signal Process. 107, 368-377, 2015.

[62] Z. Zhang, , Q. Liu, and T. Gao, *A fast explicit diffusion algorithm of fractional order anisotropic diffusion for image denoising.* Inverse Problems and Imaging, 15(6). 1451-1469, 2021.

[63] K. Zhang, W. Zuo, Y. Chen, D. Meng and L. Zhang, *Beyond a Gaussian denoiser: Residual learning of deep CNN for image denoising.* IEEE Transactions on Image Processing, 26(7), 3142-3155, 2017.

[64] Z. Zhou, Z. Guo, D. Zhang, B. Wu, *A nonlinear diffusion equation-based model for ultrasound speckle noise removal.* J. Nonlinear Sci. 28, 443-470, 2018.

[65] Y. Zhou, Y. Li, Z. Guo, B. Wu, and D. Zhang. *Multiplicative Noise Removal and Contrast Enhancement for SAR Images Based on a Total Fractional-Order Variation Model.* Fractal Fract. 7(4), 329, 2023.

Abstract

This thesis addresses the fundamental challenge of image denoising: achieving an optimal balance between noise suppression and the preservation of essential image structures. It introduces novel fractional partial differential equation (FPDE) models formulated within nonlinear diffusion and nonlinear telegraph diffusion frameworks, employing fractional derivatives in the Caputo and Caputo-Fabrizio senses to enhance modeling flexibility and denoising performance. Theoretical analysis establishes the well-posedness of the proposed models by proving the existence, uniqueness, and boundedness of weak solutions. Efficient semi-implicit numerical schemes based on additive operator splitting (AOS) are developed and shown to be unconditionally stable and computationally efficient. Comprehensive experiments evaluated using PSNR and SSIM metrics demonstrate that the proposed fractional-order models significantly outperform conventional approaches.

Keywords: Fractional PDEs; nonlinear diffusion; nonlinear telegraph diffusion; weak solutions; Schauder's fixed-point theorem; unconditionally stable numerical schemes; image denoising; image restoration.

Résumé

Cette thèse aborde le défi fondamental du débruitage d'images, qui consiste à atteindre un équilibre optimal entre la suppression du bruit et la préservation des structures essentielles de l'image. Elle introduit de nouveaux modèles d'équations aux dérivées partielles fractionnaires (FEDPs), formulés dans les cadres de la diffusion non linéaire et de la diffusion télégraphique non linéaire, en recourant aux dérivées fractionnaires au sens de Caputo et de Caputo–Fabrizio afin d'accroître la flexibilité de modélisation et d'améliorer l'efficacité du débruitage. L'analyse théorique établit le caractère bien posé des modèles proposés en démontrant l'existence, l'unicité et la bornitude des solutions faibles. Des schémas numériques semi-implicites performants, fondés sur la décomposition additive des opérateurs (AOS), sont développés et démontrés inconditionnellement stables et efficaces sur le plan computationnel. Des expériences numériques approfondies, évaluées à l'aide des indicateurs PSNR et SSIM, montrent que les modèles fractionnaires proposés surpassent de manière significative les approches classiques.

Mots-Clés: EDPs fractionnaires; diffusion non linéaire; diffusion télégraphique non linéaire; solutions faibles; théorème du point fixe de Schauder; schémas numériques inconditionnellement stables; débruitage d'images; restauration d'images.

ملخص:

تتناول هذه الأطروحة التحدي الأساسي في إزالة الضوضاء من الصور، والمتمثل في تحقيق توازن أمثل بين تقليل الضوضاء والحفاظ على البنى الأساسية للصورة. وقد تم في هذا العمل تقديم نماذج جديدة للمعادلات التفاضلية الجزئية الكسرية (FPDEs)، صيغت في اطار الانتشار غير الخطي و الانتشار التلغرافي غير الخطي، مع توظيف المشتقات الكسرية بمفهوم كابوتو(Caputo) وكابوتو–فابريزيو (Caputo– Fabrizio) لتعزيز مرونة النمذجة وتحسين أداء إزالة الضوضاء . يثبت التحليل النظري أن النماذج المقترحة جيدة الوضع، وذلك من خلال برهان وجود الحلول الضعيفة ، ووحدانيتها، وحدودها. كما تم تطوير مخططات عددية شبه ضمنية فعالة تعتمد على تفكيك المؤثرات الجمعي (AOS) ، وقد أثبتت استقراريتها غير المشروطة وكفاءتها الحسابية. وتظهر التجارب العددية الموسعة ، التي تم تقييمها باستخدام مؤشري PSNR و SSIM، أن النماذج الكسرية المقترحة تتفوق بشكل ملحوظ على الطرق التقليدية.

كلمات مفتاحية: المعادلات التفاضلية الجزئية الكسرية؛ الانتشار الغير خطي؛ انتشار التلغراف غير الخطي؛ الحلول الضعيفة؛ نظرية النقطة الثابتة لشاودر (Schauder) ؛ مخططات عددية ذات استقرار غير مشروط؛ إزالة الضوضاء من الصور؛ استعادة الصور.